DISCOVERY AND CHARACTERIZATION OF A SIGNALING MOLECULE REGULATING SOMATIC EMBRYOGENESIS IN LOBLOLLY PINE

A Dissertation
Presented to
The Academic Faculty

by

Di Wu

In Partial Fulfillment
of the Requirements for the Degree
Doctor of Philosophy in the
School of Chemistry and Biochemistry

Georgia Institute of Technology
April 2008

DISCOVERY AND CHARACTERIZATION OF A SIGNALING MOLECULE REGULATING SOMATIC EMBRYOGENESIS IN LOBLOLLY PINE

Approved by:

Dr. Sheldon May, Advisor
School of Chemistry and Biochemistry
Georgia Institute of Technology

Dr. Donald Doyle
School of Chemistry and Biochemistry
Georgia Institute of Technology

Dr. James Powers
School of Chemistry and Biochemistry
Georgia Institute of Technology

Dr. Gerald Pullman
School of Biology
Georgia Institute of Technology

Dr. Nicholas Hud
School of Chemistry and Biochemistry
Georgia Institute of Technology

Date Approved: Jan 16, 2008

Dedicated to my families and teachers

ACKNOWLEDGEMENTS

First and foremost, I would thank my dissertation advisor, Dr. Sheldon W. May, for his constant support and encouragement. I particularly appreciate his faith in me as well as the success of this tough project. I owe a huge debt of gratitude for his patience and the many hours he spent with me developing my English writing, and for his inspiration to develop into a successful scientist by sharing his philosophy of life.

Second, I would like to express my thanks to Dr. Charlie Oldham for always being available for technical discussions and assistance with operation and maintenance of equipments, and for being good listener for all my weird ideas. I would also like to thank Dr. Kristi Burns for getting me started with research, teaching me how to be a good Ph.D. student, and sharing her experience and expertise.

The success of this dissertation project attributes to a great extent to collaboration with many experts at Georgia Tech. I would like to acknowledge my coadvisor, Dr. Gerald Pullman, for his endless help and scientific advice in plant physiology and somatic embryogenesis, and for wishing me good luck all the time; Dr. M. Cameron Sullards, for developing and performing all the mass spectrometry experiments, guiding me through MS from the very beginning, and technical discussions for years; Dr. Les Gelbaum, for carrying out all the NMR experiments and scientific discussions; Dr. Yanfeng Chen, for helping me interpreting LC/MS/MS spectra; Dr. Zhen Zhou, Dr. Yonggang Wu and Dr. Jin Li, for discussing with me

about NMR spectra; other members from both Dr. May's and Dr. Pullman's research groups, Mike Foster, Elizabeth Cowan, Kylie Bucalo, Anna Griffin, Shannon Johnson, Veronica DeSilva and Jacob Lucrezi.

I gratefully acknowledge the financial support of the Institute of Paper Science and Technology at Georgia Tech, United States Department of Agriculture, the Consortium for Plant Biotechnology Research, Inc., and Monsanto, Inc. I would also like to thank the members of my thesis committee, Dr. Sheldon W. May, Dr. James Powers, Dr. Nicholas Hud, Dr. Donald Doyle, and Dr. Gerald Pullman for their guidance and suggestions about my work and for reading this dissertation.

Last but not least, I would like to thank my family and friends for supporting me during the rough times and celebrating the triumphs with me. I can never fully express my gratitude to my parents and my grandmother. My father, Qingwei Wu, has always been a wonderful resource for advice, educated and encouraged me to set high goals and to develop into an independent scholar. My mother, Peiling Shen, has provided invaluable devotion and support, and been an understanding ear. My grandmother, Xuexiu Zhou, has been a wonderful role model to be a tough woman. Special thanks would go to my uncle, Dr. Chen Zhou, who is a faculty member of School of Industrial & Systems Engineering at Georgia Tech, for his perpetual support and advice through my years in graduate school.

TABLE OF CONTENTS

LIST OF TABLES

Page

LIST OF FIGURES

Page

LIST OF SYMBOLS AND ABBREVIATIONS

myo-Inositol-1,2,3,4,5,6-hexa*kis*phosphate	$InsP_6$
SE	Somatic Embryogenesis
LP	Loblolly Pine
FG	Female Gametophyte
Ins	*myo*-Inositol
PtdIns	Phosphatidylinositol
FPLC	Fast Protein Liquid Chromatography
HPLC	High Performance Liquid Chromatography
HIC	Hydrophobic Interaction Chromatography
MS	Mass Spectrometry
TIC	Total Ion Chromatogram
XIC	Extracted Ion Chromatogram
LIT	Linear Ion Trap
ESI	Electrospray Ionization
TOF	Time of Flight
NMR	Nuclear Magnetic Resonance
COSY	Correlation Spectroscopy
HSQC	Heteronuclear Single Quantum Correlation
TFA	Trifluoroacetic Acid
SDS	Sodium Dodecyl Sulfate
ABA	Abscisic Acid
GA	Gibberellin
BR	brassinosteroid

SUMMARY

myo-Inositol-1,2,3,4,5,6-hexa*kis*phosphate ($InsP_6$), also called phytic acid, is ubiquitous in eukaryotic cells and the most abundant inositol phosphate derivative. Loblolly pine (LP, *Pinus taeda*) constitutes the primary commercial species in the southern forest of U.S. Somatic embryogenesis (SE) is an effective technique to maintain the desirable genetic composition of the progeny and to accomplish the efficiency of propagation. SE can also serve as a tool for study of plant development. Unlike angiosperm embryos with attached cotyledons as seed storage organs, the diploid conifer embryo is surrounded by the unattached haploid female gametophyte (FG). In LP SE, FG tissue is absent in the embryogenic tissue culture. We found that extracts from early-stage FG stimulate growth and multiplication of early-stage somatic embryos, whereas FG water extracts from late stage contain substance(s) inhibitory to early-stage somatic embryo growth (DeSilva et al., 2007). We now present the isolation and identification of the inhibitory substance as $InsP_6$ by means of water extraction, two gel filtrations and two ion exchange FPLC chromatographies. The results represent the first complete structural characterization of $InsP_6$ from a natural product using LC/MS, LC/MS/MS, exact MS, 1D- and 2D-NMR analyses. We also report that there is a good correlation between the amount of $InsP_6$ purified from FG tissue (1.3 nmoles per full-term FG) and the amount of $InsP_6$ which inhibits somatic embryo growth. This novel approach of isolating and characterizing $InsP_6$ from plant tissue, and investigating its role on SE can allow us to improve SE technology by circumventing current bottleneck, to elucidate enigmatic functions of $InsP_6$ in plants, and most importantly, to utilize this molecule properly.

CHAPTER I

INTRODUCTION

Somatic Embryogenesis

Importance and History of Somatic Embryogenesis

With the growing demand for wood products all over the world, an increasing need for production of high-value tree species is becoming more and more prominent. Innovative technology for the generation of new hybrids, early selection and testing of desirable genotypes, rapid vegetative propagation of selected genotypes needs to be developed to meet the rapidly growing demand. Among all the tree improvement programs, there are two basic factors to determine its success: the quality of the product and the economy of propagation. Vegetative propagation is superior to sexual reproduction in that it can not only maintain the desirable genetic composition of the progeny, but also accomplish the efficiency of propagation.

The commercial applications of cell and tissue culture to mass propagation enable the growth of tissue or organ segments in proper media which allow their development through one specific pathway. The most common pathway, known as "micropropagation", involves the regeneration of whole plants or multiple shoots from stem segments or from excised shoot apices. Another pathway, known as "somatic embryogenesis (SE)", which is also the most promising and desirable so far, is to reproduce whole plants from callus and suspension cultures (Jain et al., 1995). Well

controlled SE is not only able to maintain the genetic stability and assure juvenile plants of normal growth habit, but also liable to mass production and planting.

Zygotic embryos resulting from gametic fusion are structurally observed bipolar with root and shoot on opposite ends. Somatic embryos or embryoids are "embryo-like" structures in tissue cultures of various plant species. The formation and development of somatic embryos is termed "somatic or asexual embryogenesis" (Jain et al., 1995).

The idea of SE first started with the regeneration of adventitious buds from cambial tissue of *Ulmus campetris* (Gautheret, 1940). In this work, some root was formed, but complete plantlets were not generated. Winton (Winton, 1970) reported the first regeneration of complete plants from tissue culture from leaf explants of aspen. Due to the discovery of cytokinins, explant sources were managed to be cultured in vitro for callus and plantlet production. Since Sommer and Wetzstin published more than 100 species of angiospermic woody plants reproduction from zygotic embryos and/or young seedlings in 1984 (Sommer and Wetzstein, 1984), the number of hardwood species able to reproduce *in vitro* has almost doubled.

Sharp (Sharp et al., 1982) differentiated two patterns of the origin of somatic embryos from *in vitro* grown explants:

a. Pro-embryonic-determined cells (PEDC), somatic embryos originate from explant cells in which only an in vitro environment is needed to be released from some suppressive condition. Examples of PEDC in woody angiosperms include *Citrus, Ilex aquifolium, Malus domestica, Mangifera indica, Theobroma cacao,* and *Pyrus* spp.

b. Induced embryogenic-determined cells (IEDC), also known as indirect production of somatic embryos from an unorganized callus/tissue mass. In this case, a series of growth regulators are needed to first form callus, then to reproduce somatic embryos. IEDC requires the release of previously differentiated state through mitotic cell divisions, and an induction of the new pattern of cell divisions to form organized embryos. Examples of IEDC span both monocots and dicots including *Cocos nucifera, Chamedorea costaricana, Phoenix dactylifera, Elaeis guineensis, Coffea Arabica, Pyrus communis, Santalum album.* Although plants follow either pattern of somatic embryo development, they are not mutually exclusive.

The commercial plantation of SE was first presented by Blake for oil palms (Blake, 1983). A major problem for most commercial somatic embryos since then was the low frequency of maturation and germination into whole plants. Various attempts were made to improve both the quality and yield of mature somatic embryos to germinate in multiple species of *Picea (Roberts et al., 1993).* Von Arnold and Hakman (von Arnold and Hakman, 1988) demonstrated that light can inhibit the germination of somatic embryos.

The use of large-scale bioreactors in liquid cultures has proved to be the ideal approach to increasing the efficiency of SE in gymnosperms, including *Picea abies, Picea mariana, Pinus caribaea, Pinus strobus*, etc. Additionally, Chen and Kartha reported that cryopreservation was ideal for maintaining superior genotypes in an embryogenic state for a long period (Chen and K.K., 1987).

Somatic embryogenesis *in vivo* and *in vitro*

Natural asexual embryos were reported in several angiosperm families. Although other tissues including integuments, synergids and embryo-suspensors are able to generate asexual embryos, they originate predominantly from the nucellus. Therefore, seeds contain multiple embryos in addition to the zygotic embryo. This phenomenon is called "polyembryony". There are two possibilities that cause polyembryony in conifers:

A) sperm nuclei contained in one or more pollen tubes fertilize more than one archegonium or egg cell

B) the cleavage of the embryonal segments of one or more zygotic embryos

The natural occurrence of "cleavage polyembryony" *in vivo* inspired the idea of somatic embryogenesis in conifers, since four genera of the Pinaceae family, including *Pinus, Cedrus, Keteleeria* and *Tsuga*, show cleavage polyembryony (Jain et al., 1995). Four major steps involved in the process of SE in culture were summarized as following:

A) Initiation or induction of somatic embryos from primary explants which could be female or megagemetophytes without embryos, female gametophytes with intact zygotic embryos, precotyledonary zygotic embryos, cotyledonary embryos from fresh seed cones and stored dry seeds, seedling explants.

B) Multiplication or proliferation of embryogenic cultures. After the initiation of embryogenic tissue occurs, the tissue needs to be mainteined on fresh media gelled or in liquid suspension cultures to sustain proliferation.

C) Development and maturation of somatic embryos, which includes free nuclear somatic proembryo phase, cellular somatic proembryo phase, precotyledonary somatic embryo phase and cotyledonary somatic embryo phase.

D) Germination in which plantlets exhibit a well formed root, an elongated hypocotyl and cotyledons.

Importance of LP

The pine (Pinaceae) family belongs to the Pinales order of gymnosperms which are a group of vascular plants whose seeds are not enclosed by a ripened ovary (fruit) (Mirov, 1967). Loblolly pine (LP, *Pinus taeda*), a species of pine family, constitutes the primary commercial species in the southern forest of U.S. covering 13.4 million ha., approximately 45% of commercial forestland. Over 1.5 billion loblolly pine seedlings are planted in U.S. each year (Schultz, 1999). In the southern U.S., one of nine manufacturing jobs can be linked to southern pine forests, from planting to the production of forest-based products.

Somatic embryogenesis in Loblolly Pine

Implementation of clonal tree production is a major trend for the forest industry. For many softwood trees including LP, SE is the most promising method to overcome both economic barriers (investments vs. returns) and biological barriers (Timmis, 1998). The successful development of SE will allow superior, faster-growth LP trees to be replicated in large-scale, commercial numbers for replanting initiatives, which will in turn benefit our society and economy by conserving national forestland, sequestering carbon dioxide and revitalizing the U.S. forest products industry. In addition to its practical application, SE can serve as a tool for study of plant development (Zimmerman, 1993).

SE in LP is also comprised of four major steps initiation, maintenance and multiplication, maturation and germination (Figure 1). In initiation, zygotic seed embryos are used to initiate a culture in which cleavage polyembryony continues to form masses of early-stage somatic embryos through the application of plant hormones. The numbers of the resulting somatic embryos are increased by transferring to a gelled or liquid multiplication medium, which contains plant hormones to continue cleavage polyembryony and somatic embryo multiplication. Cultures may replicate 2-6 times weekly, rapidly producing large numbers of somatic embryos. After a sufficient population of somatic embryos is obtained, embryos are placed on a development and maturation medium, in which a different set of plant hormones and environment conditions are provided. During this step, somatic embryos continue their growth to a maxium of stage 9.1 compared to zygotic embryos that complete development with another 7-10 weeks of growth (stage 9.7-9.10). In the last step, germination, somatic embryos are taken out of the tissue culture to produce somatic seedlings ready for planting in the field. Our most advanced LP somatic embryos resemble stage 7-8 zygotic embryos in germination performance.

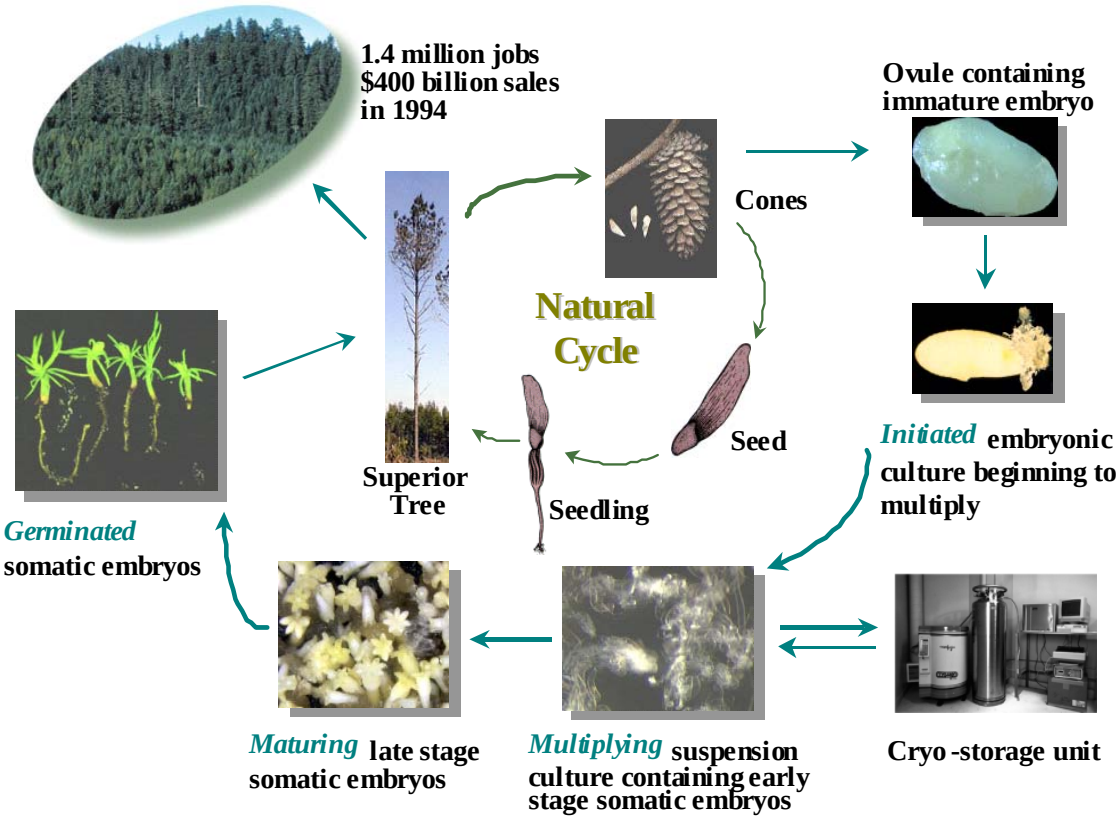

Figure 1. Somatic embryogenesis in loblolly pine (Pullman et al., 2003a).

The failure of somatic embryos to fully mature is the bottleneck in the increased utilization of somatic seedlings. Figure 2 shows an embryo staging system established by (Pullman and Webb, 1994), in which developmental stages of zygotic embryos of LP were determined by appearance, size, dry weight, germination ability and gene activity profiles (Cairney et al., 2000). Figure 3 presents the corresponding staging system for somatic embryos of LP. Zygotic embryos continue growth through stages 9.2-9.10 and acquire the ability to germinate at stage 7, whereas somatic embryos develop to a stage of 8-9.1 vs. full development at 9.10. Thus, only a low percentage of the most advanced genotypes of our LP somatic embryos are able to germinate and grow into seedlings.

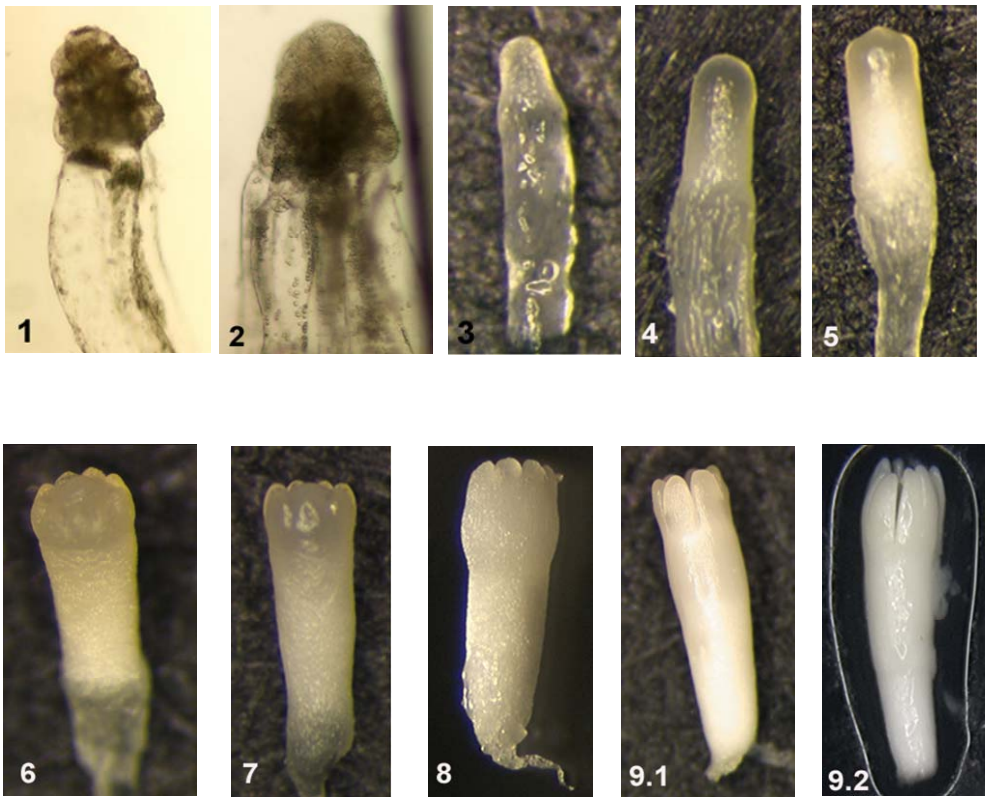

Figure 2. Zygotic embryos of loblolly pine, stages 1 through 9.2, modified from (Cairney and Pullman, 2007).

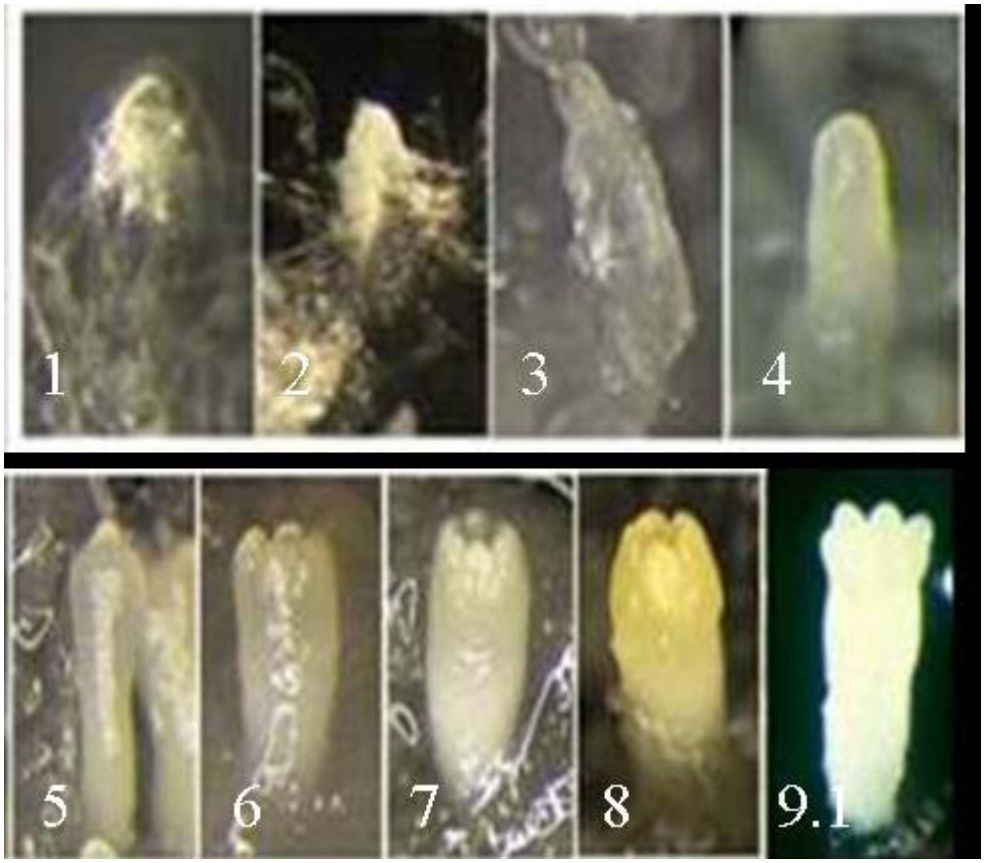

Figure 3. Somatic Embryos of loblolly pine, Stages 1 through 9.1, modified from (Cairney and Pullman, 2007).

Plant Polypeptide Hormones

Peptide hormones are the most extensive signaling molecules in the animal kingdom, controlling cell interaction, differentiation and proliferation. In contrast, in the world of plants, only five small organic compounds have traditionally been thought to regulate cell to cell communication. The first of these five phytohormones are auxins, such as indole-3-acetic acid and 2,4-D; auxins stimulate cell elongation, cell division, and differentiation of phloem and xylem, and mediate gravitropic response, root initiation and root development (Mauseth, 1991; Raven, 1992; Salisbury and Ross, 1992; Davies, 1995). The second group is cytokinins, such as zeatin, whose structures resemble adenine. Cytokinins are involved in transportation of metabolites into plants and stimulation of cell division and morphogenesis (Mauseth, 1991; Raven, 1992; Salisbury and Ross, 1992; Davies, 1995; Kulaeva and Prokoptseva, 2004). The third group is gibberellins that regulate seed and tuber dormancy release and transition to flowering in response to day length (Kulaeva and Prokoptseva, 2004). The fourth group is abscisic acid, a sesquiterpenoid that induces and maintains dormancy in buds, tubers, bulbs and roots, and regulates the synthesis of storage proteins in seeds (Kulaeva and Prokoptseva, 2004). The fifth group is ethylene, which can induce defoliation, accelerate senescence and stimulate flower and fruit abscission (Kulaeva and Prokoptseva, 2004). In addition to these five traditional groups, two other new classes of molecules brassinosteroids and jasmonates, have been counted as plant hormones as well. The former group is polyhydroxylated steroid hormones mediating multiple physiological and developmental processes, including stem elongation, leaf expansion, xylem differentiation, seed germination, etc (Wang and He, 2004). Jasmonates, which include jasmonic acid and its

cyclopentane derivatives, regulate root growth, fruit ripening, leaf abscission and senescence; they also mediate responses to stress, wounding, pathogen infection and UV damage (Shan et al., 2007).

During the early 1990s, the discovery of systemin by Pearce *et al*. (1991) introduced us a new class of plant hormones, peptides, which changed the old idea that only small lipophilic compounds could serve as signaling molecules in plants. This 18-amino acid peptide was first discovered during the search for the systemic wound signal which induces the expression of defensive genes in response to wounding by predator attacks. It activates the synthesis of protease inhibitors in young tomato plants at low nanomolar concentrations through their cut stems (Pearce et al., 1991). The mature systemin is produced by proteolysis from a 200-amino acid precursor, called prosystemin (Pearce et al., 1991; McGurl et al., 1992). Unlike animal peptide hormones, prosystemin lacks a signal sequence or any post-translational modifications, indicating that it is not processed through the secretory pathway (McGurl et al., 1992). With the subsequent identification of homologs of the tomato prosystemin gene in other solanaceous species (Constabel et al., 1998) and the discovery of two hydroxyproline rich tobacco systemins (Pearce et al., 2001a), the systemin family has greatly expanded.

Since the discovery of systemins, a number of additional peptides have been discovered that play a wide range of roles in the regulation of plant growth and development. Among these are: phytosulfokine (PSK), which regulates callus formation and proliferation (Matsubayashi and Sakagami, 1996); SCR/SP11, which is involved in self-incompatibility (Takayama and Isogai, 2005); CLV3, which plays an important role in regulating the growth of the shoot apical meristem (Brand et al., 2000; Trotochaud et

al., 2000); ENOD, which plays a central role in nodule development and symbiotic interaction (van de Sande et al., 1996); DVL and ROT 4, which are critical to leaf morphogenesis (Narita et al., 2004; Wen et al., 2004); and IDA, which determines floral organ abscission (Butenko et al., 2003; Stenvik et al., 2006).

Table 1 summarized 17 plant peptide hormones, containing identification and isolation, structures, functions, receptor and signaling pathway of these peptides. Both PSK and CLV3 have been reported to promote SE, whereas RALF (Pearce et al., 2001b) can inhibit root growth and development in tomato. All this information leads to the original proposal that plant peptide hormones absent from the SE culture might cause the maturation block in LP.

Table 1. Summary of plant peptide hormones.

Name		Plant Species	Tissue	Role/Function	Peptide Isolation	Peptide Isolation Protocol	Bioassay	No. of a.a.	Sequence	Molecular Weight (Da)	Precursor (a.a.)	Receptor	Cofactor	Post-translational modification	Family
Systemins	tomato proline -rich systemin (original)	Tomato, potato, pepper, and nightshade	leaves	Defense signaling: triggers the production of jasmonic acid, which induces the production of defensive proteins	Y	DEAE cellulose reversed-phase C18 flash chromatography Sephadex G-25 strong cation exchange chromatography C18 reversed phase chromatography a. pH6 b. pH2.5 strong cation exchange chromatography C18 HPLC	Protease Inhibitor-inducing Assay	18	[1]AVQSKPPSKRDPPKMQTD[18]	2010	200 no secretory pathway	SR 160 Mr: 160kD (tomato plasma membrane)	No	No	Systemin
	tobacco hydroxyproline -rich systemin (TobHypSys I and II)	Tobacco	leaves	Defense signaling	Y	C18 reversed phase chromatography Sephadex G-25 semi-preparative reversed-phase C18 chromatography cation exchange chromatography narrow-bore reversed-phase chromatography	Alkalinization Assay	18	[1]RGANLPOOSOASSOOSKE[18] and [1]NRKPLSOOSOKPADGQRP[18]	Tob Sys1:3060 Tob Sys2: 2784	165 involved in the secretory pathway	N/D	No	glycosylation, hydroxylation of prolines	
	tomato hydroxyproline -rich glycopeptides TomHypSys I, II and III	Tomato	leaves	Defense signaling	Y	reversed-phase C18 flash chromatography Sephadex G-25 semipreparative C18 reversed phase chromatography strong cation exchange chromatography analytical C18 reversed phase chromatography narrow-bore C18 HPLC	Alkalinization Assay	18, 20, 15	[1]RTOYKTOOOOTSSSOTHQ[18] [1]GRHDYVASOOOOKPQDEQRQ[20] [1]GRHDSVLPOOSOKTD[15]	2076 2530 1651	146	N/D	No	glycosylation, hydroxylation of prolines	
***At* Pep1**		Arabidopsis	leaves	Defense signaling against pathogens	Y	reversed-phase semipreparative C18 flash chromatography Sepharose G-25 C18 reversed phase chromatography ion exchange chromatography narrow-bore HPLC	Alkalinization Assay	23	[1]ATKVKAKQRGKEKVSSGRPGQHN[23]	2491.7	*At* proPep1 92 aa	PEPR1 1124 aa, 170 kD	No	No	N/D
Phytosulfokine (PSK)		asparagus, rice, zinnia, carrot, Arabidopsis	mesophyll	promote cell division and development	Y	DEAE Sephadex A-25 column Bio-Gel P-2 extra fine column Develosil ODS-HG-5 column	mitogenic activity	PSK-α: 5 PSK-β: 4	PSK-α: H-Tyr(SO3H)-Ile-Tyr(SO3H)-Thr-Gln-OH PSK-β: H-Tyr(SO3H)-Ile-Tyr(SO3H)-Thr-OH	PSK-α: 846	OsPSK 89 aa 9.8 KD post-translational processing	PSKR Mr: 120kD (membrane fractions of carrot cells)	No	sulfation of tyrosines	N/D
Leginsulin		legume species	radicles of germinated seeds	stimulate cell proliferation and differentiation	Y	an affinity column a C18 reverse-phase column on HPLC	N/A	37	[1]ADCNGACSPFEVPPCRSR DCRCVPIGLFVGFCIHPTG[37]	3925.6 pI 6.74	13045.9 Da 119 aa	43 kD globulin, glycosylated pI 9.05 to 9.26	N/D	No	N/D
IDA		*Arabidopsis*	floral abscission zone	deficient in floral abscission	N	N/A	mutation screening	77	[1]MAPCRTMMVLLCFVLFLAASSSCVA AARIGATMEMKKNIKRLTFKNSHIFG YLPKGVPIPPSAPSKRHNSFVNSLPH[77]	N/D pI 11.87	N/D	HAESA	N/D	N/D	IDL
BRICK		maize, conserved in plants and animals	leaf epidermis	promotes multiple, actin-dependent cell polarization events	N	N/A	mutation screening	84	[1]MGRGGGMGNP VNVGIAVQAD WENRHFISN ISLNVRRLFD FLLRFEATTK SKLASLNEKLD ILERKLEVLE VQVGSATTNPSVFN[84]	8kD	N/D	Scar/WAVE-related plant ARP2/3 activator proteins	N/D	N/D	N/D
Plant Natriuretic Peptides (PNP)		*Hedera helix* potato *Arabidopsis thaliana*	leaves	promote stomatal guard cell opening maintein water and salt homeostasis	Y	Sephadex G25-80 Sepharose 4B immunoaffinity (ANP antisera)	stomatal opening bioassay	126	[1]MAVKFVVVMIVFAQILAPIAEAAQGKAVYY DPPYTRSACYGTQRETLVVGVKNNLWQNGR ACGRRYRVRCIGATYNFDRACTGRTVDVKV VDFCREPCNGDLNLSRDAFRVIANTDAGNI RVVYTP[126]	14016 pI 9.22	N/D	N/D	N/D	N/D	N/D
ENOD40		18 species, legume, non-legumes, monocots and dicots, including tobacco, maize, alfalfa, tomato and rice	cells surrounding vascular bundles, low levels in stem and root cells rapidly growing tissues: meristems, fruits and ovules	induce root nodule organogenesis	N	N/A	N/A	Soybean: 12 aa 24 aa Alfalfa: 13 aa 27 aa	Peptide A: MELCWLTTIHGS Peptide B: MVLEEAWRERGVRGEGAHSSHSLT	N/D	N/D	soybean nodulin 100	cytokinin	No	N/D

Continued

RALF	16 species, 9 families	a variety of tissues including roots, shoots, leaves, flowers, ovules and ovaries	inhibit root growth and development in tomato and *rabidopsis* specific roles in growth unknown	Y	reversed-phase C18 flash chromatography semipreparative reversedphase C18-HPLC polySULFOETHYL Aspartamide column strong cation exchange-HPLC narrow-bore reversed-phase C18-HPLC column	Alkalinization Assay	49	[1]ATKKYISYGALQKNSV PCSRRGASYYNCKPGA QANPYSRGCSAITRCRS[49]	5,346.80	115	25kD and 120kD two protein components	No	No	N/D	
DEVIL1 (DVL1)	*Arabidopsis*	non- specific	development of multiple plant organs	N	N/A	mutation screening	51	[1]MEMKRVMMSSAERSKEKKRSISRRLG KYMKEQKGRIYIIRRCMVMLLCSHD[51]	6209D pI 10.52 (predicted)	N/D	N/D	N/D	N/D	RTFL/DVL	
ROTUNDIFOLIA4 (ROT4)	*Arabidopsis*	shoot apex and young leaves	restrict polarity-dependent cell proliferation during wt leaf morphogenesis	N	N/A	mutation screening	53	[1]MAPEENGTCEPCKTFGQKCSHVVKKQRA KFYILRRCIAMLVCWHDQNHDRKDS[53]	6.2kD (predicted)	N/D	N/D	N/D	N/D		
CLAVATA3 (CLV3)	*Arabidopsis*	shoot apical meristems (SAM)	balance cell proliferation and differentiation	N	gel chromatography, HR 10/30 column with superose 6 resin CLV3 in each fraction assayed by dot blots G-50 Sephadex column	mutation screening	12	[1]RTVP[h]SGP[h]DPLHH[12]	1344.6	96	CLV1/CLV2 complex	No	hydroxylation of prolines	CLE	
POLARIS (PLS)	*Arabidopsis*	embryonic and seedling root, with low expression in aerial parts.	correct auxin-cytokinin homeostasis to modulate root growth & leaf vascular pattering	N	N/A	N/A	36	[1]MKPRLCFNFRRRSISPCY ISISYLLVAKLFKLFKIH[36]	4.6kD	N/D	N/D	ethylene/ cytokinn & auxin	N/D	N/D	
SCR/SP11	*Brassica*	expressed post-meiotically in both the microspores and the tapetum	male determinant of Self incompatibility	N	N/A	Pollination	50	SP11-S8: NLMKRCTRGFRKLGKCTTLEEEKCK TLYPRGQCTCSDSKMNTHSCDCKSC	<8 kD	74-81	SRK female determinant of SI	SLG, enhance the strength of the SI reaction	No	SCRL	
HT	*Nicotiana alata*	stigma and style	S-allele-specific pollen rejection in the style	N	N/A	N/A	77	[1]RDMVDPSISLLEPNNDKKTNGMNDATL QKIGGKVGMFFDFMCAACKCQKGNND NNDNDNDNDNDNNNNNDIVCQTVCC[77]	8.6 kD calculated pI 3.76 (predicted)	101	N/D	N/D	N/D	N/D	
Egg Apparatus 1	maize	egg apparatus (egg cell and two synergids)	short-range pollen tube attraction by the female gametophyte	N	N/A	N/A	94	[1]MSSCPAIVNMKDDDGIGAMGAAVAFA AMGVFGIYFLWPVVGPTSAGMMMKAPG AAGWVICRAVFEANPQLYPTILRTAGA AAAAATFAACSIAS[94]	N/D	N/D	N/D	N/D	N/D	EAL	
TLA1	maize	egg cells and microspores	development and maturation of leaf and reproductive tissues	N	N/A	N/A	27	[1]MLWGVLFQFMWAVVSLVVTALVACWAK[27]	N/D	N/D	N/D	N/D	N/D	N/D	

myo-Inositol-1,2,3,4,5,6-hexa*kis*phosphate

History background

myo-Inositol-1,2,3,4,5,6-hexa*kis*phosphate ($InsP_6$), also called phytic acid, is *myo*-inositol (Ins) with six phosphate groups attached to its six carbons. Ins is a member of the B vitamins, playing a central role in growth and development, and several pathways in plant cells including IAA metabolism, cell-wall polysaccharide and cyclic alcohol synthesis, and the phosphatidylinositol (PtdIns)/Ins phosphate pathways (Loewus and Murthy, 2000). $InsP_6$ was first brought to attention in 1872 by Pfeffer who reported that subcellular particles in wheat endosperm contain a calcium/magnesium salt of organic phosphate. In 1908, Neuberg proposed a structure that contained three cyclic pyrophosphate moieties, whereas in 1914, Anderson proposed a structure in which the six hydroxyl groups on *myo*-inositol are esterified with orthophosphate moieties (Cosgrove, 1980a; Lasztity and Lasztity, 1990; Harland and Morris, 1995). In 1969, NMR spectroscopy eventually resolved the dilemma in favor of the latter (L.F. Johnson, 1969). $InsP_6$ is known to be ubiquitous in eukaryotic cells and is the most abundant inositol phosphate derivative in late 1980s and 1990s (Sasakawa et al., 1995).

myo-Inositol-1,2,3,4,5,6-hexa*kis*phosphate in plant seed

$InsP_6$ is the major form of phosphorus in seeds and it also accumulates in other plant tissues and organs, including pollen, roots, tubers and turions (Cosgrove, 1980b; Raboy, 1997). It can represent from 1 to several percent of a typical seed's dry weight, about 75 ± 10% of a seed's total P, and normally more than 90% of a mature seed's total, acid-extractable Ins phosphates (Raboy, 1997).

Plants take up phosphorus from soils to develop seeds and seeds use most of the phosphorus in $InsP_6$. A recent global estimate (Lott et al., 2000) of net $InsP_6$ production by seed crops represented more than 50% of all phosphorus fertilizer consumed annually, suggesting that seed $InsP_6$ represents a major pool in phosphorus flux through the global agricultural ecology. As a result, $InsP_6$ and its degradation products comprise the most abundant organic phosphorus form in soils.

$InsP_6$ usually exists as mixed phytate salts of the mineral cations K^+, Mg^{2+}, Ca^{2+}, Mn^{2+} and Zn^{2+} in mature seeds. During seed development, it serves as a counter-ion for the mineral storage and retrieval processes in a mineral-, tissue- and stage-specific fashion. A recent paper (Otegui et al., 2002) reported that developing *Arabidopsis thaliana* seeds store K^+, Mg^{2+} and Ca^{2+} as phytates in protein storage vacuoles globoids in the embryo, Zn^{2+} as phytates in the chalazal vacuolar compartment, and Mn^{2+} as phytates in the chalazal endoplasmic reticulum. The transient storage of Mn^{2+} and Zn^{2+} as phytates and subsequent redistribution during seed development reflects different physiological or metabolic demands for Mn^{2+} and Zn^{2+}.

$InsP_6$ accumulates in a linear fashion throughout seed development and degrades to lower-phosphate inositol phosphates during germination. Early studies hypothesized these results are due to the maintenance of homeostasis of both Pi and cellular P (Strother, 1980; Raboy and Dickinson, 1987). Nonetheless, recent studies of transgenic plants with *low phytic acid* (*lpa*) mutations revealed that $InsP_6$ metabolism during seed development is not essential to P homeostasis, in that numerous pathways depends on Ins or Pi supply and/or homeostasis and many plant *lpa* genotypes exhibited viability as well as relatively normal appearance of seed. This result also suggested that $InsP_6$ accumulation in seeds

may attribute mainly to efficient storage and retrieval of P and minerals essential for survival and successful germination in natural environment (Raboy et al., 2000; Dorsch et al., 2003).

Metabolism in eukaryotic cells

Since the discovery of Ins(1,4,5)P_3 as a second messenger in signal transduction, the metabolism of this compound and its derivatives has been widely studied. Among these derivatives, the relatively massive and more polar InsP_6 present in many cells has been brought to researchers' attention. Later on, similar chromatographic methods led to the discovery of its more highly phosphorylated pyrophosphate-containing (PP-Ins phosphate) derivatives such as the 5-PP-Ins(1,2,3,4,6)P_5 and 5,6-bis-PP-Ins(1,2,3,4)P_4 (Figure 4). The same process also led to the discovery of a non- InsP_6 inositol phosphate, containing the same 6 moles of phosphate per mole of Ins, such as 5-PP-Ins(1,3,4,6)P_4 (Raboy, 2003).

Understanding the metabolism of InsP_6 and its derivatives facilitates elucidation of molecular mechanisms of their biological functions. Figure 5 shows the modified structural metabolic pathways comprised of five parts and centered on InsP_6 (Raboy, 2003). The early or substrate supply pathway is focused on Ins synthesis and supply in which D-glucose 6-phosphate is converted to Ins, Ins(3)P_1 and phosphatidylinositol (PtdIns). The inositol phosphate early intermediate pathway located in the top left proceeds via soluble inositol phosphates to Ins(3,4,6)P_3, and then to Ins(1,4,5)P_3. In the top right is the phosphatidylinositol phosphate early intermediate pathway, where Ins(1,4,5)P_3 is produced via PtdIns phosphate intermediates. The hub pathway in the

center converts Ins *tris*phosphates to Ins(1,3,4,5,6)P_5 or other Ins pentaphosphates followed by their conversion to InsP_6. The late inositol polyphosphate pathways are at the bottom, where InsP_6 or other Ins polyphosphates are utilized to produce PP-Ins phosphates.

Ins(3)P_1 is produced from D-glucose 6-phosphate by *myo*-inositol (3) P_1 synthase (MIPS). In plants, Ins is involved in various metabolic pathways including phospholipid or InsP_6 synthesis, biogenesis of cell wall polysaccharides and stress-related responses (Loewus and Murthy, 2000). MIPS has been shown to mobilize in a tissue-specific manner in response to salinity stress (Nelson et al., 1998). It is induced by ABA which leads to subsequent accumulation of InsP_6 by Ins synthesis (Flores and Smart, 2000). Additionally, MIPS is induced at sites proximal to InsP_6 accumulation in rice seeds (Yoshida et al., 1999).

The first strong evidence for sequential phosphorylation of Ins(3)P_1 was from investigation in *Dictyostelium* (Stephens and Irvine, 1990) in which Ins(3)P_1 was converted to Ins(3,6)P_2, Ins(3,4,6)P_3, Ins(1,3,4,6)P_4 Ins(1,3,4,5,6)P_5 and InsP_6. A similar pathway to InsP_6 was found in duckweed, *Spirodela polyrrhiza* (Brearley and Hanke, 1996), consisting of a complete sequence – Ins(3)P_1, Ins(3,4)P_2, Ins(3,4,6)P_3, Ins(3,4,5,6)P_4, Ins(1,3,4,5,6)P_5.

Ins P_6 synthesis via PtdIns phosphate early intermediates is well established. The action of phospholipase C on the lipid PtdIns(4,5)P_2 yields Ins(1,4,5)P_3 and diacylglycerol. In yeast (York et al., 1999), *Drosophila melanogaster* (Seeds et al., 2004) and *Arabidopsis thaliana* (Stevenson-Paulik et al., 2002), Ins(1,4,5,6)P_4 is produced from Ins(1,4,5)P_3 via IPK2 (Ins P_3 3-/5-/6-Kinase), and then Ins(1,3,4,5,6)P_5 from this InsP_4

isomer also via IPK2, and finally IPK1 produces $InsP_6$. Nonetheless, in human cells (Verbsky et al., 2005), the synthesis of $InsP_6$ works through the isomerization of $Ins(1,4,5)P_3$ to $Ins(1,3,4)P_3$, and the sequential phosphorylation of $Ins(1,3,4)P_3$ to $Ins(1,3,4,6)P_4$ by the 5/6 kinase, of $Ins(1,3,4,6)P_4$ to $Ins(1,3,4,5,6)P_5$ by a 5-kinase, and of $InsP_5$ to $InsP_6$ by a 2-kinase.

More importantly, $InsP_6$ was reported to inhibit tumor promotion by targeting phosphatidylinositol-3 kinase (PtdIns 3-Kinase) (Huang et al., 1997), although there is no pathway established linking PtdIns 3-Kinase to $InsP_6$ synthesis. In mammals and yeast, PtdIns 3-kinases are involved in mitogenesis, apoptosis, trafficking of membrane proteins, glucose uptake, and activation of intracellular signaling molecules such as *rac*, *ras*, *rab*, MAP kinase, protein kinase B/Akt, protein kinase C and JNK/p38 kinase (Munnik et al., 1998; Leevers et al., 1999; Meijer and Munnik, 2003). Additionally, the structure of $InsP_6$ is similar to D-3-deoxy-3-fluoro-ptdIns, a potent PtdIns 3-kinase inhibitor (Powis et al., 1995). It is likely that $InsP_6$ can inhibit PtdIns 3-kinase in plants to regulate plants growth and development.

Enzymes hydrolyzing Ins P_6/phytic acid are termed phytases, a special class of phosphatases catalyzing the sequential hydrolysis of phytic acid (Cosgrove, 1980a). Two classes of acid phytases, 6-phytase (EC 3.1.3.26) and 3-phytase (EC 3.1.3.8), hydrolyze $InsP_6$ to $Ins(2)P_1$ (Cosgrove, 1980a). An usual alkaline phytase present in lily pollen and seeds starts dephosphorylation on the 5 position of $InsP_6$ (Barrietos et al., 1994). Multiple phytases with different specificity and biochemical properties are involved in the hydrolysis of $InsP_6$. The hydrolysis of $InsP_6$ to lower-phosphate inositol phosphates via phytases might be involved in seed germination and dormancy in plants.

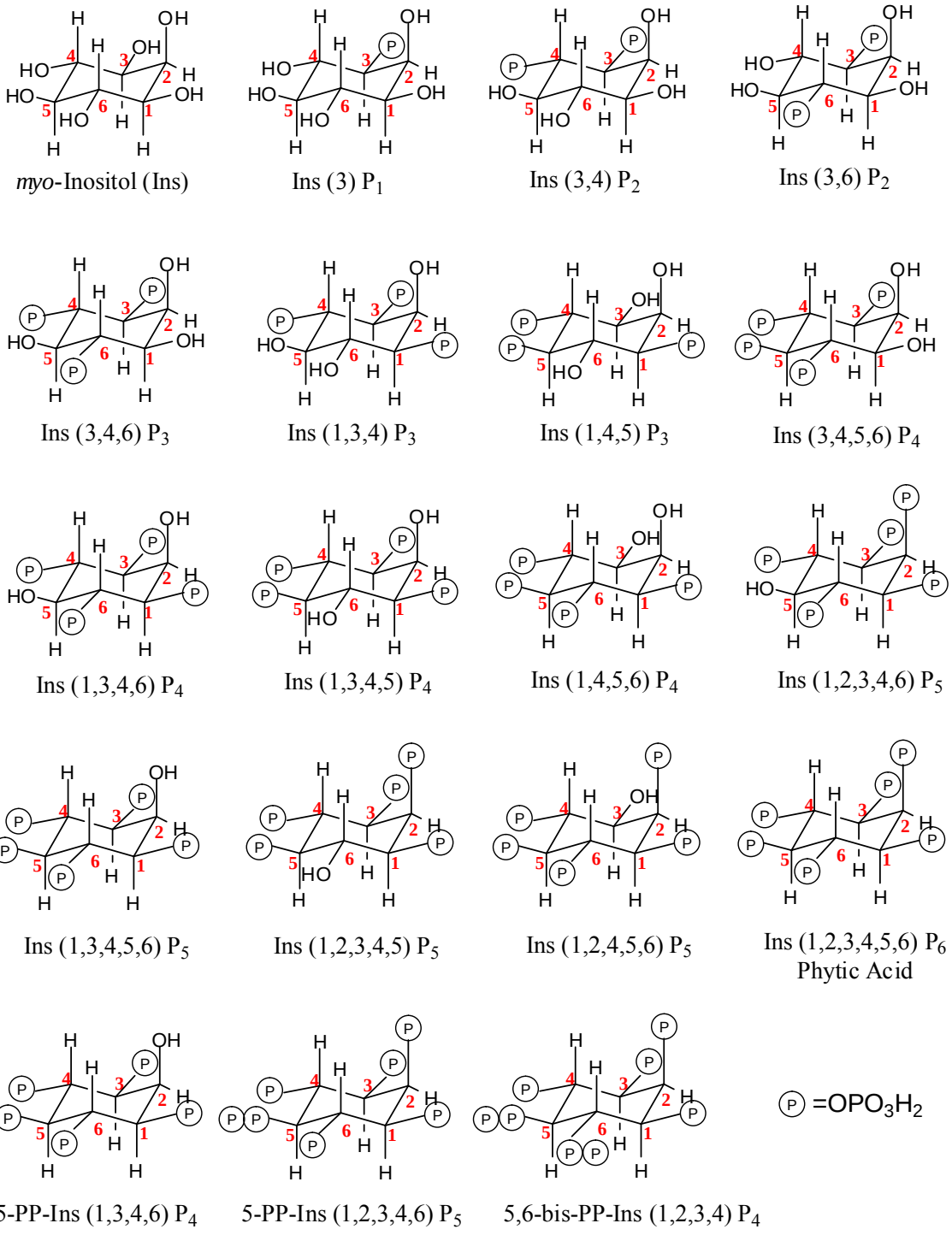

Figure 4. Structures of *myo*-inositol (Ins) and various inositol phosphates including Ins (1,2,3,4,5,6) P_6 or phytic acid modified from (Raboy, 2003)

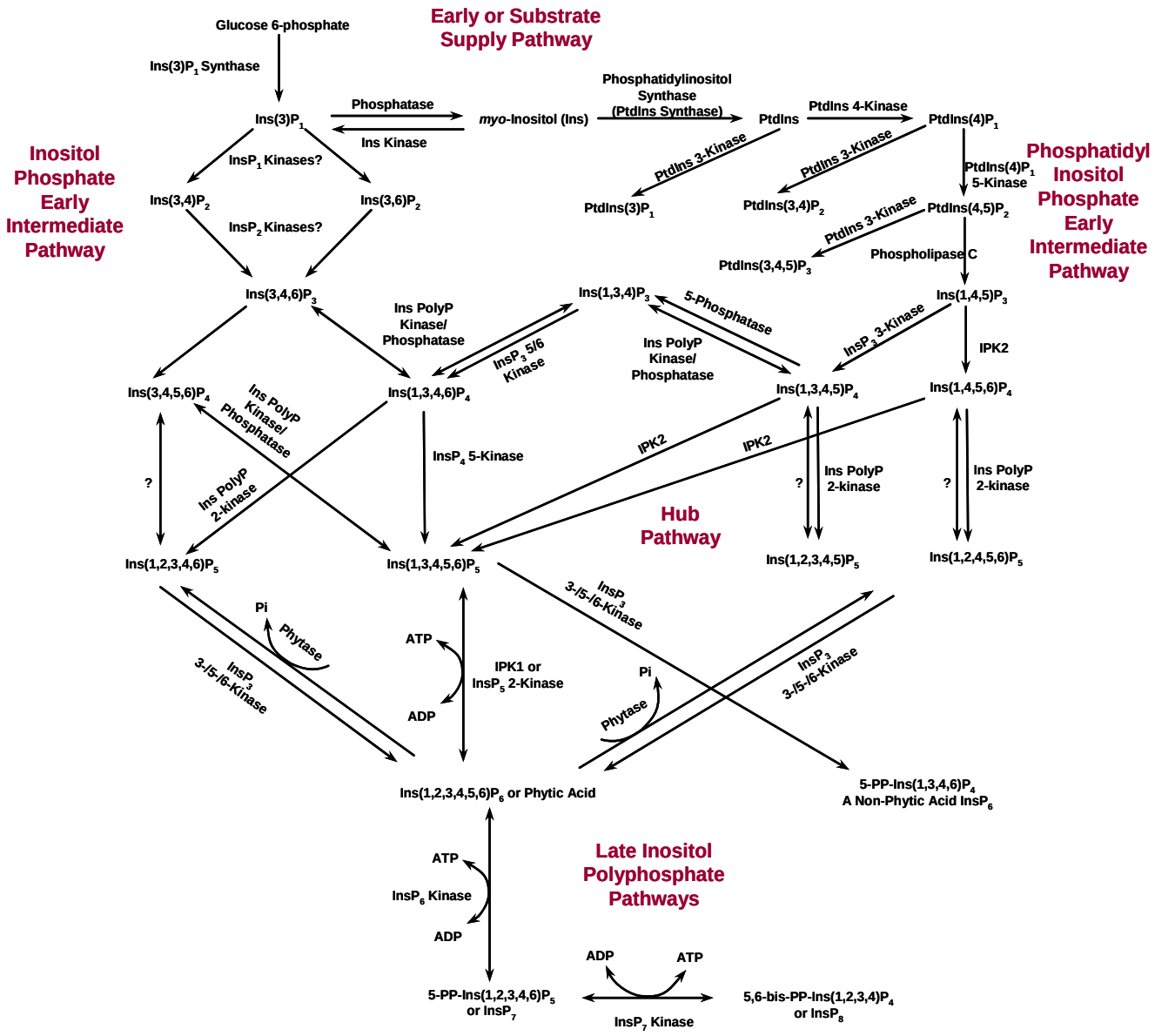

Figure 5. Structural metabolic pathways from glucose 6-P to Ins(3)P_1, and from Ins(3)P_1 to $InsP_6$, and beyond, in eukaryotic cells, modified from (Raboy, 2003). The early or substrate supply pathway is focused on Ins synthesis and supply in which D-glucose 6-phosphate is converted to Ins, Ins(3)P_1 and phosphatidylinositol (PtdIns). The inositol phosphate early intermediate pathway located in the top left proceeds via soluble inositol phosphates to Ins(3,4,6)P_3, and then to Ins(1,4,5)P_3. In the top right is the phosphatidylinositol phosphate early intermediate pathway, where Ins(1,4,5)P_3 is produced via PtdIns phosphate intermediates. The hub pathway in the center converts Ins *tris*phosphates to Ins(1,3,4,5,6)P_5 or other Ins pentaphosphates followed by their conversion to $InsP_6$. The late inositol polyphosphate pathways are at the bottom, where $InsP_6$ or other Ins polyphosphates are utilized to produce PP-Ins phosphates.

Cellular functions and signaling transduction

In addition to storage and retrieval of phosphorus, mineral and Ins in plant seeds, $InsP_6$ has a wide-ranging array of important physiological activities (Shears, 2001). Larsson et al. reported that $InsP_6$ inhibited serine-threonine protein phosphatases and activated L-type Ca^{2+} channels (Larsson et al., 1997). The plant drought-stress hormone, abscisic acid (ABA), elevates $InsP_6$ levels in *Solanum tuberosum* stomatal guard cells. $InsP_6$ in turn inactivates the plasma membrane K^+-inward conductance which is a well characterized target of ABA response, in a cytosolic calcium-dependent manner (Lemtiri-Chlieh et al., 2000). $InsP_6$ also functions as an endomembrane-acting calcium release signal (Lemtiri-Chlieh et al., 2003). These findings suggest that $InsP_6$ is a downstream component of the ABA signaling pathway.

$InsP_6$ stimulates insulin exocytosis by the activation of protein kinase C (Efanov et al., 1997). The 1, 2, 3 (axial-equatorial-axial) phosphate grouping in $InsP_6$ provides a specific interaction with iron during iron transport through the cytosol or cellular organelles, so that $InsP_6$ inhibits the catalysis of hydroxyl radical formation by iron and acts as a cellular antioxidant (Graf et al., 1987; Hawkins et al., 1993). Additionally, $InsP_6$ was purified from HeLa cell-free extracts. It is bound by DNA-protein kinase and stimulates DNA-protein kinase-dependent end-joining *in vitro* (Hanakahi et al., 2000). $InsP_6$ also has specific inhibitory effects on the agonist-induced loss of responsiveness of the rat substance P receptor (Sasakawa et al., 1994). Other functions of $InsP_6$ include regulation of mRNA export (York et al., 1999), priming of stimulus-dependent respiratory burst in neutrophils (Eggleton et al., 1991), preventing kidney stone formation

(Grases et al., 1998), mediation of neurotransmission (Vallejo et al., 1987), inhibition of cancer cells (Vucenik and Shamsuddin, 1994), etc.

Nevertheless, $InsP_6$ was historically considered as an antinutrient in that it can decrease the bioavailability of essential dietary minerals in human beings due to its ability to bind them. In the late 1980s, $InsP_6$ was shown to possess striking anticancer action. $InsP_6$ inhibited the growth of all tested cell lines in a dose- and time-dependent manner (Shamsuddin and Vucenik, 2005). Reduction of the elevated rate of cell proliferation to the normal level has been observed both in intact animals (Wattenberg and Chalcones, 1995; Challa et al., 1997; Gupta et al., 2003) and in cultures of human malignant cells (Shamsuddin et al., 1992; Sakamoto et al., 1993; Shamsuddin and Yang, 1995; Ferry et al., 2002; Singh et al., 2003). Moreover, cells from different origins have different sensitivities to $InsP_6$, indicating that the mechanism of $InsP_6$ anticancer action varies in cell types. Can inhibition of somatic embryo growth by $InsP_6$ in plants share the same mechanism as some cancer cells in animals? A proposed mechanism regarding inhibition to early-stage somatic embryos is described in the discussion section.

CHAPTER II

EXPERIMENTAL PROCEDURES

Materials and Equipment

Materials

LP cones were collected weekly throughout the sequence of embryo development from multiple open-pollinated mother trees over the last ten years. Seeds from Union Camp tree UC5-1036, located in a seed orchard near Bellville, GA, were collected in years 1996 to 1998. Seeds from tree S4PT6, located in a Boise Cascade breeding orchard near Lake Charles, Louisiana, were collected in year 1997, 1998 and from Texas in years 2002, 2003 and 2005. Cones were shipped to IPST in a cooler with blue ice, received within 24-48 hours after the collection period and stored at 4 ^{o}C.

Tris base, deuterium oxide (min. 99.96 atom% D), tributylphosphine (TBP), iodoacetamide, trypsin, bromophenol Blue, Dowex resin 50WX8-200, and phytic acid dodecasodium salt hydrate from rice were obtained from Sigma-Aldrich (St Louis, MO). 50% (w/w) phytic acid water solution was obtained from Chromadex (Irvine, CA). HPLC grade acetonitrile and methanol, sodium chloride, sodium phosphate monobasic and dibasic, ammonium acetate, trifluoroacetic acid (TFA), formic acid, ammonium sulfate, triethylammonium acetate (TEAA), sodium dodecyl sulfate (SDS), glycerol, and β-mercaptoethanol were purchased from Fisher Scientific (Pittsburgh, PA).

Abscisic acid, ammonium nitrate, 6-benzylaminopurine (BAP), biotin, boric acid, calcium nitrate tetrahydrate, cobalt chloride hexahydrate, copper sulfate pentahydrate, folic acid, Gelrite, glutamine, glycine, iron sulfate heptahydrate, kinetin, magnesium chloride hexahydrate, magnesium nitrate hexahydrate, magnesium sulfate heptahydrate, manganese sulfate heptahydrate, N-morpholinoethanesulfonic acid (MES), myo-inositol, nicotinic acid, potassium iodide, potassium hydroxide, thiamine hydrochloride and zinc sulfate heptahydrate were obtained from Sigma Aldrich (St Louis, MO). Casamino acids were purchased from Beckton Dickinson (Franklin Lanes, NJ). 2,4-Dichlorophenoxyacetic acid was purchased from Chem Service (West Chester, PA). Potassium dihydrogenphosphate, potassium hydrogenphosphate, potassium nitrate, sodium ethylenediaminetetraacetic acid and sucrose were obtained from JT Baker (Phillipsberg, NJ). Acrodisc Syringe filter (0.2 μm HT Tuffryn Membrane Low Protein Binding Non-Pyrogenic) was purchased from Pall Life Sciences (East Hills, NY).

Equipment

All FPLC purification was performed at 4 ^{o}C by column chromatography on an ÄKTA™ Explorer (GE Healthcare, formerly Amersham Bioscicences, Piscataway, NJ) with a fraction collector 950 installed. The separation unit was controlled by the UNICORN software (GE Healthcare, Piscataway, NJ). All centrifugation was performed in a table top Eppendorf microcentrifuge 5415C (Brinkmann Instruments, Inc., Westbury, NY). Ultrafiltration was accomplished using stirred cells (Amicon, Beverly, MA) with Millipore YM1 or YM3 membranes (Millipore, Bedford, MA).

All reversed-phase HPLC purification and characterization were performed at room temperature either on a Waters™ LC Module I plus HPLC system (Waters, Milford, MA) or on a Beckman Coulter HPLC system (Beckman Coulter, Fullerton, CA). The former was controlled by Millennium Chromatography Manager Software. The latter consisted of a System Gold 126 Solvent Module, a System Gold 508 Autosampler and was controlled by 32 Karat software. All capillary electrophoresis were carried out on a Proteolab PA 800 (Beckman Coulter, Fullerton, CA), also under the control of 32 Karat software. All SDS-PAGE and Native-PAGE were performed on a Pharmacia PhastSystem (GE Healthcare, formerly Amersham Bioscicences, Piscataway, NJ)

All lyophilization was carried out on a Labconco Centrivap system (Labconco, Kansas City, MO), which consisted of a cold trap, a concentrator and a Welch DirecTorr 8915 vacuum pump (Welch Vacuum, Skokie, IL). All osmolalities were measured on a Wescor 5500 vapor pressure osmometer (Wescor, Logan, Utah)

The LC/MS and LC/MS/MS characterization were accomplished on an Applied Biosystems/MDS SCIEX 4000 QTRAP™ (Linear Ion Trap Quadrupole) LC/MS/MS system (Applied Biosystems, Foster City, CA), which was interfaced with two Shimadzu LC-10AD*VP* HPLC pumps (Shimadzu, Columbia, MD) and a PE200 autosampler (Perkin Elmer, Waltham, MA). The capillary flow was obtained by an LC Packings Acurate precolumn flow splitter (Dionex, Sunnyvale, CA). The exact mass measurement was carried out on an Applied Biosystems/MDS SCIEX QSTAR® XL Hybrid (hybrid quadrupole time-of-flight mass spectrometer) LC/MS system (Applied Biosystems, Foster City, CA), which was interfaced with an UltiMate nano and capillary LC system by LC Packings (Dionex, Sunnyvale, CA) and a TriVersa™ NanoMate (Advion, Ithaca,

NY). The MALDI characterization was performed on an Applied Biosystems 4700 Proteomics Analyzer with TOF/TOF^{TM} Optics (Applied Biosystems, Foster City, CA).

All NMR spectra were recorded on a Bruker DRX 500 spectrometer (Bruker Biospin, Billerica, MA).

Female Gametophyte Collection and Water Extraction

Collection

Cones were pried open and seeds were isolated. Seeds were then cracked open with a hemostat. The FG tissue was split with fine-tipped forceps, and integuments and nucellar tissue were removed from the ovule. The dominant zygotic embryo was removed from the FG and individual embryos were observed through a dissecting microscope, evaluated for stage of development (Pullman and Webb, 1994), sorted by stage and tissue type, and placed in vials partially immersed in liquid nitrogen. Stage 9 embryos were categorized by the week they were collected: 9.1 (stage 9, week 1), 9.2 (stage 9, week 2), etc. Twenty same-staged embryos or FGs were collected per vial, frozen and stored in a -70^{o}C freezer. Collections for each tree and tissue type ranged from stage 1 (collected 1 to 2 weeks after estimated fertilization) to stage 9.12 (shortly before cone harvest).

Water extraction

The stored FG tissue (from 40 FGs) was powdered by crushing with a mortar and pestle under liquid nitrogen, and extracted with 10 ml of deionized water and stirred at 4 ^{o}C for an hour. The resulting mixture was aliquoted into mirocentrifuge tubes; the

supernatant was combined and collected after centrifugation (Baxter Scientific, Biofuge 13 at 13000 rpm) for 10 min; the pellet was washed with deionized water, vortexed for 1 min, and centrifuged as above. The wash was combined with the previous supernatant; the resulting solution was filtered with a 0.2 μm syringe filter (Pall life sciences), and lyophilized overnight to dryness.

Identification

Preparation of maintenance and multiplication media (1133 and 1250)

Media components and concentrations (1133 and 1250) are listed in Table 2. Both the media were prepared by mixing all the reagents with the exception of abscisic acid (ABA) and glutamine, adjusting the pH to 5.7 with 1N KOH and autoclaving the resulting mixture in the absence (1133) or the presence (1250) of Gelrite using the liquid cycle (highest temperature of 121 ^{o}C). ABA and glutamine were filter-sterilized through a 0.2 μm syringe filter (Pall, East Hills, NY) and added to the autoclaved media mixture. Two ml of the subsequent media mixture was poured into each well of a 24-well Costar #3526 cluster plate (Corning, Corning, NY).

Embryogenic Cell Culture Maintenance

Embryogenic cultures were maintained as described in (Pullman et al., 2003c). Cultures were stored in 250-ml Erlenmeyer flasks incubated in the dark at 20 to 22 ^{o}C. Every seven days, the contents of the culture flask were poured into sterile centrifuge tubes and settled for 20 min. The old liquid media was decanted, settled cell volumes were measured to monitor the cell growth, and cells were resuspended in media 1133 at a

density of 1 ml settled cells/9 ml medium (5 ml of settled cells/45 ml of media 1133). The cultures were rotated at 90-100 rpm and maintained with weekly transfers at the same ratio of cells to medium.

Early-stage Somatic Embryogenic Multiplication Bioassay

Single stage 2 or 3 somatic embryos were isolated by forceps from suspension culture and placed on 2 ml of multiplication medium 1250 contained in 24-well Costar #3526 cluster plates. Genotypes of early-stage somatic embryos used in bioassays were 500, 112, 387, 51 and 279. Each treatment was composed of 40 single early-stage somatic embryos in four replicates of 10 embryos each. The female gametophyte (FG) extract lyophilized fractions were each dissolved in 2 ml of deionized water, adjusted to pH 5.7 with 0.1 M NaOH or 0.1 M HCl. Each fraction was filter sterilized by a 0.2 μm syringe filter (Pall, East Hills, NY) and topically applied on early-stage somatic embryos at 50 μl/well, which corresponded to a concentration of approximately ½ FG per embryo. The embryos grew in the dark at 23-25 ^{o}C; after four to seven weeks, the diameter of the embryogenic tissue was measured with a dissecting microscope using a calibrated eyepiece reticle.

Statistic Analysis

All the data were evaluated by multifactor analysis of variance. The significant differences between means of each treatment were determined by the Multiple Range Test at 95% level of significance. Both analyses were performed using Statgraphics Plus Version 4.0 (Manugistics, Rockville, MD).

Table 2. Media ingredients of media 1133 and 1250 (Pullman et al., 2006).

Components	Media and components (mg/l)	
	1133	**1250**
NH_4NO_3	603.8	603.8
KNO_3	909.9	909.9
KH_2PO_4	136.1	136.1
$Ca(NO_3)_2 \bullet 4H_2O$	236.2	236.2
$MgSO_4 \bullet 7H_2O$	246.5	246.5
$Mg(NO_3)_2 \bullet 6H_2O$	256.5	256.5
$MgCl_2 \bullet 6H_2O$	101.7	101.7
KI	4.15	4.15
H_3BO_3	15.5	15.5
$MnSO_4 \bullet H_2O$	10.5	10.5
$ZnSO_4 \bullet 7H_2O$	14.4	14.4
$Na_2MoO_4 \bullet 2H_2O$	0.125	0.125
$CuSO_4 \bullet 5H_2O$	0.125	0.125
$CoCl_2 \bullet 6H_2O$	0.125	0.125
$FeSO_4 \bullet 7H_2O$	6.95	9.95
Na_2EDTA	9.33	9.33
Sucrose	30,000	30,000
Myo-inositol	1,000	1,000
Casamino acids	500	500
L-Glutamineb	450	450
Thiamine _HCl	1	1
Pyridoxine HCl	0.5	0.5
Nicotinic acid	0.5	0.5
Glycine	2	2
MES	–	250
Biotin	–	0.05
Folic acid	–	0.5
2,4-D	1.1	1.1
BAP	0.45	0.45
Kinetin	0.43	0.43
Abscisic acid	1.3	1.3
Gelrite	–	2500
pH	5.7	5.7

Liquid Chromatography Isolation

Gel filtration chromatography I

A Superdex 75 10/300 GL gel filtration column (10×300 mm, GE Healthcare, Piscataway, NJ) was used as the first isolation column. Lyophilized powder corresponding to the water extract of 30 FGs was dissolved in 250 µl of 150 mM NaCl. After centrifugation at 14000 rpm for 10 minutes, the supernatant was separated by the Superdex 75 column at a flow rate of 0.5 ml/min using 150 mM NaCl as an eluent. The column was pre-equilibrated with the same eluent for 118 min at 0.5 ml/min. The elution was monitored at wavelengths of both 254nm and 280 nm at 4 ^{o}C. The isocratic elution lasted for 118 min. Fractions were grouped and numbered according to the elution of each peak. Each collected fraction was ultrafiltered against a Millipore YM 1 membrane (1000 Da cutoff), which was contained in an Amicon ultrafiltration cell (Amicon 8200). Deionized water was added three times and the duration of ultrafiltration was approximately six hours. The retentate was collected, divided into aliquots and lyophilized overnight to dryness. Each fraction was assayed as described above.

Reversed Phase Chromatography

The reversed phase columns attempted for the second-step liquid chromatography were a Phenomenex Jupiter C5 column (5 µm, 300 Å, 4.6×250 mm, Phenomenex, Torrance, CA), an Alltech ProSphere C18 column (5 µm, 300 Å, 4.6×150 mm, Alltech, Deerfield, IL) and a Vydac 218TP C18 column (3 µm, 300 Å, 1.0×250 mm, Vydac, Deerfield, IL).

The Phenomenex Jupiter C5 column attached to a wide-pore C5 guard cartridge (3.0×4 mm, Phenomenex, Torrance, CA) was connected to a Beckman Coulter HPLC system. Water containing 0.1% TFA was used as mobile phase A; mobile phase B consisted of acetonitrile in 0.085% TFA. The flow rate was 1 ml/min and a wavelength of 215 nm was used for the detector. The linear gradient started at 15% B for 3 min, increased to 35% B over 30 min, and returned to 15% B in 3 min.

Hydrophobic Interaction Chromatography (HIC)

The hydrophobic interaction columns attempted for the second-step liquid chromatography were a HiPrep Butyl FF column (16 × 100 mm, GE Healthcare, Piscataway, NJ), a HiPrep Phenyl FF column (high sub, 16×100 mm, GE Healthcare, Piscataway, NJ) and a HiPrep Octyl FF column (16 × 100 mm, GE Healthcare, Piscataway, NJ). For the HiPrep Butyl FF column, various concentrations of sodium phosphate and sodium acetate were used as the buffer depending on the desired pH in the range from 2.5 to 7.0. Various amounts of ammonium sulfate were added to eluent A in order to adjust the retention of compounds on the HiPrep Butyl FF column, and various gradients were carried out to adjust the resolution of separation. For the other two HIC columns, similar attempts were made for the same purpose. The final conditions of the HiPrep Butyl FF column used for collecting fractions that were bioassayed were: eluent A consisted of 50 mM sodium phosphate buffer containing 1.5 M ammonium sulfate and eluent B consisted of 50 mM sodium phosphate buffer, both at pH 2.5. The flow rate was maintained at 5 ml/min, and the elution profile was monitored at 215 nm. A 48-min elution with linear gradient segments was applied: 0% B for 10 min, 0% to 50% B over

20 min, 50% to 100% B for 8 min, and 100% B for 10 min. All fractions were pooled, collected, ultrafiltered against a Millipore YM3 membrane (3000 Da cutoff), lyophilized to dryness, and assayed.

Ion Exchange Chromatography

Strong cation exchange chromatography

A Mono S strong cation exchange column (5 × 50 mm, GE Healthcare, Piscataway, NJ) was used as the second isolation column. Bioactive fraction F2 corresponding to 40 FGs was re-dissolved in 300 µl of eluent A, 20 mM sodium phosphate buffer at pH 2.5, and further separated by the Mono S column at 1.5 ml/min and 4 ^{o}C. The elution was monitored at a wavelength of 215 nm in a 56-min gradient. Eluent B was eluent A containing 2 M NaCl. The gradient started at 0% B for 9 min, 0% to 50% B over 27 min, 50% to 100% B for 2 min, and 100% B for 18 min. All fractions from the Mono S column were pooled and grouped, ultrafiltered against a Millipore YM1 (1000 Da cutoff) membrane, and lyophilized to dryness.

Strong anion exchange chromatography

The third-step LC was achieved on a Mini Q strong anion exchange column (4.6 ×50 mm, GE Healthcare, Piscataway, NJ). After each fraction was assayed for early-stage embryo multiplication, amount corresponding to 40 FGs of the bioactive fraction F2-S1 eluting from 0.5 to 2.5 min was re-dissolved in 300 µl of eluent A, 20 mM Tris-Cl buffer at pH 8.0, and loaded on the Mini Q column which was pre-equilibrated with 10 ml of the eluent A at 0.5 ml/min. Eluent B was eluent A containing 2 M NaCl. The flow

rate of elution was 0.5 ml/min, and the elution profile was monitored at 215 nm. An 89-min gradient was applied: 0% B for 23 min, 0% to 30% B over 58 min, 30% to 100% B for 4 min, and 100% B for 4 min. Fractions were pooled, ultrafilted against a Millipore YM3 (3000 Da cutoff) membrane, and lyophilized. Each fraction was submitted to embryo multiplication assay. An optimized desalting procedure was carried out by treating the bioactive fraction F2-S1-Q6 eluting from 52 to 69 min from Mini Q pooled and lyophilized directly after elution, without ultrafiltration.

Weak anion exchange chromatography

A HiPrep DEAE (16×100 mm, GE Healthcare, Piscataway, NJ) column was used in an attempt to fractionate F2 for the second liquid chromatography separation after the Superdex 75 column. Both 20 mM bis-Tris and Tris were used as the buffer at various pH values ranging from 6.5 to 7.7 to adjust the resolution of separation and the retention of compounds on the column, and various gradients were applied for the same purpose.

Gel filtration chromatography II

The last-step purification was accomplished on a Superdex Peptide 10/300 GL gel filtration column (10×300 mm, GE Healthcare, Piscataway, NJ). The lyophilized bioactive fraction F2-S1-Q6 (corresponding to 10 FGs) was re-dissolved in 150 μl of 100 mM ammonium acetate buffer at pH 5.5, the eluent of the Superdex Peptide column. F2-S1-Q6 was desalted and further fractionated at a flow rate of 0.2 ml/min for 158 min. The detecting wavelengths were set at 215 nm and 280 nm. The column was equilibrated

with the same buffer at 0.5 ml/min for 138 min before sample loading. Fractions were pooled, collected and lyophilized to dryness. Aliquots of each fraction was applied onto bioassay and analyzed by LC/MS.

Mass Spectrometry Characterization

LC/MS

LC/MS under positive polarity

The mass spectrometer was an Applied Biosystems 4000 QTRAP (Linear Ion Trap Quadrupole) LC/MS/MS system. The ESI interface was operated in positive mode at 5500 V. A Vydac C8 capillary column (5μ, 300 Å, 0.3×250 mm, Deerfield, IL) was coupled to a Shimadzu LC-10AD*VP*. Full scan mass spectra were recorded from *m/z* 500 to 2000 amu at 1000 amu/s by the linear ion trap as an enhanced mass spectrometric (EMS) scan, with declustering potential at 90 V. The total flow rate was 0.6 ml/min, which was split to 5 μl/min to the column. Mobile phase A consisted of 2% acetonitrile, 98% water and mobile phase B was 80% acetonitrile, 20% water both containing 0.1% formic acid as the ion pair reagent. The elution protocol was comprised of a 1 min column pre-equilibration with 100% A, followed by 10.0 μl sample injection, a 5 min sample load and wash with 100% A. The gradient was 105 min in total: 0% B for 12 min, 0 to 40% B over 63 min, 40 to 100% B for 5 min, 100% B for 8 min, back to 0% B for 5 min, re-equilibration for 12 min.

LC/MS under negative polartiy

LC/MS under negative ion polarity was achieved on the same Applied Biosystems 4000 QTRAP LC/MS/MS system by two different LC approaches. The first approach used a C5 Jupitor reversed phase column (4.6 × 250 mm, Phenomenex, Torrance, CA) with mobile Phase A consisting of 95% water, 5% acetonitrile and mobile phase B comprised of 70% acetonitrile, 30% water both containing 10 mM ammonium acetate at pH 5.5. An 80-min gradient was applied at a flow rate of 1 ml/min: 0% B for 5 min, 0 to 50% B over 40 min, 50 to 100% B for 15 min, 100% B for 5 min, back to 0% B for 5 min, re-equilibration for 10 min. The second approach used a Vydac C8 capillary column (0.3×250 mm, Deerfield, IL). Mobile phase A was comprised of 2% acetonitrile, 98% water and mobile phase B was 80% acetonitrile, 20% water both containing 10 mM triethylammonium acetate buffer at pH 7.0. The flow rate was maintained at 5 µl/min. The gradient was 105 min in total: 0% B for 12 min, 0 to 55% B over 63 min, 55 to 100% B for 5 min, 100% B for 8 min, back to 0% B for 5 min, re-equilibration for 12 min.

For both methods, the ESI interface was operated under negative ion polarity. The turbo ion spray needle was held at negative 4500 V. Full scan mass spectra were recorded from *m/z* 500 to 2500 amu at a scan rate of 400 amu/s under quadrupole mode, with declustering potential at -200 V.

Exact Mass Analysis

Exact mass analysis under positive polarity

The exact mass analysis under positive polarity of the active fraction from the Mini Q column desalted against YM3 membrane (F2-S1-Q6) was carried out on an Applied Biosystems QSTAR XL system (Applied Biosystems, Foster City, CA). The

turbo ion spray needle was held at 5500 V. TOF-MS spectrum was recorded over a mass range of *m/z* 300-2000. 20 FG of F2-S1-Q6 was dissolved in 100 µl of a water/acetonitrile (50:50, v/v) mixture and infused to QSTAR XL through an injection loop. The declustering potential was set at 40 V and the focusing potential at 100 V.

Exact mass analysis under negative polarity

Exact mass analysis under negative polarity was obtained from the final active fraction from the Superdex Peptide column (F2-S1-Q6-D1B). The stock solution of F2-S1-Q6-D1B was prepared by dissolving 25 FG of F2-S1-Q6-D1B in 50 µl of a water/methanol (50:50, v/v) mixture containing 0.1% formic acid. The resulting stock solution (5 µl) was diluted in 1 ml of methanol. Because it was too concentrated for the detector limit, a further dilution was performed by mixing 100 µl of the last dilute solution with another 1 ml of methanol. The phytic acid standard used was a 50% water solution (w/w, Chromadex, Irvine, CA), 0.2 µl of which was dissolved in 200 µl of a water/methanol (50:50, v/v) mixture containing 0.1% formic acid, and 5 µl of the resulting mixture was then diluted with 1 ml of methanol.

The exact mass measurement under negative ion polarity was conducted on the QSTAR XL system, with F2-S1-Q6-D1B and phytic acid standard directly infused with an automated chip-based nanoelectrospray TriVersa^{TM} NanoMate system (Advion, Ithaca, NY). The NanoMate was controlled by the ChipSoft software (version 7.1.1) and comprised of a liquid handling robot equipped with a 96-well plate and a rack of 96 disposable conductive pipette tips, as well as a microchip containing a 10×10 array of nanoelectrospray nozzles (ESI chip, Advion, Ithaca, NY). The system can automatically

infuse 96 samples. The ESI chip used was chip D (4.1 μm i.d.) containing 100 nozzles. For each analysis, a new tip and a nozzle were used. A low delivery pressure of 0.15 psi of nitrogen gas and a negative voltage of 1.6 kV were applied to generate a nanoelectrospray plume from a given nozzle when infusing the sample of interest. TOF-MS spectra were recorded over the mass range of *m/z* 300-2000. The declustering potential was held at -150 V and the focusing potential at -200 V. Data acquisition and QSTAR instrument control were performed by Analyst QS software (version 1.1).

MS/MS

LC/MS/MS under positive polarity

LC/MS/MS spectra of the precursor ion at *m/z* 661 under positive polarity were acquired subsequent to the LC/MS on the QTRAP. Enhanced product ion (EPI) scans were performed subsequent to the enhanced mass spectrometric (EMS) scan at a scanning rate of 1000 amu/s over the mass range *m/z* 50-700 with collision energies at both 40 eV and 80 eV. Data acquisition, and instrument control were performed by Analyst software (version 1.4.2).

MS/MS under negative polarity

Tandem mass spectra of the precursor ion at *m/z* 659 under negative polarity were acquired subsequent to the exact mass measurement on the QSTAR XL interfaced with the NanoMate system. The spectra were recorded from *m/z* 50-700 with collision energies at both 40 eV and 80 eV.

NMR Characterization

Standard preparation

Phytic acid dodecasodium salt hydrate (Sigma, St Louis, MO) from rice was converted to $InsP_6$ through cation exchange resin Dowex 50WX8-200 (Sigma, St Louis, MO). The resin (4g) was mixed with 12 ml of 1M NaOH in a beaker, poured onto a filter paper and washed with deionized water until the pH of the eluate decreased to 5-6 (tested by pH paper). The resulting resin was transferred to another beaker containing 12 ml of 1M HCl, mixed thoroughly, poured onto a filter paper and washed until eluate is at neutral pH. A column was packed with the resulting resin in a 10-ml syringe barrel which had a small amount of glass wool at the bottom. Phytic acid dodecasodium salt (300.2 mg) was dissolved in approximately 20 ml of water. The resulting solution was loaded onto the column and rinsed with deionized water. The eluate, which contained the $InsP_6$, was collected, divided into 10 aliquots and lyophilized to dryness. The lyophilized product was dissolved in 500 µl of deuterium oxide (min. 99.96 atom% D) and the pH adjusted to 8.22 by adding aliquots of concentrated NaOD. Additional ^{1}H and ^{31}P spectra were recorded at different pH values over the range 8.0 – 8.5.

1-Dimensional NMR

NMR spectra of the final purified active fraction (F2-S1-Q6-D1B) were recorded in D_2O at 500.13 MHz for ^{1}H with 32 scans, 202.46 MHz for ^{31}P with 64 scans and 125.77 MHz for ^{13}C with 16386 scans using a multinuclei probe maintained at 280 K on a Bruker DRX 500 spectrometer. F2-S1-Q6-D1B was dissolved in 500 µl of D_2O (min. 99.96 atom% D) and lyophlized to dryness, repeated for three times. The final

lyophilized product was dissolved in 200 μl of D_2O (min. 99.96 atom% D) and transferred to a symmetrical 5 mm NMR tube (Shigemi, Allison Park, PA) matched with D_2O containing a pair of insert (4.1×190 mm) and outer tube (4.52 mm ID, 4.965 mm OD×180 mm). The 5mm-OD NMR tube (Wilmad, Buena, NJ) designed for 500 MHz NMR instrument was used for all standard recording which share the same conditions as those of F2-S1-Q6-D1B, except fewer scans. ^{1}H, ^{31}P, and ^{13}C chemical shifts were reported in ppm and assignments for both F2-S1-Q6-D1B and the standard are labeled above their respective peaks in the proton spectra with reference to the 4.67 ppm water peak. Coupling constants were determined using the MestRe-C software package and spectra were analyzed by MestReNova software.

F2-S1-Q6-D1B: ^{1}H NMR analysis δ 4.59 (d, 1, H_2), 4.09 (q, 2, $H_{4/6}$), 3.82 (m, 1, H_5), 3.76 (t, 2, $H_{1/3}$). ^{31}P NMR analysis δ 2.54 (s, 1, P_5), 2.29 (s, 2, $P_{1/3}$), 2.06 (s, 1, P_2), 1.63 (s, 2, $P_{4/6}$). ^{13}C NMR analysis δ 77.40 (s, 1, C_5), 75.89 (s, 2, $C_{4/6}$), 74.51 (s, 1, C_2), 73.39 (s, 2, $C_{1/3}$).

Commercial $InsP_6$: ^{1}H NMR analysis δ 4.56 (d, 1, H_2), 4.08 (q, 2, $H_{4/6}$), 3.79 (m, 1, H_5), 3.74 (t, 2, $H_{1/3}$). ^{31}P NMR analysis δ 2.72 (s, 1, P_5), 2.54 (s, 2, $P_{1/3}$), 2.30 (s, 1, P_2), 1.75 (s, 2, $P_{4/6}$). ^{13}C NMR analysis δ 77.47 (s, 1, C_5), 75.77 (s, 2, $C_{4/6}$), 74.72 (s, 1, C_2), 73.38 (s, 2, $C_{1/3}$).

^{1}H-^{1}H COSY

The correlation spectroscopy (COSY) experiment was carried out using the standard Bruker program cosygpqf during the 1.5-s relaxation delay on the HOD signal, 1024 data points in the F2 dimension, and 128 increments in F1. The data matrix was

processed to give a matrix of 1024 ×1024 points, and a sine bell apodization function was applied before Fourier transformation.

^{1}H-^{31}P HSQC

The two-dimensional heteronuclear single quantum correlation (^{1}H - ^{31}P HSQC) experiment was carried out using the standard Bruker program hsqcetgpsi2 modified for ^{31}P gradient strength. The parameters were 1.5-s recycle delay, 1024 data points in F2, 128 increments in F1, GARP (globally optimized alternating phase rectangular pulse) ^{31}P decoupling during acquisition, and shifted sine-squared apodization before Fourier transformation.

^{1}H-^{13}C HSQC

The two-dimensional heteronuclear single quantum correlation (^{1}H – ^{13}C HSQC) experiment was carried out using the standard Bruker program hsqcetgpsi2. The parameters were 1.5-s recycle delay, 1024 data points in F2, 128 increments in F1, GARP ^{13}C decoupling during acquisition, and shifted sine-squared apodization before Fourier transformation.

Gel Electrophoresis -- SDS-PAGE

All SDS-PAGE and Native-PAGE were performed on a Pharmacia PhastSystem. PhastGel high density (GE Healthcare, Piscataway, NJ), a homogeneous polyacrylamide gel designed for the separation of peptides and low molecular weight proteins, was used for SDS-PAGE. The gel was run with PhastGel SDS buffer strips made of 3% Agarose

IEF, containing 0.20 M Tris, 0.55% SDS at pH 8.1. The sample buffer stock solution was prepared by mixing 1.2 ml of 0.5M Tris-HCl at pH 6.8, 1.0 ml of glycerol, 4.8 ml of deionized water, 2.0 ml of 10% (w/v) SDS stock solution and 0.5 ml of 0.1% (w/v) Bromophenol Blue stock solution. 285 µl of the buffer stock solution was mixed with 15 µl of β-mercaptoethanol at a ratio of 19:1 to make the final fresh buffer on the day of the experiment. The low-MW ladder standard (Biorad, Hercules, CA) was diluted at 1:20 in the final buffer. Samples of interest were diluted in various ratios with the final buffer to make the consequent volume 20 µl each. All sample solutions and the ladder solution were heated in a water bath at 100^{o}C for 5 min, followed by cooling to room temperature. Samples and the ladder were loaded by an 8-well sample applicator and separated at 500 V, 5.0 mA, 3.0 W, 15 ^{o}C for 190 Vh. Samples were fixed by 2.5% glutaraldehyde in deionized water for 4 min, stained by 0.1% PhastGel Blue R solution in 30% methanol and 10% acetic acid in deionized water for 60 min, destained by 30% methanol and 10% acetic acid in deionized water for four rinses with 44 min in total and preserved by 10% glycerol and 10% acetic acid in deionized water for 5 min. All these staining and destaining procedures were performed at 50 ^{o}C.

Capillary eletrophoresis -- SDS-gel MW analysis

The SDS-gel MW analyses were performed on a Proteolab PA 800 (Beckman Coulter, Fullerton, CA) under the control of 32 Karat software. The capillary (50 µm ID, 57 cm length, bare-fused silica, Beckman Coulter, Fullerton, CA) was first activated by 0.1 M NaOH basic wash for 5 minutes at 50 psi, followed by 0.1 M HCl acidic wash for 2 minutes at 50 psi, water rinse for 2 minutes at 50 psi, then filled with SDS-MW gel buffer for 10 minutes at 40 psi (Beckman Coulter, CA) and equilibrated with the SDS gel

at 15 kV for 10 minutes. For analyses of samples with reduced disulfide bonds, samples of interest were diluted with 38 µl of SDS sample buffer (100 mM Tris-HCl pH 9.0/ 1% SDS) and 5 µl of β–mercaptoethanol. The mixture was heated in a water bath at 100 ^{o}C for 3 minutes. After cooling down in a room-temperature water bath for 5 minutes, the sample was injected for 20 seconds at 5 kV and separated for 30 minutes at 15 kV (reverse polarity), with 20 psi on both inlet and outlet. Samples with non-reduced disulfide bonds were diluted with 38 µl of SDS sample buffer (100 mM Tris-HCl pH 9.0/ 1% SDS) and 5 µl of 250 mM iodoacetamide solution. The mixture was heated in a water bath at 70 ^{o}C for 3 minutes. The capillary electrophoresis method used was for samples with reduced disulfide bonds.

CHAPTER III

RESULTS

Female Gametophyte Collection and Embryogenic Multiplication Bioassay

Female gametophyte collection

The female gametophyte (FG), also called megagametophyte or the embryo sac, is the ovule of one or more zygotic embryos in Gymnosperm seeds. It contains a haploid number of chromosomes and provides nourishment to embryo development. This pattern is different from angiosperm embryos, which have attached cotyledons as seed storage organs. Figure 6 shows the anatomy of a loblolly pine seed.

In LP SE, FG tissue is absent in the embryogenic tissue culture. In culture, important compounds produced by FG such as vitamins are absent and need to be added as medium supplements.

Effect of LP stage-specific FG water extracts on Bioassay

Figure 7A exhibits the performance of early-stage somatic embryogenic multiplication bioassay. Typically, a single early-stage embryo is on average 1.0 mm in diameter and will grow to form an embryogenic mass 5 to 9 mm in diameter in four to six weeks depending on the genotype of somatic embryo. The typical duration for each genotype to continue multiplying in liquid culture is about one to two years. However, some genotypes such as 500 survive longer. The majority of bioassays in this dissertation were using genotype 500 as the early-stage somatic embryo.

Preliminary experiments were conducted to investigate the effect of LP stage-specific FG tissue water extracts on early-stage somatic embryo growth. Female gametophyte tissue collected in 1997 from tree UC5-1036 from stages 1, 2, 3, 4, 6, 8, 9.1, 9.3, 9.5, 9.7 and 9.9 was water extracted and applied onto multiplication bioassay. Statistic analysis of bioassay results revealed that FG water extracts from stages 1, 2, 3, and 8 contain compound(s) that stimulate growth of early-stage somatic embryo (genotype 500) in a statistically significant manner at $p = 0.05$ compared to the control treatment without extract, whereas FG water extracts from stages 9.7 and 9.9 FG contain substance(s) inhibitory to early-stage somatic embryo growth, illustrated in Figure 7B. Further bioassay experiments were carried out using FG water extracts from stage 2 and 9.12 of tree S4PT6 collected in 1997. The results were identical to those from tree UC5-1036, with stage 2 FG extract stimulatory and stage 9.12 FG extract inhibitory to the embryo growth in a statistically significant manner.

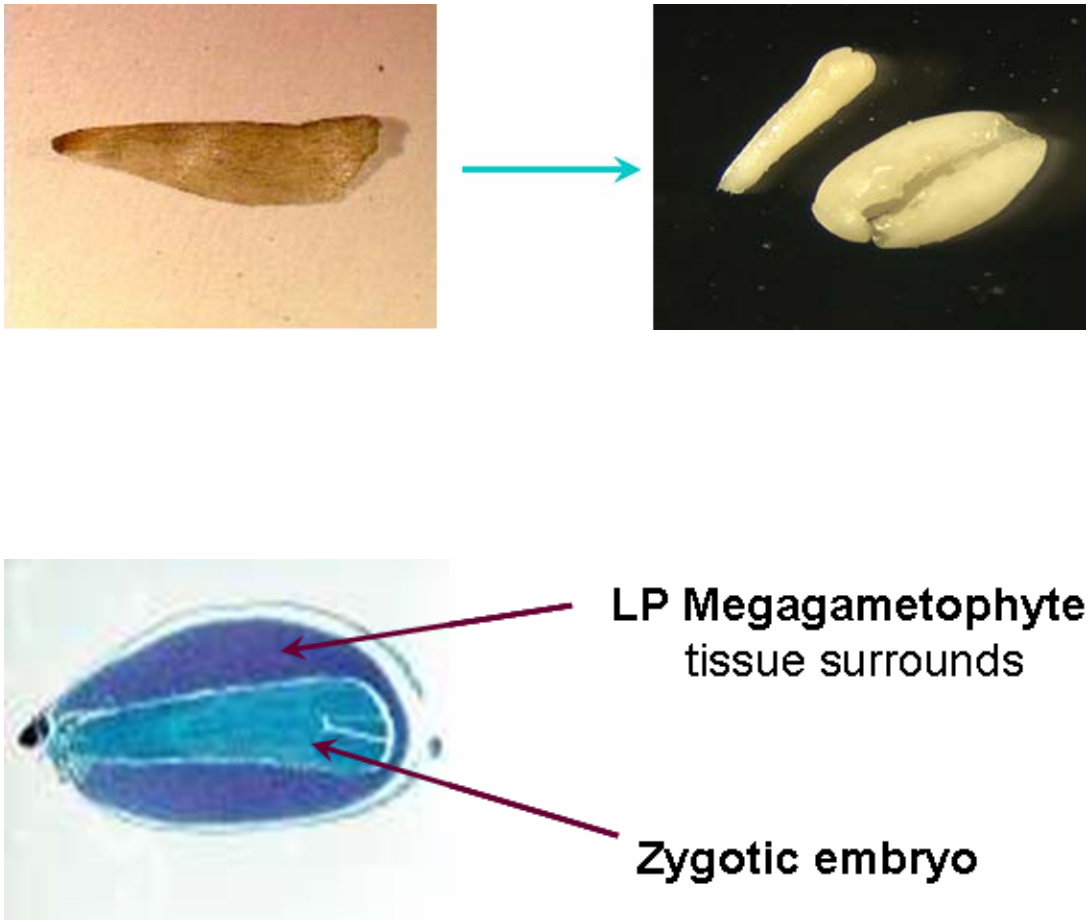

Figure 6. Anatomy of loblolly pine seed.

A

B

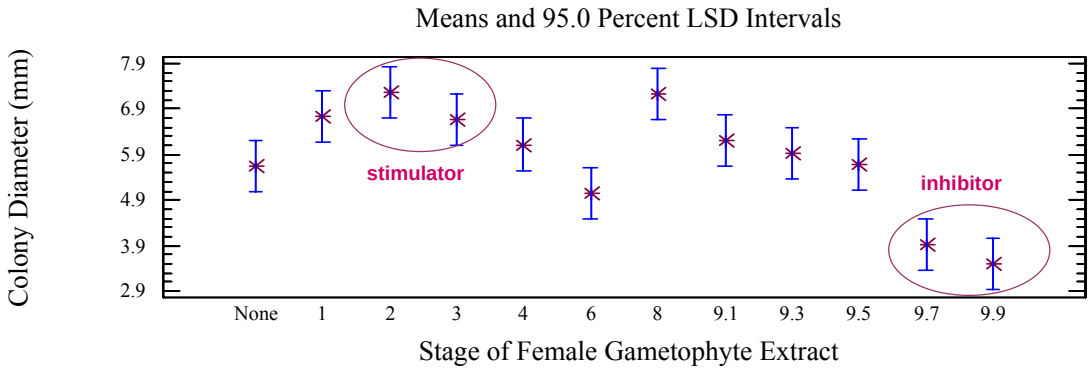

Figure 7. (A) Early-Stage Somatic Embryogenic Multiplication Bioassay. (B) Water Extracts from Staged Female Gametophyte Tissue.

Liquid Chromatography Isolation and Identification

Gel filtration chromatography I

All Superdex (GE Healthcare, Piscataway, NJ) gel filtration columns are formed by the dextran chains covalently bonded to a highly cross-linked agarose gel matrix. The first chromatography isolation step was achieved on a Superdex 75 gel filtration column which is designed for biomolecule separations from 3000 Da up to 600 kD (globular proteins).

Eluent selection

Plain water was originally used as the eluent. However, water elution gave rise to inconsistencies in the bioassay and MS results, causing difficulties in tracking the inhibitory molecule.

The eluent was then switched to 150 mM NaCl solution. After the FG water extract was lyophilized to dryness, it was re-dissolved in 150 mM NaCl and centrifuged; the resulting supernatant was loaded on a Superdex 75 10/300 GL gel filtration column. Fractions were grouped and numbered according to the elution of each peak. Each fraction was lyophilized and applied to the SE multiplication bioassay directly. The bioassay results showed that all fractions eluted from the Superdex 75 column inhibited somatic embryo growth in a statistically significant manner at $p = 0.05$. A later bioassay with salt control corresponding to the minimum and maximum amount of salt contained in each fraction was carried out, which revealed that even the lowest amount of salt could inhibit the embryo growth in a statistically significant manner. These results suggest that

salt depletion is essential for the preciseness of the bioassay to identify the bioactive compound.

Selection of desalting method

Estimation of MW range of the active fraction F2 was based on calibration curve using four globular proteins, albumin, ovalbumin, chymotrypsinogen A and ribonuclease A. Since F2 falls into the range of 9kD to 16kD, it is very likely that the active molecule is a small protein. But the possibility of a small molecule which is associated with proteins with MW in that range could not be excluded. Dialysis using membrane tubing (Spectra CE, Spectrum Laboratories, Rancho Dominguez, CA) with 100 Da cutoff was first used as the salt depletion method. However, due to large fraction volume and large amount of salt collected from the Superdex 75 column, this method was not efficient to remove salt. Alternative desalting was achieved by ultrafiltration with either an Amicon stirred cell containing an YM1 (1000 Da cutoff) membrane or a Centricon centrifugal device (3000 Da cutoff).

Osmolality measurement was performed to correlate between the optimal ultrafiltration duration, number of times of water change and concentration of remaining salt in BSA solution. According to Table 3, after three times of water change and six hours, the osmolality of the retentate was close to that of water, implying that these conditions were the optimal for desalting after the Superdex 75 column.

Elution and bioassay

Consequently, fractions obtained were salt depleted by ultrafiltration (1000 Da cutoff). Since the elution of gel filtration is isocratic, the time length of ultrafiltration is based on previous osmotic pressure measurement. The retention time for each fraction is as follows: F1 from 15.08 to 27.00 min, F2 from 27.00 to 34.04 min, F3 from 34.04 to 55.06 min, F4 from 59.07 to 77.08 min, as illustrated in Figure 8A. The retentate of each fraction was lyophilized overnight to dryness. Dry fractions obtained were re-dissolved with deionized water, pH adjusted at 5.7 and applied to bioassay. The subsequent bioassay data is shown in Figure 8B. F2 eluting from 27.00 min to 34.04 min was the only fraction which statistically significantly inhibited the embryo growth compared to the blank control. The rest treatments exhibited similar embryo growth to that of the control.

Table 3. Osmolality of pure water, filtrate and retentate after Centricon and Amicon membranes

ID	Osmolality (mM)	Osmolality (mM)	Osmolality (mM)	Ave (mM)
12.9mg BSA in 150 mM NaCl	292	307	295	298
pure water	39	41	41	**40.333**
Centricon filtrate after 1st change	372	371	370	371
Centricon filtrate after 2nd change	102	110	116	109.33
Centricon filtrate after 3rd change	51	52	53	52
Centricon BSA retentate	47	45	44	**45.333**
Amicon filtrate after 1st change	57	65	59	60.333
Amicon filtrate after 2nd change	46	47	47	46.667
Amicon filtrate after 3rd change	42	43	46	43.667
Amicon BSA retentate	46	42	45	**44.333**

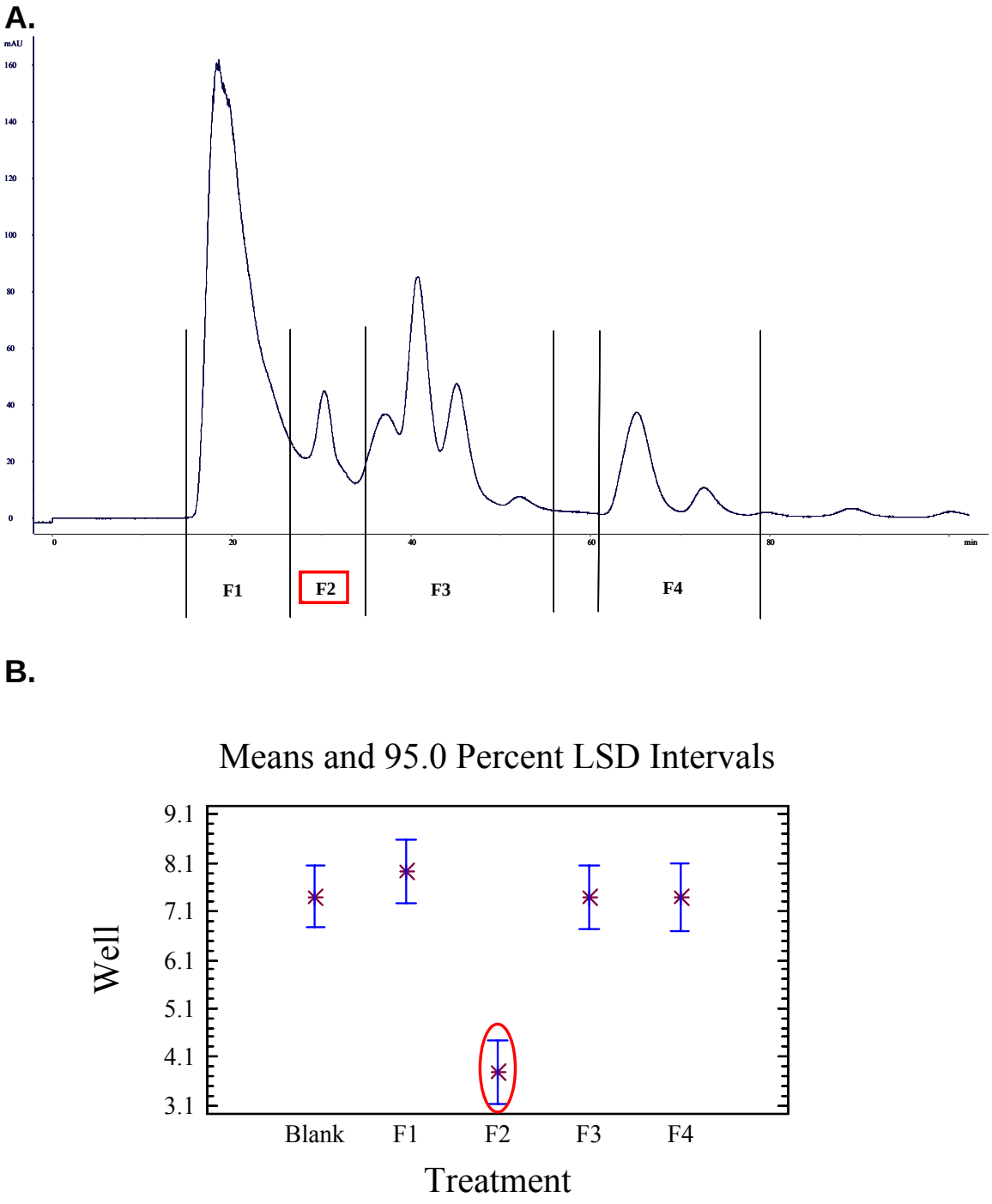

Figure 8. (A) Superdex 75 FPLC elution profile for the inhibitor 1st fractionation eluted with 150 mM NaCl, 280 nm. (B) Bioassay of the fractions eluted from a Superdex 75 column.

Calibration and Molecular Weight Estimations

Four globular proteins, Ribonuclease A, Chymotrysinogen A, Ovalbumin and Albumin, packed in a low molecular weight gel filtration calibration kit, were used to calibrate the Superdex 75 column. The molecular weight of the inhibitory fraction F2 obtained from calibration curve of gel filtration column was to correlate with that acquired from mass spectrometry. Figure 9 is the calibration elution profile of these four protein standards and Figure 10 shows the molecular weight calibration curve defining the relationship between the elution volumes of these standards and the logarithm of their respective molecular weights. The void volume of the column was determined using Blue Dextran 2000.

According to this calibration curve, the mass range of F2 was calculated spanning from 9kD to 16kD, whereas mass analysis of the purified inhibitory molecule was only 660 Da, described in later mass spectrometry characterization. This inconsistency was caused by co-elution of multiple proteins or peptides falling in this mass range with the inhibitory molecule from the gel filtration column, supported by the detection of various proteins in LC/MS spectra of the first two active fractions (F2 and F2-S1).

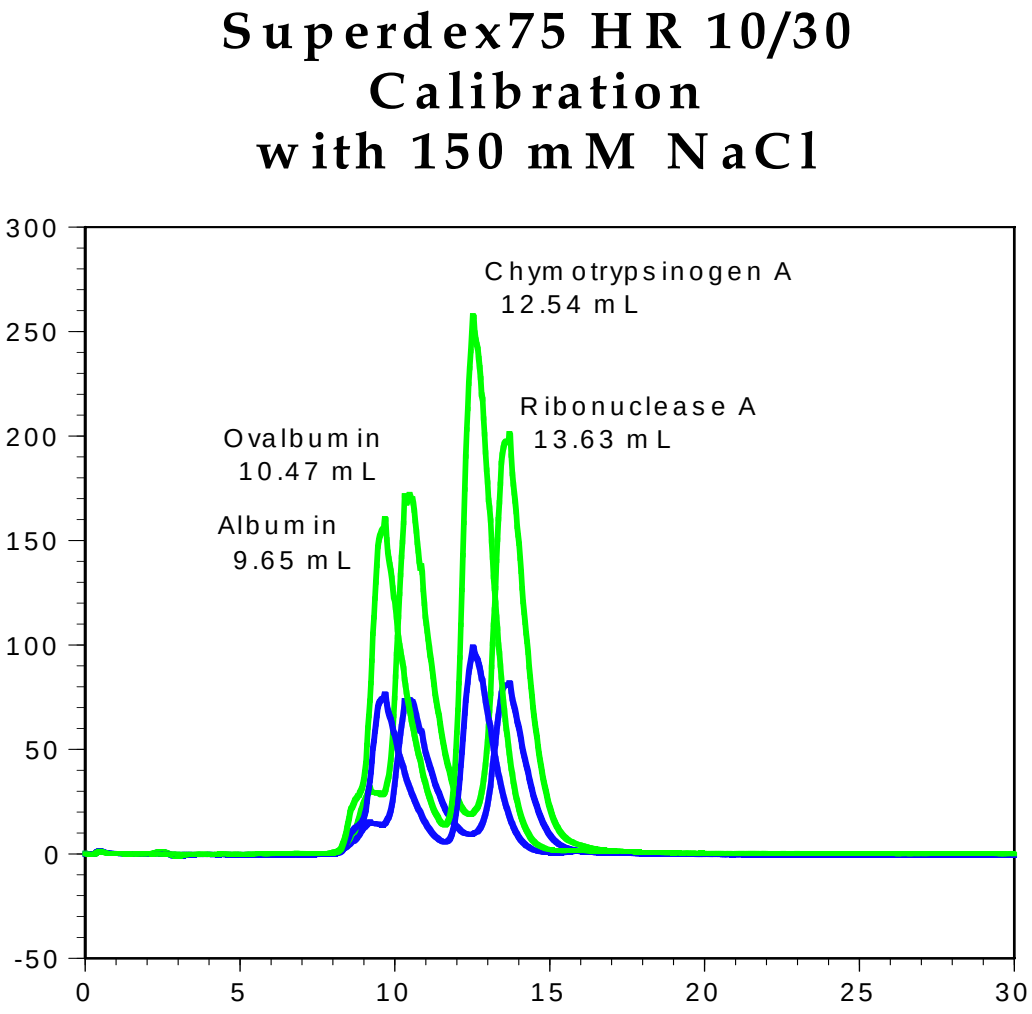

Figure 9. Superdex 75 FPLC Calibration Elution Profile monitored at 254 nm (blue) and 280 nm (green).

Eluent	150 **mM NaCl**
Vo	8.22 **mL**
Vt	23.56 **mL**
Vt - Vo	15.34 **mL**

Protein	Concentration (mg/ml)	MW kDa	Log(MW)	Ve	Kav
Albumin	7	64.7	1.810904	9.65	0.09322
Ovalbumin	7	45.8	1.660865	10.47	0.146675
Chymotrypsinogen A	3	19.9	1.298853	12.54	0.281617
Ribonuclease A	10	15.4	1.187521	13.63	0.352673

$K_{av}=(V_e-V_0)/(V_t-V_0)$
V_e = elution volume for the protein
V_0 = column void volume
V_t = total bed volume

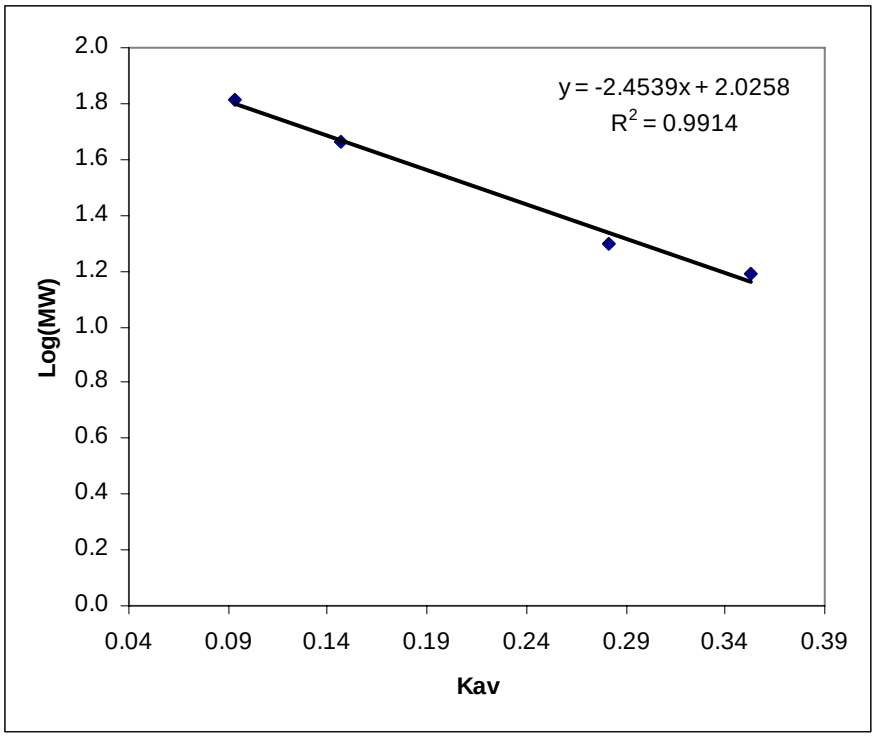

Figure 10. Molecular weight calibration curve of the Superdex 75 column.

Reversed Phase Chromatography

The reversed phase columns used in attempts to separate F2 were the Phenomenex Jupiter C5 column (5 μm, 300 Å, 4.6×250 mm, Phenomenex, Torrance, CA), the Alltech ProSphere C18 column (5 μm, 300 Å, 4.6×150 mm, Alltech, Deerfield, IL) and the Vydac 218TP C18 column (3 μm, 300 Å, 1.0×250 mm, Vydac, Deerfield, IL).

All above three reversed phase columns have wide pore size of 300 Å, which allows access of large proteins while still maintaining resolution of small peptides. The Vydac 218 TP C18 column is a microbore column packed with polymerically bonded endcapped n-octadecyl reversed phase based on 300 Å TP silica. Both methanol and acetonitrile were used as the organic modifier; TFA and formic acid were used as the ion pair reagent. Various concentrations of ion pair reagents and various gradients were applied to adjust the retention of compounds on columns and the baseline separation.

For the Vydac 218 TP C18 column, chromatogram with a single peak was obtained, with no indication of separation under these conditions. Chromatograms of both the Phenomenex Jupiter C5 column and the Alltech ProSphere C18 column exhibited three distinct peaks, and the performance of the former was more consist than the latter; therefore, the Phenomenex Jupiter C5 column was consequently selected for further separation of F2 and for the subsequent bioassay as well. All fractions were manually collected and retention times are: P1, 2.5 to 6.0 min, P2, 16.0 to 22.4 min, P3, 22.4 to 26.0 min (Figure 11A). However, several later bioassays did not show any inhibitory bioactivity from any subfraction. Figure 11B shows the result of one of the bioassays. The F2 control from the Superdex 75 column consistently inhibited the early-

stage somatic embryo growth in a statistically significant manner, whereas treatments of all subfractions and the mixture of subfraction P2 and P3 (labeled P23) did not affect the embryo growth compared to the blank control. This result showed that the inhibitory bioactivity could not be recaptured from this elution condition.

A

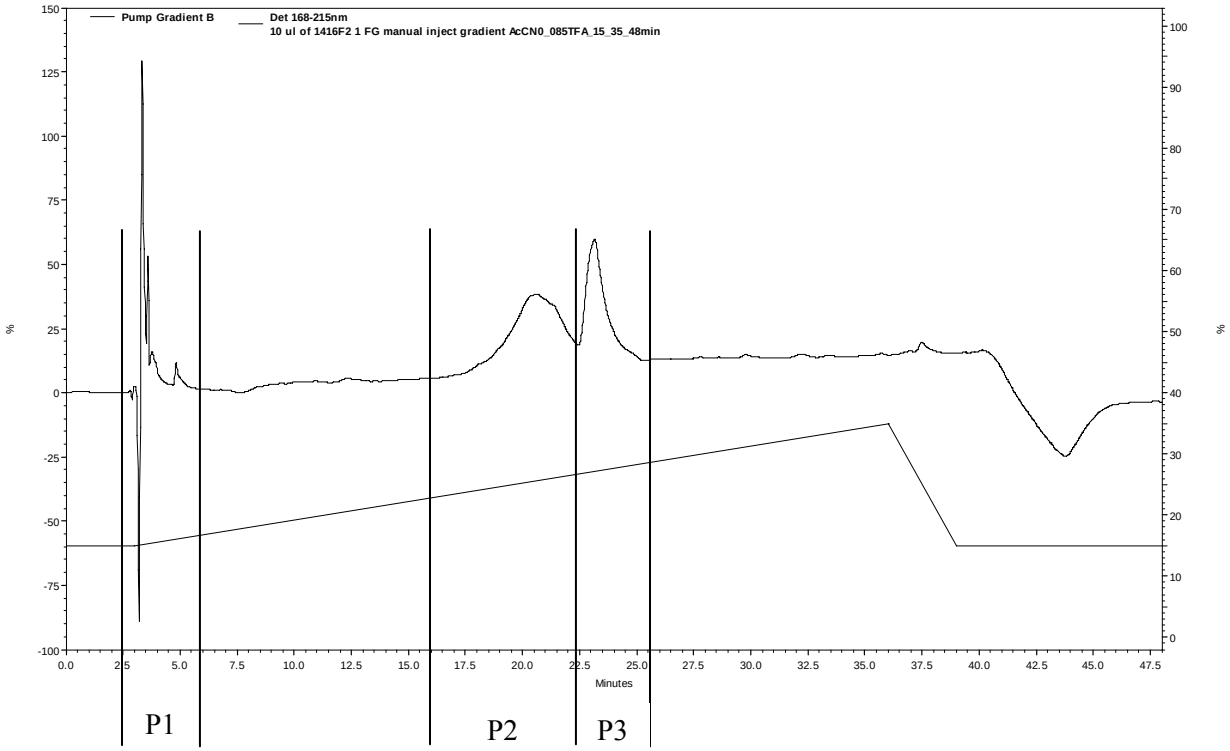

B

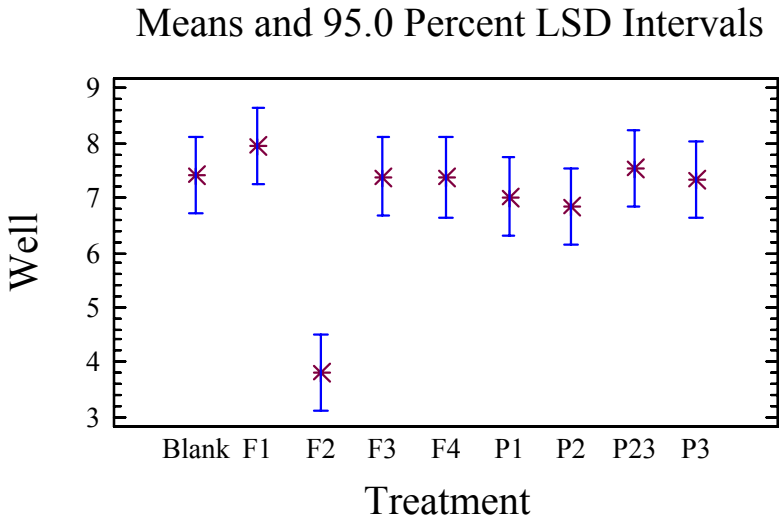

Figure 11. (A) Phenomenex Jupiter C5 RP HPLC elution profile for the subfractionation of F2, 215 nm. (B) Bioassay of the HPLC-isolated fractions eluted from a Phenomenex Jupiter C5 RP column.

Hydrophobic Interaction Chromatography (HIC)

Many theories based on interactions between hydrophobic solutes and water have been proposed regarding HIC (Tanfor and sons, 1973; Creighton and Freeman, 1984), but none of them have been universally accepted. Only the central role played by the structure-forming salts is common to these theories: the structure-forming salts affect the individual components (i.e., solute, solvent and adsorbent) of the chromatographic system to bring about the binding of solute to adsorbent (Porath, 1986). One of the most acceptable theories is that close to the surface of the hydrophobic ligand attached to polymer matrix and solute molecules, water molecules are more highly ordered than in the bulk water, resulting in shielding off the hydrophobic ligand and solute molecules. Salt added in the eluent interacts strongly with water molecules and leaves less water available for the shielding off effect, which is the driving force for hydrophobic ligand and hydrophobic patch on surface of solute molecules to interact with each other (Hjertén, 1977).

There are several main factors affecting HIC, including type of ligand and degree of substitution, type of base matrix, type and concentration of salt, pH effect, temperature effect, and additives (Jennissen and Heilmeyer, 1975; Visser and Strating, 1975; Srinivasan and Ruckenstein, 1980; Hjertén et al., 1986; Narhi et al., 1989).

The commercially available HIC media include butyl, octyl, phenyl groups linked to the glycidyl ether group. This coupling procedure generates gels of free charge and having interactions with proteins only.

Selection of column, eluent and gradient

Three HIC columns were used in attempt to improve the retention of compounds on them, including the HiPrep Butyl FF (-O-CH_2-CHOH-CH_2-O-$(CH_2)_3$- CH_3) column, the HiPrep Phenyl FF (-O-CH_2-CHOH-CH_2-O-C_6H_6) column and the HiPrep Octyl FF (-O-CH_2-CHOH-CH_2-O-$(CH_2)_7$-CH_3) column. Ammonium sulfate was chosen as the salt in eluent A due to its high precipitation effect. Increased amount of ammonium sulfate was added up to 1.5 M, but for both Phenyl and Octyl HIC columns, chromatograms only exhibited a single peak before the start of gradient. Sodium phosphate and sodium acetate buffers at pH ranging from 2.5 to 7.0 were also attempted to adjust the retention. Only the Butyl column can retain the F2 fraction under the condition of eluent A, 50 mM sodium phosphate buffer containing 1.5 M ammonium sulfate and eluent B, 50 mM sodium phosphate buffer, both at pH 2.5. Various gradients were attempted to achieve the baseline separation and shortest time consumption. A four-segment stepwise gradient was chosen as described in experimental procedure.

Elution and desalting

Fractions were pooled and collected as follows: F21, 2.57 to 14.67 min; F22, 14.67 to 34.82 min; F23, 34.82 to 38.40 min; F24, 38.40 to 41.40 min, as shown in Figure 12A. YM1 membrane continued to be used as the desalting procedure at first, but it was replaced by YM3 (3000 Da cutoff) membrane due to its high efficiency to ultrafiltrate high amount of salt. Osmolality was measured to ensure the completeness of salt depletion from each fraction.

Bioassay

Three bioassays were carried out, but none of them were consistent to each other. Figure 12B shows the best result for this HIC separation. Both subfraction F22 and F23 inhibited embryo growth in a statistically significant manner, but only inhibition from F22 was more statistically significant than that from the F2 control (F20) from the Superdex75 column. However, in the later two bioassays, either F22 did not inhibit embryo growth in a statistically significant manner, or the subfraction F21 also inhibited embryo growth. The bioassay result in Figure 12B was not reproducible. Due to inconsistency in bioassay results from this elution condition and requirement of use of huge amount of salt for HIC columns, an alternative sub-fractionation procedure of F2 was needed.

A

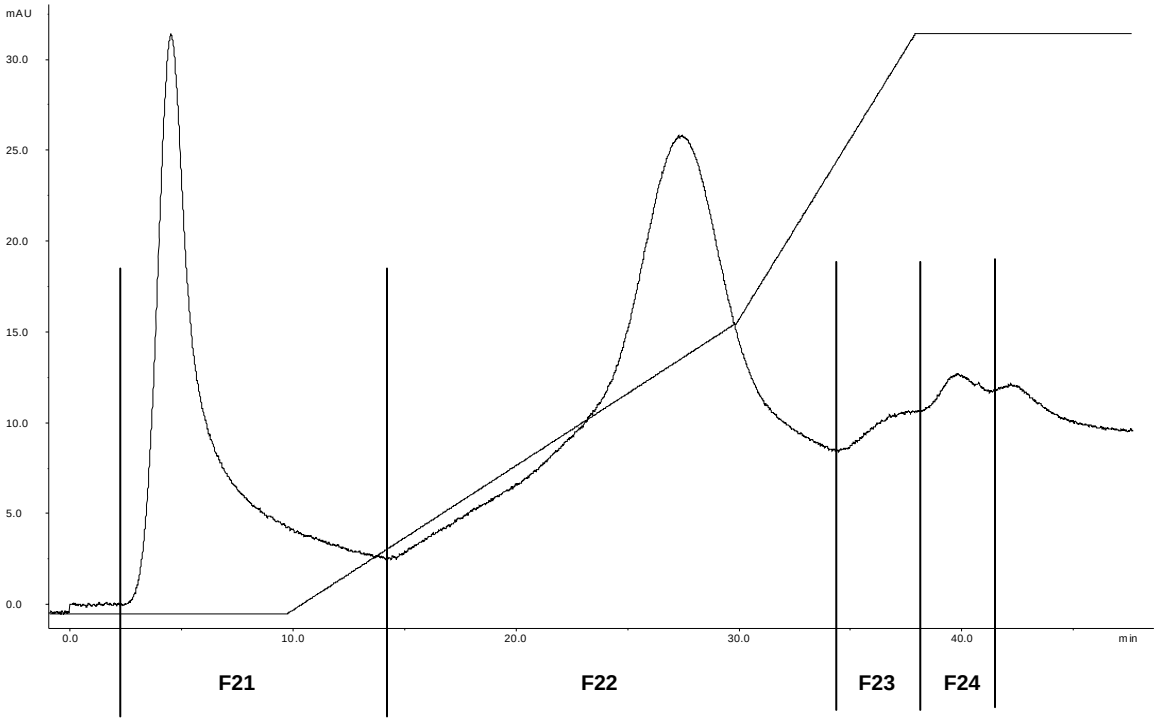

B

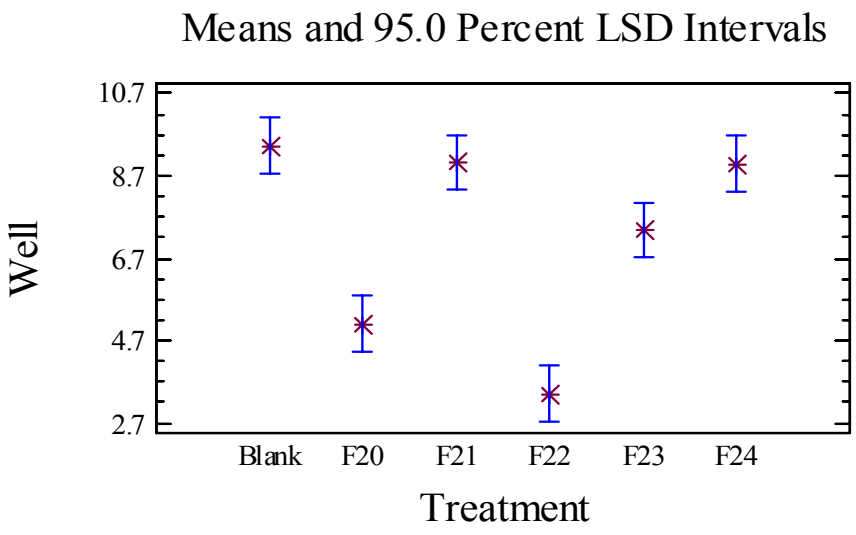

Figure 12. (A) HiPrep 16/10 Butyl FF HIC FPLC elution profile for the subfractionation of F2, 215 nm. (B) Bioassay of the FPLC-isolated fractions eluted from a HiPrep 16/10 Butyl FF HIC column.

Ion Exchange Chromatography

The definition of strong and weak ion exchangers is based on the extent of variation of ionization with pH, not the strength of binding. Strong ion exchangers are characterized by complete ionization over a wide pH range; as for weak ion exchangers, the degree of dissociation and exchange capacity changes remarkably with pH. Sulphonic and quaternary amino groups are used to generate strong ion exchangers, whereas diethylaminoethyl (DEAE) and carboxymethyl (CM) groups form weak ion exchangers. Compared with the weak ion exchangers, strong ion exchangers have several advantages, including stable loading capacity, simple mechanism of interaction and easiness of control.

Strong cation exchange chromatography

Consequently, the column selected for the second isolation chromatography is Mono S. The cation exchanger of Mono S column is mehtyl sulphonate (-O-CH_2-CHOH-CH_2-O-CH_2-CHOH-$CH_2SO_3^-$).

Selection of eluent and gradient. 50 mM sodium formate at pH 3.75 was attempted to use as the buffer for the Mono S column. Formate buffer itself has high UV absorbance during the wavelengths below 300 nm. This resulted in limited detection in that sample peaks were not distinct enough to be distinguished from the baseline. Lower pH can facilitate compounds retention to cation exchange columns. Eluent A, 20 mM sodium phosphate buffer at pH 2.5, and eluent B, eluent A containing 2 M NaCl, were consequently used. Various gradients were attempted to achieve the baseline separation

and shortest time consumption. A four-segment stepwise gradient was chosen as described in experimental procedure.

Elution and Desalting. Fractions were pooled and grouped as follows: F2-S1: 0.68 to 2.02 min, F2-S2: 2.02 to 3.37 min, F2-S3: 13.29 to 21.30 min, F2-S4: 21.30 to 27.30 min, F2-S5: 37.54 to 41.53 min (Figure 13A). Desalting for each fraction was accomplished by an Amicon stirred cell containing an YM1 (1000 Da cutoff) membrane. The duration of ultrafiltration applied to each fraction varied depending on the calculated salt amount it contained from the salt elution gradient. Retentate was divided into aliquots and lyophilized to dryness.

Bioassay. Dry fractions were re-dissolved with 2ml of deionized water, pH adjusted at 5.7 and applied to bioassay. F2-S1 eluting during the wash of unbound compounds was the only fraction which showed statistically significant inhibition to embryo growth compared to the blank control, in exactly the same manner as that of the F2 control from the Superdex75 column (Figure 13B), indicating that the active molecule is highly anionic and can not be retained on a strong cation exchange column. F2-S2 and F2-S3 were weakly inhibitory to the growth, but not in a statistically significant manner. F2-S4 and F2-S5 treatments exhibited similar embryo growth to that of the blank control.

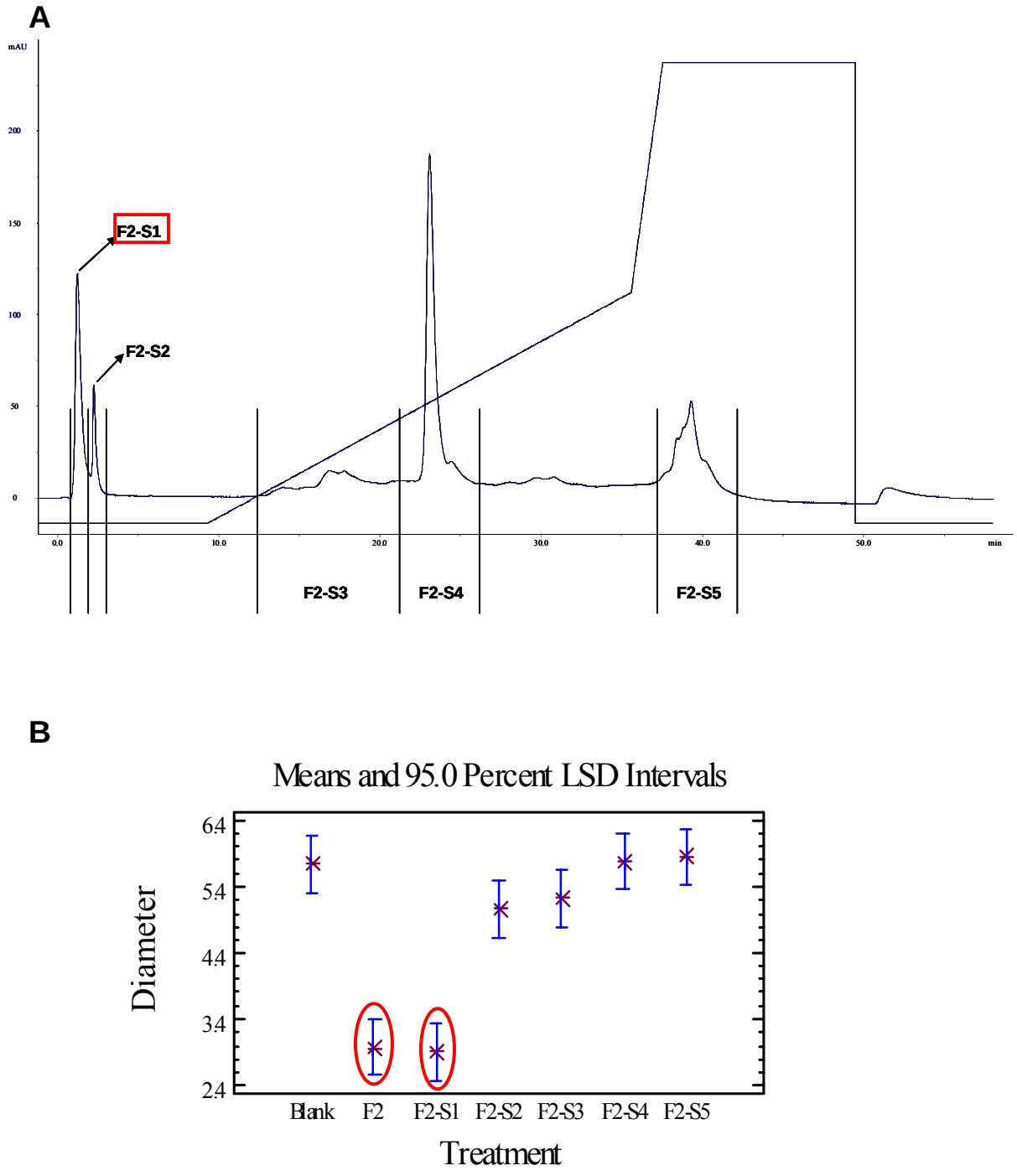

Figure 13. (A) Mono S FPLC elution profile for the inhibitor 2nd fractionation eluted with 20 mM sodium phosphate buffer at pH 2.5, 215 nm. (B) Bioassay of the fractions eluted from a Mono S column.

Strong anion exchange chromatography

The incapability of the active compound to bind to a Mono S column indicated that this compound is very anionic. A strong anion exchange column, Mini Q, is selected for the third-step chromatography isolation. Mini Q is composed of monodisperse 3 μm nonporous beads coupled to the anion exchanger, quaternary ammonium (-O-CH_2-CHOH-CH_2-O-CH_2-CHOH-CH_2-$N^+(CH_3)_3$). The nonporous matrix of Minibeads offers improved resolution and separation for analytical scale.

A four-segment gradient was applied to accomplish the baseline separation. Retention time of each fraction is listed as follows: F2-S1-Q1, 2.10 to 6.05 min; F2-S1-Q2, 6.05 to 11.12 min; F2-S1-Q3, 25.38 to 30.37 min; F2-S1-Q4, 30.37 to 36.34 min; F2-S1-Q5, 36.34 to 43.34 min; F2-S1-Q6, 49.38 to 58.32 min (Figure 14A).

All the resulting fractions were also processed desalting against YM3 membrane (3000 Da cutoff). 20 FG aliquot of each fraction was applied to the bioassay, which included treatments of blank control, active control from the previous Mono S column (F2-S1), all individual fractions from Mini Q and one combination of F2-S1-Q4 and F2-S1-Q5. The bioassay results (Figure 14B) revealed that both F2-S1-Q5 and F2-S1-Q6 had the statistically significant inhibition to the embryo growth compared to the blank control. However, the significance of inhibition was not as great as that of F2-S1 control. Treatment of the combination of F2-S1-Q4 and F2-S1-Q5 exhibited similar statistical significance of inhibition as that of F2-S1-Q5 alone, whereas F2-S1-Q4 alone did not inhibit embryo growth. Neither did the remaining fractions from Mini Q, indicating F2-S1-Q5 and F2-S1-Q6 were the only two inhibitory fractions. However, collection of F2-

S1-Q6 as two individual fractions based on the split of the peak did not retain any inhibitory bioactivity (data not shown).

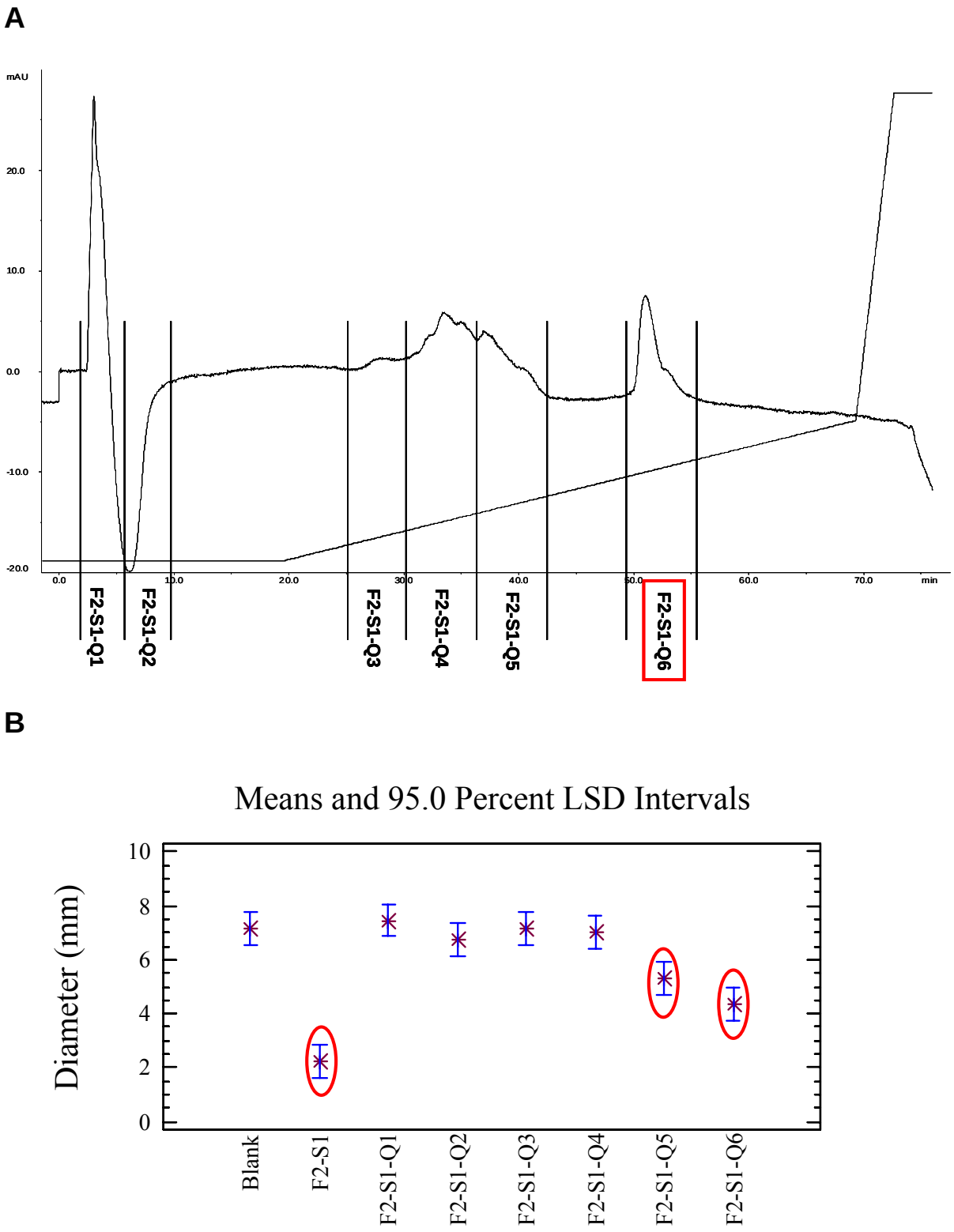

Figure 14. (A) Mini Q FPLC Elution profile for the inhibitor 3rd fractionation eluted with 20 mM Tris-Cl buffer at pH 8.0, 215 nm. (B) Bioassay of the fractions eluted from a Mini Q column.

Weak anion exchange chromatography

The weak anion exchanger DEAE is the abbreviation for diethylaminoethyl (-O-CH_2-CH_2-$N^+H(CH_2CH_3)_2$). The DEAE column was attempted to fractionate F2 for the second column separation after the Superdex 75. Tris and *bis*-Tris buffers were used at various pH values ranging from 6.5 to 7.7 to adjust ionization of compounds with pH. Various gradients and concentrations of sodium chloride were applied to adjust the resolution of the separation and the retention of compounds on the column. However, chromatograms with a single peak were obtained, indicative of no separation. Or, chromatograms of blank runs showed inconsistently unknown peaks. Therefore, this column was consequently abandoned.

Gel filtration chromatography II

Column selection

The weaker inhibition of Q5 and Q6 compared to that of the F2-S1 control and the absence of molecules above 1000 Da in both Q5 and Q6 indicated that the 3000 Da cutoff ultrafiltration membrane might not retain molecules of a lower molecular weight and a portion of the active molecule might have lost during the process. Besides separation according to size, gel filtration columns are sometimes used as the final step in isolations, in that they can separate contaminants such as salt carried over from previous chromatography. Superdex 75 was used in attempts to desalt and separate other small molecules from the active one. Unfortunately, the subsequent MS results revealed a mixture of small molecules below 1000 Da in the subfraction in which the candidate active molecule is. Therefore, a Superdex Peptide column was selected as the alternative desalting procedure. This column is the only gel filtration column commercially available offering high-resolution separation of small biomolecules in the fractionation range of 100-7000 Da.

Elution

A volatile buffer such as ammonium acetate would be an ideal eluent, in that the Superdex Peptide column was selected mainly for desalting, and residual buffer salts would suppress ionization in subsequent MS characterization and mask the bioassay results by generating extra inhibition to embryo growth. Flow rate was decreased from 0.5 ml/min (lower value in the room temperature recommended by the manufacturer) to 0.2 ml/min to adjust the resolution of the separation. Fractions were pooled and grouped

based on absorbance at both 215 nm and 280 nm. Elution times of each fraction are shown in Figure 15A: F2-S1-Q6-D1A, 62.06 to 80.14 min; F2-S1-Q6-D1B, 80.14 to 90.13 min; F2-S1-Q6-D2, 90.13 to 95.06 min; F2-S1-Q6-D3, 95.06 to 98.12 min; F2-S1-Q6-D4, 98.12 to 100.11 min. Components eluting after D4 were Tris-Cl buffer, NaCl from the Mini Q column and water peak, supported by individual control runs with injections of corresponding amount of each of them. Additionally, conductivity recorded on-line with UV detection also indicated the retention times of Tris-Cl and NaCl elution.

Bioassay

Treatments in this bioassay included:

- a blank control;
- bioactive control fractions F2-S1 and F2-S1-Q6-YM3 (from the Mini Q column followed by desalting against YM3 ultrafiltration membrane, labeled as Q6-YM3);
- buffer control (6ml of 100mM ammonium acetate lyophilized to dryness, corresponding to the highest amount of ammonium acetate contained in treatments before lyophilization), labeled as NH_4Ac;
- all individual fractions from the Superdex Peptide column, labeled as Q6-D1A, Q6-D1B, Q6-D2, Q6-D3 and Q6-D4;
- one combination of F2-S1-Q6-D1A and F2-S1-Q6-D1B, labeled as Q6-D1.

Figure 15B shows the bioassay results of the fractions eluted from a Superdex Peptide column. F2-S1-Q6-D1B and F2-S1-Q6-D1 are the most statistically significant inhibitory treatments of this set of bioassay. Active control fractions F2-S1 and F2-S1-

Q6-YM3 along with subfraction F2-S1-Q6-D2 also exhibited statistically significant inhibition to the embryo growth, but much less inhibitory than F2-S1-Q6-D1B and F2-S1-Q6-D1.

A

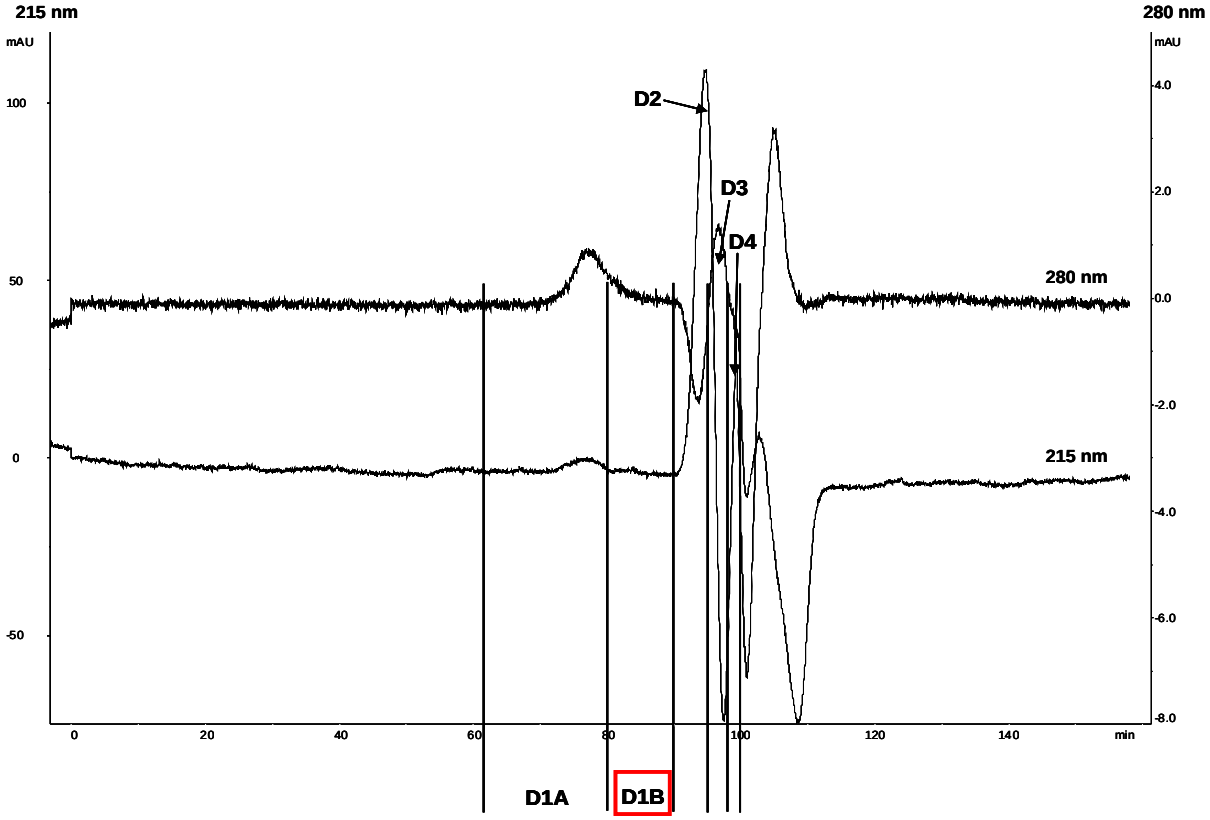

B

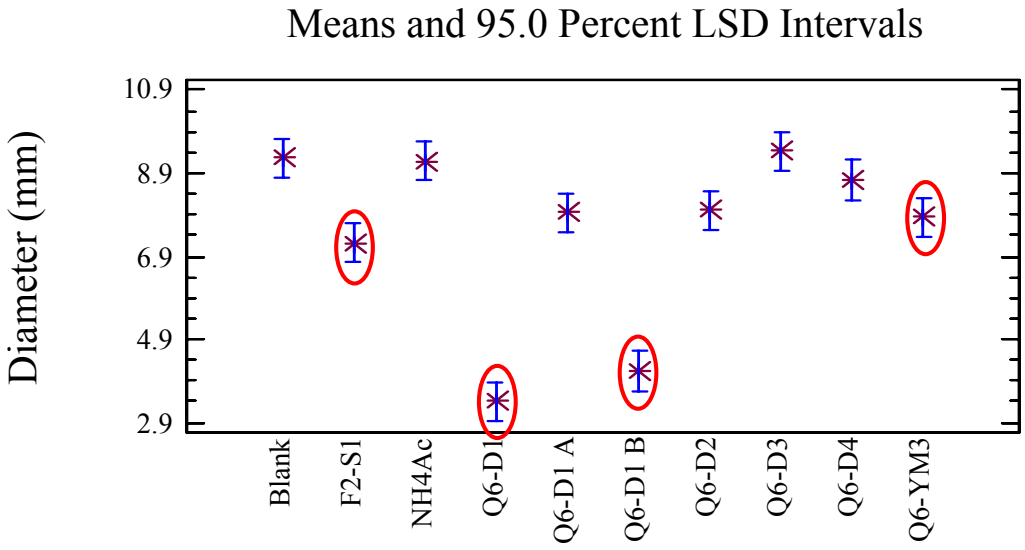

Figure 15. (A) Superdex Peptide FPLC elution profile for the inhibitor 4th fractionation eluted with 100 mM ammonium acetate buffer at pH 5.5, 215 and 280 nm. (B) Bioassay of the fractions eluted from a Superdex Peptide column.

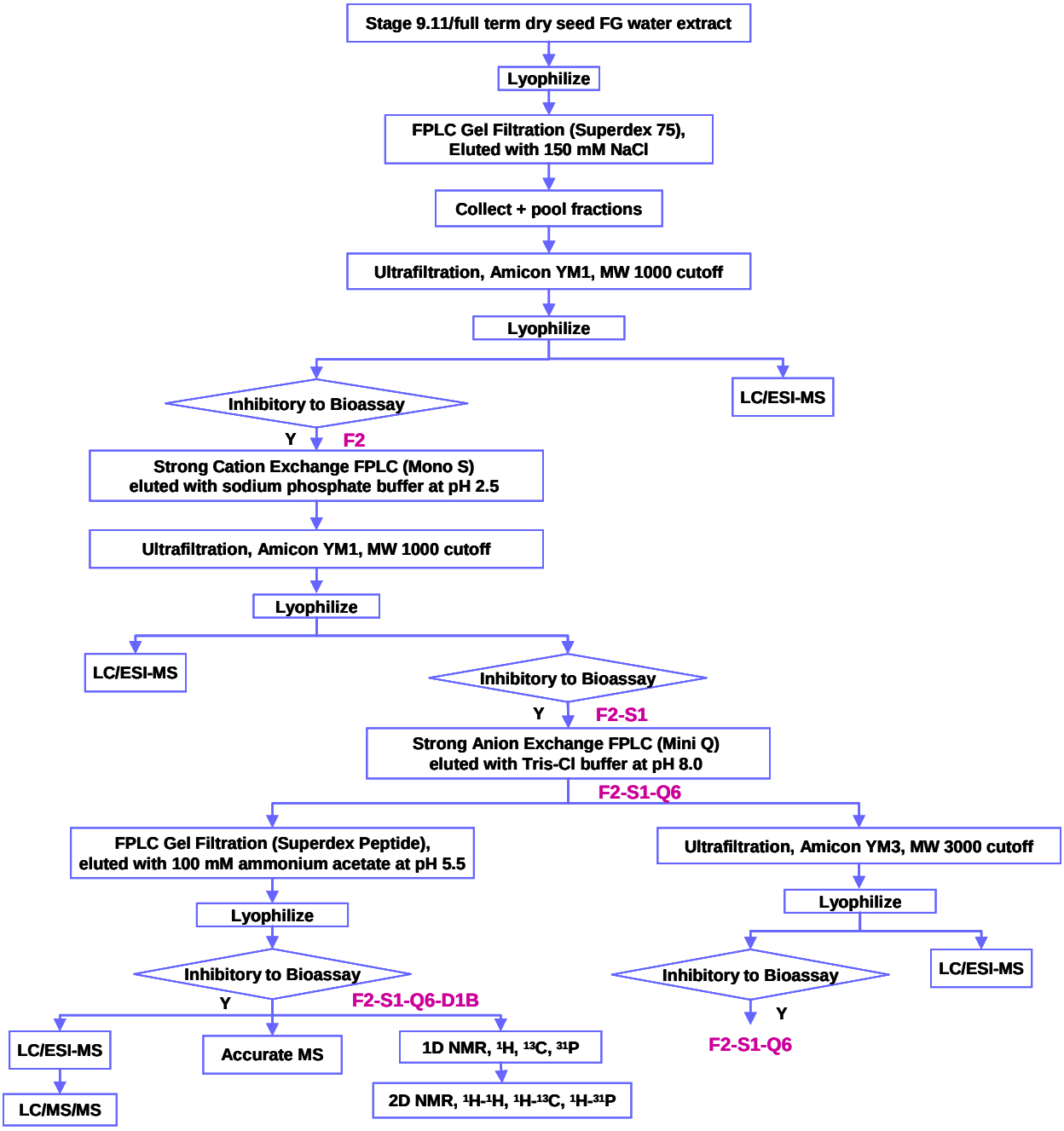

Figure 16. Final flow chart of isolation and characterization of $InsP_6$ from FG tissue.

Scale-up collection

Scale-up collection of the final active fraction F2-S1-Q6-D1B for NMR and MS analyses required 800 full-term dry seeds from tree S4PT6 of year 2006. Each seed was cracked open and the FG tissue was collected and water extracted within three days. Every step of purification conformed to the protocol shown in the flow chart (Figure 16). 800 FG was divided evenly into two batches, and each batch was performed sequentially. The amount of FG loaded onto each column was adjusted higher within the column capacity than previous analytical collections to improve scale-up efficiency. Fresh FG, lyophilized water extract, aliquots of lyophilized active fractions from Superdex 75 (ultrafiltered against YM1 membrane), Mono S (ultrafiltered against YM1 membrane) and Superdex Peptide columns were weighed out and yield was calculated in Table 4. F2-S1-Q6 directly from the Mini Q column was not included in the yield calculation due to high concentration of NaCl involved in this fraction.

Table 4. Yield of active fractions from successive processing steps.

FG and sequential active fractions	Number of FG weighed	Weight (mg)	Number of Normalized FG	Normalized Weight (mg)	Yield
Fresh FG collected from dry seed	60	812.5	100	1354.17	---
Lyophilized FG water extract	50	37.05	100	74.10	5.5×10^{-2}
Lyophilized F2	50	4.55	100	9.10	6.7×10^{-3}
Lyophilized F2-S1	100	1.32	100	1.32	9.7×10^{-4}
Lyophilized F2-S1-Q6-D1B	100	0.11	100	0.11	8.1×10^{-5}

Mass Spectrometry Characterization

LC/MS

LC/MS positive polarity

Instrument overview. Atmospheric pressure ionization (API) mass spectrometry (MS), particularly electrospray ionization (ESI), allows the analysis of thermolabile compounds of low molecular mass. The Applied Biosystems/MDS SCIEX 4000 QTRAP™ LC/MS/MS system is a combination of a triple quadrupole MS and linear ion trap (LIT) technology. The ion path of this system is identical to that of a standard triple quadrupole with a series of four rod quadrupoles. The final quadrupole, Q3, can be operated either in the normal RF/DC (quadrupole) mode or in LIT mode in a mass-selective fashion. Figure 17 shows a schematic ion path of QTRAP.

In the LIT mode, ions generated at atmospheric pressure flow through the orifice and skimmer regions, through the milli-torr pressure Q0 ion guide, through Q1 also operated as an ion guide, through the pressurized Q2 collision cell, and into the Q3 LIT. Ions are trapped in Q3 by the RF voltage operating in the radial direction and by the DC-biased aperture plates operating in the axial direction. After the trapped ions are cooled briefly, they are scanned out of Q3 in an axial direction toward the ion detector to yield a high sensitivity survey MS scan, named enhanced mass spectrometry (EMS) scan (Le Blanc et al., 2003; Hopfgartner et al., 2004)

LC/MS analyses under positive polarity of the fractions from the Superdex 75, Mono S and Mini Q columns were performed with quadrupole scans. LC/MS analyses of fractions from the Superdex Peptide column and analyses of F2-S1-Q6 before LC/MS/MS of the *m/z* 661 precursor ion under positive polarity were carried out with

EMS scans. No difference in either resolution or sensitivity between the Q1 and Q3 quadrupoles was observed when operating Q3 in either the RF/DC mode or the LIT mode.

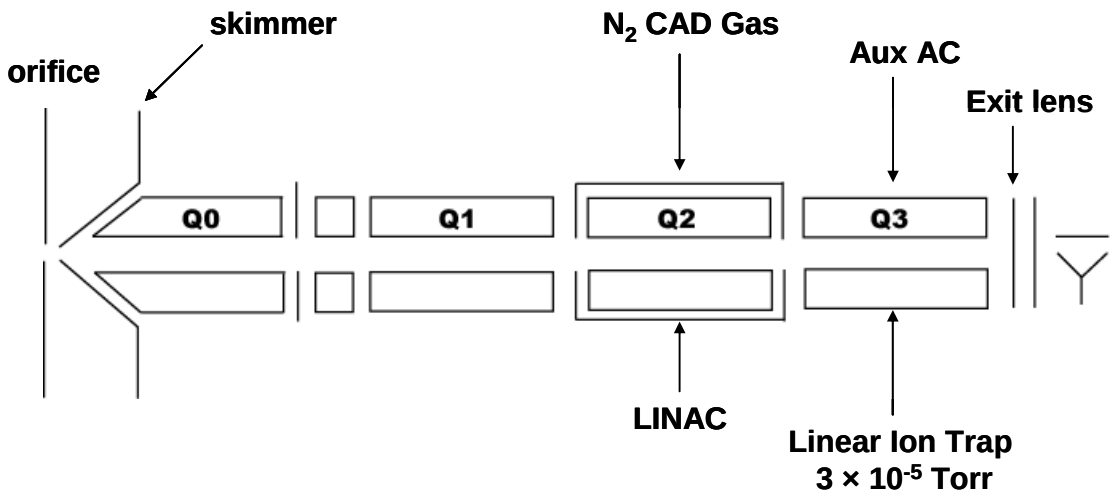

Figure 17. A schematic representation of the ion path of the QTRAP instrument, modified from (Le Blanc et al., 2003). Q1 is a standard RF/DC quadrupole mass filter; the final quadrupole, Q3, can be operated either in the normal RF/DC (quadrupole) mode or in linear ion trap mode.

Selection of column and mobile phase. Several reversed phase columns were used for LC/MS in attempts to characterize F2. The columns tried were the Discovery C5 Bio Wide Pore column (5 μm, 300 Å, 3.2×150 mm, Supelco, Bellefonte, PA), the Discovery C18 Bio Wide Pore column (5 μm, 300 Å, 3.2×150 mm, Supelco, Bellefonte, PA), the polymer-based monolithic PS column (200 μm ×50 mm, Dionex, Sunnyvale, CA), the Agilent Hypersil ODS amino acid column (2.3×200 mm, Foster City, CA), the C18 PepMap capillary column (3 μm, 100 Å, 0.3×250 mm, Dionex, Sunnyvale, CA) and the Vydac C8 capillary column (5μ, 300 Å, 0.3×250 mm, Deerfield, IL). Among them, the Vydac C8 capillary column packed with 5μm particles with 300 Å pore size exhibited the best performance based on separation and consistency, and was consequently selected.

TFA and formic acid can both serve as ion pair reagents, but TFA suppresses the ESI signals of analytes due to its ability to form gas-phase ion pairs with positively-charged analyte ions (Kuhlmann et al., 1995). Therefore, formic acid was included in the mobile phase. In terms of the organic modifier, acetonitrile showed stronger retention of the F2 fraction on columns than methanol. The consequent mobile phase A was comprised of 2% acetonitrile, 98% water and mobile phase B was 80% acetonitrile, 20% water, both containing 0.1% formic acid.

LC/MS of active fractions. LC/MS of F2, the active fraction collected from the Superdex 75 column and ultrafiltered against a YM3 membrane exhibited a mixture of singly charged and hundreds of multiply charged ions, indicating that the active F2 fraction contained various proteins as well as small molecules (Figure 18). Mass spectra

at different retention times revealed that the ion at *m/z* 661 was co-eluting with various multiply charged ions. An extracted ion chromatogram (XIC) of ion at *m/z* 661 confirmed that it eluted over the entire time course (data not shown).

F2-S1, the active fraction collected from the Mono S column (ultrafiltered against a YM3 membrane), only contained three peptides, the deconvoluted masses of which are 2649, 2102 and 2426 Da. The *m/z* 661 molecule co-eluted with peptides of 2649 and 2102 Da (Figure 19). XIC of ion at *m/z* 661 revealed that the majority of this molecule eluted from four to ten min, where most unbound molecules such as salt and plasticizer contaminants elute, whereas some of this ion was retained on the column up to approximately 40 min.

LC/MS of F2-S1-Q6, the active fraction collected from Mini Q (ultrafiltered against a YM3 membrane), exhibited one distinct ion at *m/z* 661 and a polymer plasticizer co-eluting with this ion near the void volume (Figure 20), as well as a number of species of low molecular mass at different retention times. The lack of multiply charged ions suggests that the inhibitory molecule is unlikely to be a polypeptide. Among several LC/MS runs of F2-S1-Q6, only one of them showed retention of the ion at *m/z* 661 from 26.6 to 29.7 min, and the rest exhibited its elution near the void volume. An array of sodium adduct ions with mass difference of 22 amu (the mass difference between sodium Na^+ and proton H^+) were observed downstream of the ion at *m/z* 661. However, the number of sodium adduct ions varied through the elution. From 26.6 to 29.7 min, a maximum of eight sodium adduct ions, corresponding to the +1 (Na^+), +2 (Na^+), and up to +8 (Na^+) salts of the species at m/z 661, were observed, whereas only two to six sodium adduct ions showed near the void. In the other active fraction from the

Mini Q, F2-S1-Q5, the ion at *m/z* 661 was also present (data not shown). But for the remaining inactive fractions F2-S1-Q1 through F2-S1-Q4, no such ion was detected in their mass spectra. These results indicated that the ion at *m/z* 661 corresponds to the active molecule to be pursued.

In the LC/MS run of F2-S1-Q6-D1B (Figure 21), the active fraction from the Superdex Peptide column, only the ion at *m/z* 661 and its three sodium adduct ions were present, suggesting that the improved desalting procedure using the Superdex Peptide column removed plasticizers and other small molecules, and isolated the pure compound.

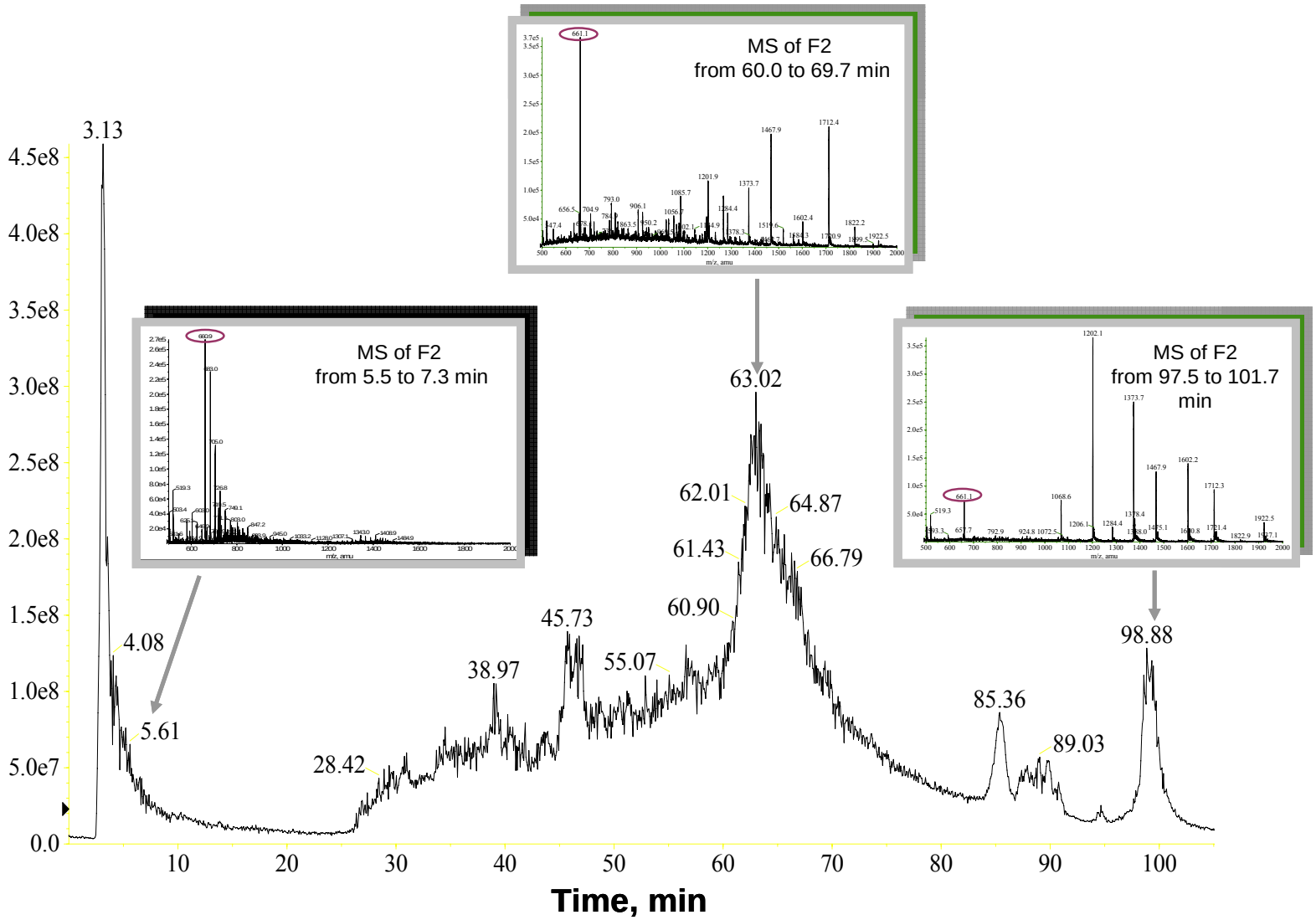

Figure 18. Total ion chromatogram and MS spectra of F2 (the active fraction from Superdex 75).

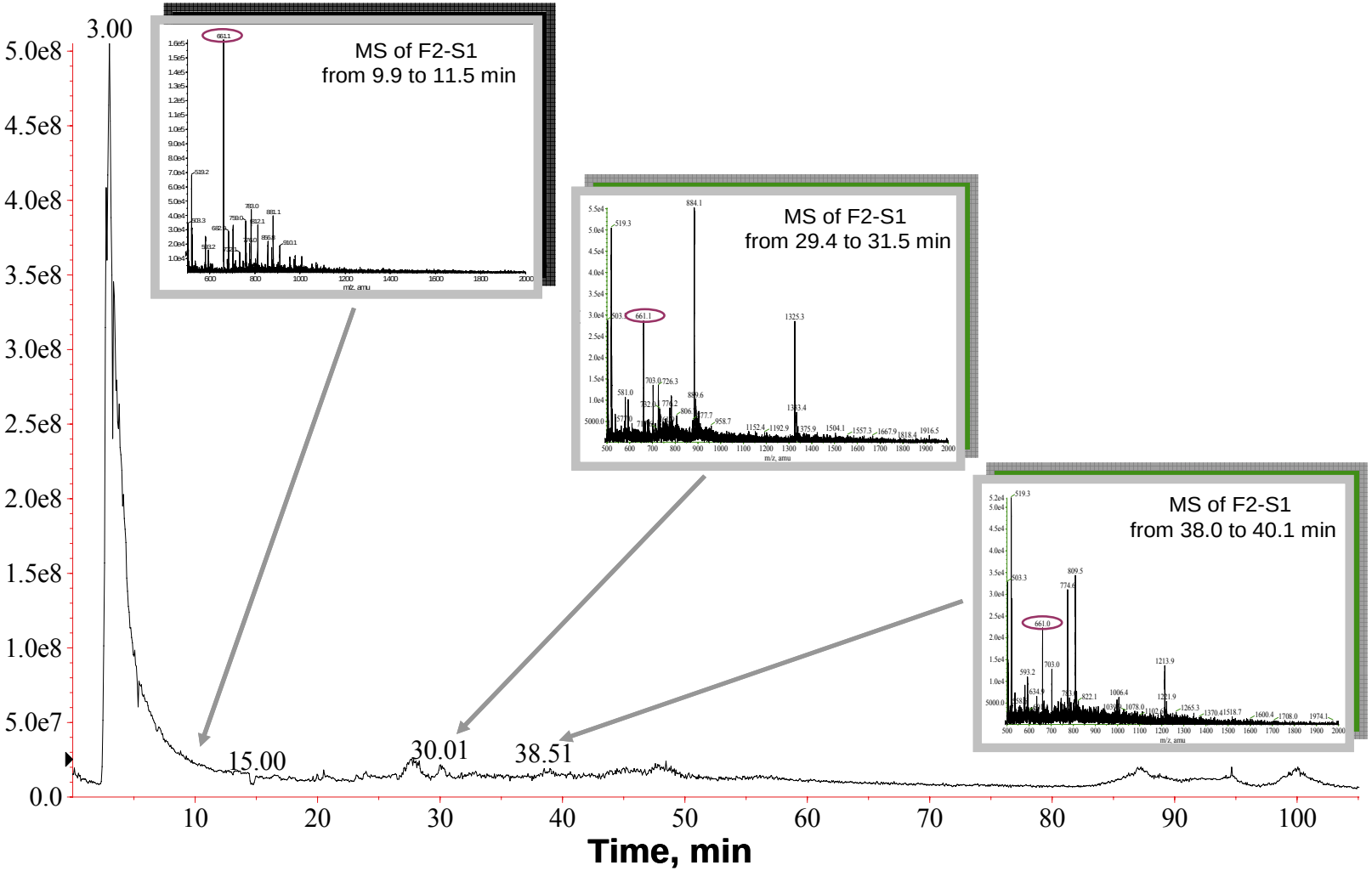

Figure 19. Total ion chromatogram and MS spectra of F2-S1 (the active fraction from Mono S).

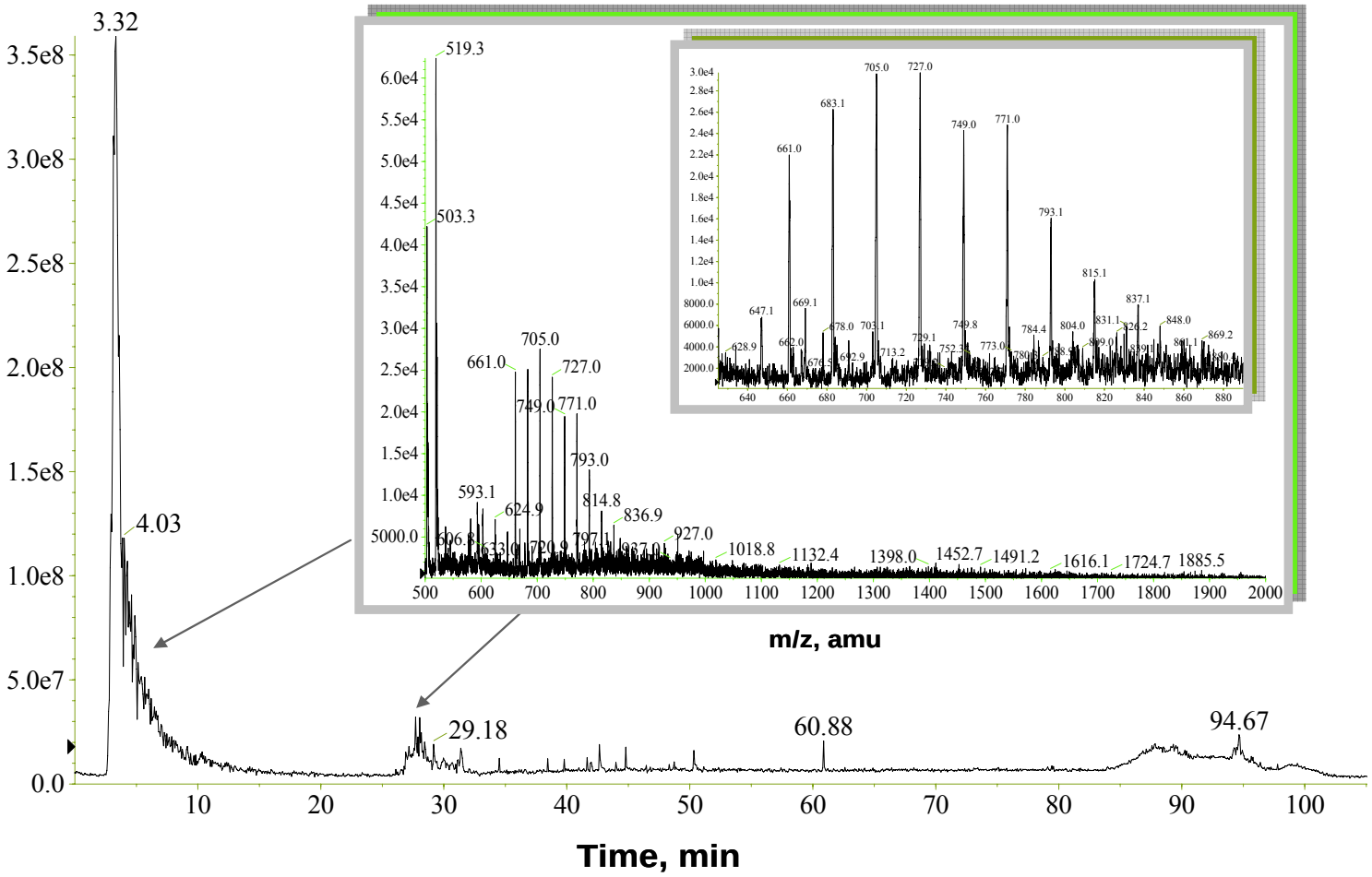

Figure 20. Total ion chromatogram and MS spectra of F2-S1-Q6 (the active fraction from Mini Q, desalted by 3000 Da cutoff membrane).

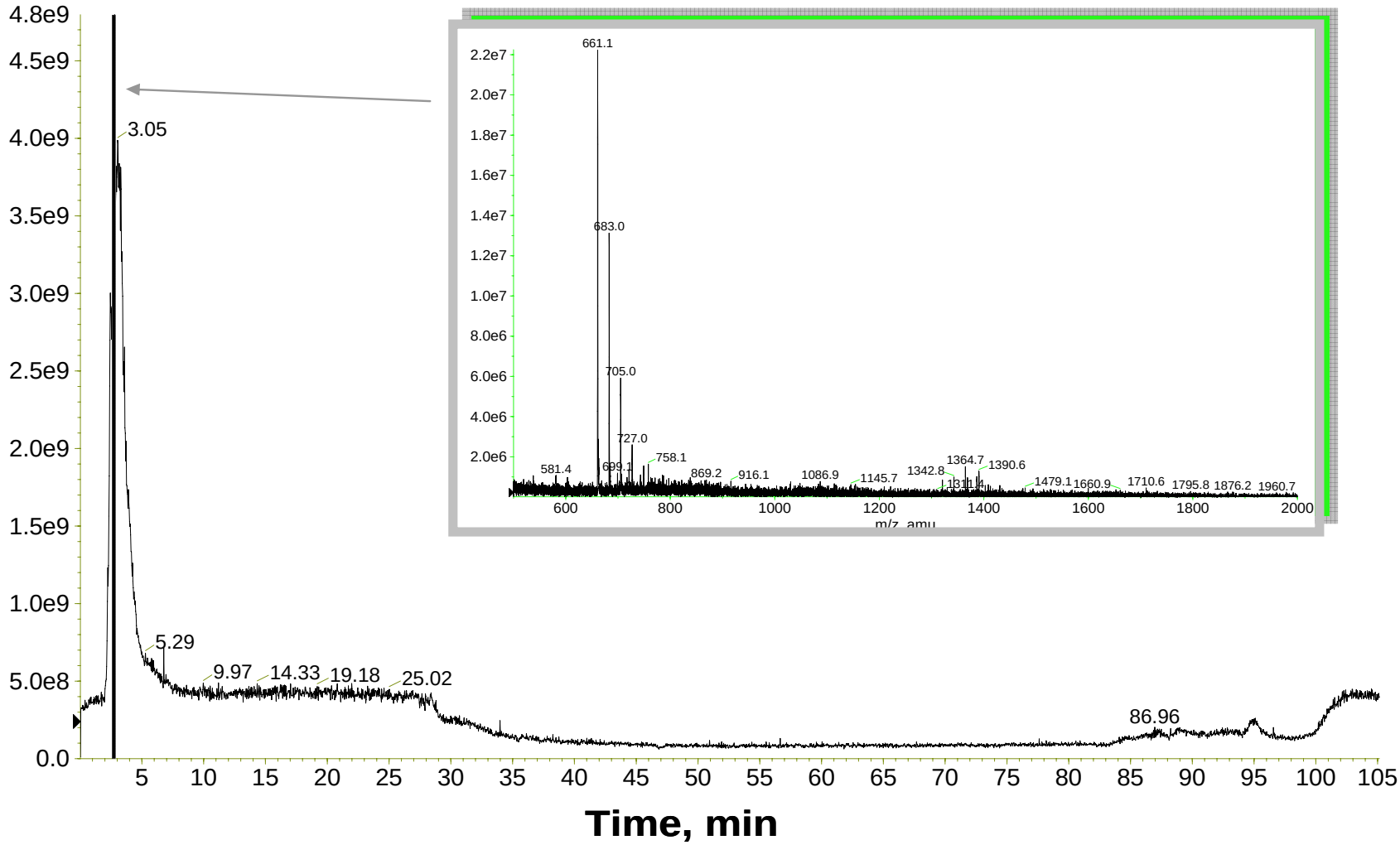

Figure 21. Total ion chromatogram and MS spectrum of F2-S1-Q6-D1B (the active fraction from Superdex Peptide column).

LC-MS negative polarity

Two different LC approaches for the LC/MS characterization under negative quadrupole scan mode of all fractions from the Mini Q column were accomplished using either a Phenomenex C5 analytical column or a Vydac C8 capillary column. Elutions were performed at pH 5.5 and pH 7.0, respectively. LC/MS results from both LC approaches were identical to those obtained from the positive scans. The corresponding ion at *m/z* 659 was only detected in the active fractions F2-S1-Q5 and F2-S1-Q6, but not in any of the other inactive fractions (data not shown). No multiply charged ions were observed in F2-S1-Q5 and F2-S1-Q6, suggesting that the inhibitory molecule is unlikely to be a polypeptide or nucleic acid. These results confirmed that ion at *m/z* 659 corresponds to the active molecule to be pursued. The *m/z* difference of 2 amu between ion at *m/z* 661 from the positive scan and ion at *m/z* 659 from the negative scan indicated that both ions are singly charged and the average mass of this molecule is 660 Da.

Exact Mass Analysis

Instrument overview

The inhibitory molecule was originally postulated to be a plant peptide hormone. The Applied Biosystems QSTAR XL Hybrid LC/MS system was selected for LC/MS analyses due to its sensitivity for the identification and characterization of low-abundance proteins. QSTAR is a hybrid quadrupole time-of-flight mass (TOF) spectrometer. The quadrupole analyzer allows high transmission and high scan speeds, and TOF offers a broad mass scan range up to 40,000 *m/z* as well as exact mass measurement down to ± 0.0001 ppm, which is perfect for protein database searching. After all LC/MS analyses were transferred to the QTRAP instrument, QSTAR was used only for exact mass measurement and the subsequent tandem MS analysis.

Exact Mass Analysis under positive polarity

Due to the limited amount of FG available to acquire NMR spectra of the active fraction, an exact mass measurement under positive polarity of F2-S1-Q6 (desalted against a YM3 membrane) was carried out to generate empirical formulas of candidate molecules to investigate the possible structure. F2-S1-Q6 showed an exact mass $(M+H)^+$ of 660.8476. The $(M+2H)^{2+}$ and $(M+3H)^{3+}$ ions constituted 7.30 % and 6.12 % relative intensities of $(M+H)^+$, respectively. This result indicated that the maximum number of carbon atoms included in this molecule would not exceed ten, since the natural abundance of ^{13}C is 1.11% and the $(M+2H)^{2+}$ ion of a molecule containing ten carbons constitutes 11.1% relative intensitiy of $(M+H)^+$. This percentage is already 3.8% higher than the observed 7.3% without contributions from other elements. Additionally, silicon,

sulfur, chlorine and bromine are unlikely to be present, due to their high M+2 peaks. Phosphorus is monoisotopic and known for its presence in many biomolecules, therefore, it is very likely to be one of the elements. Nitrogen is also known to be one common element in natural products and it only contributes 0.38% to the M+1 peak. The involvement of iodine and fluorine could not be completely excluded, in that they are also monoisotopic elements. Nevertheless, iodine and fluorine are not very common elements in biomolecules. Therefore, the elements were likely to be a combination of carbon (1-10), hydrogen (0-30), oxygen (0-30), nitrogen (0-10) and phosphorus (0-8). A list of 130 candidate formulas was generated under the error tolerance of ±30 ppm.

Formulas with either unreasonable elemental combinations or unreasonable relative intensities of isotope peaks were excluded. The remaining 14 formulas were submitted to a database search, including CAS registry (Scifinder), SDBS (spectral database of organic compounds from Japan), and the NIST library (National Institute for Standards and Technology). None of the formulas were found to have a match in any of these three databases. Possible structures were hypothesized based on both candidate empirical formulas and the LC/MS/MS spectra under positive polarity. However, none of the structures were feasible.

Exact Mass Analysis under negative polarity

After the TriVersa^{TM} NanoMate (Advion, Ithaca, NY) was installed on QSTAR, the sensitivity of the instrument was comparable to that of the QTRAP down to the fmol level. The NanoMate combines the strengths of LC, fraction collection and chip-based infusion in one integrated system. The ESI microfluidics chip contains an array of

nanoelectrospray nozzles, each one-fifth the diameter of a human hair, etched in a silicon wafer. The unique field strength created by the nanoelectrospray nozzles allows for a more efficient and stable spray (Figure 22A). As shown in Figure 22B, LC/MS is performed while simultaneously collecting fractions in a 96/384 well sample plate and software links the chromatographic peaks with collected fractions in the sample plate; a robot picks up one pipette tip from the rack; moves the tip to the 96/384 well sample plate and the target fraction is aspirated; the tip with the targeted sample then engages to the back of the ESI chip; the targeted fraction is infused and ions spray into the mass spectrometer. The long infusion times allow signal averaging for increased sensitivity (Advion).

A

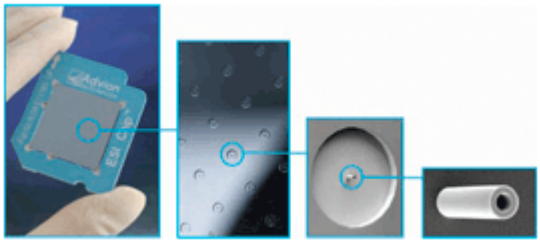

B

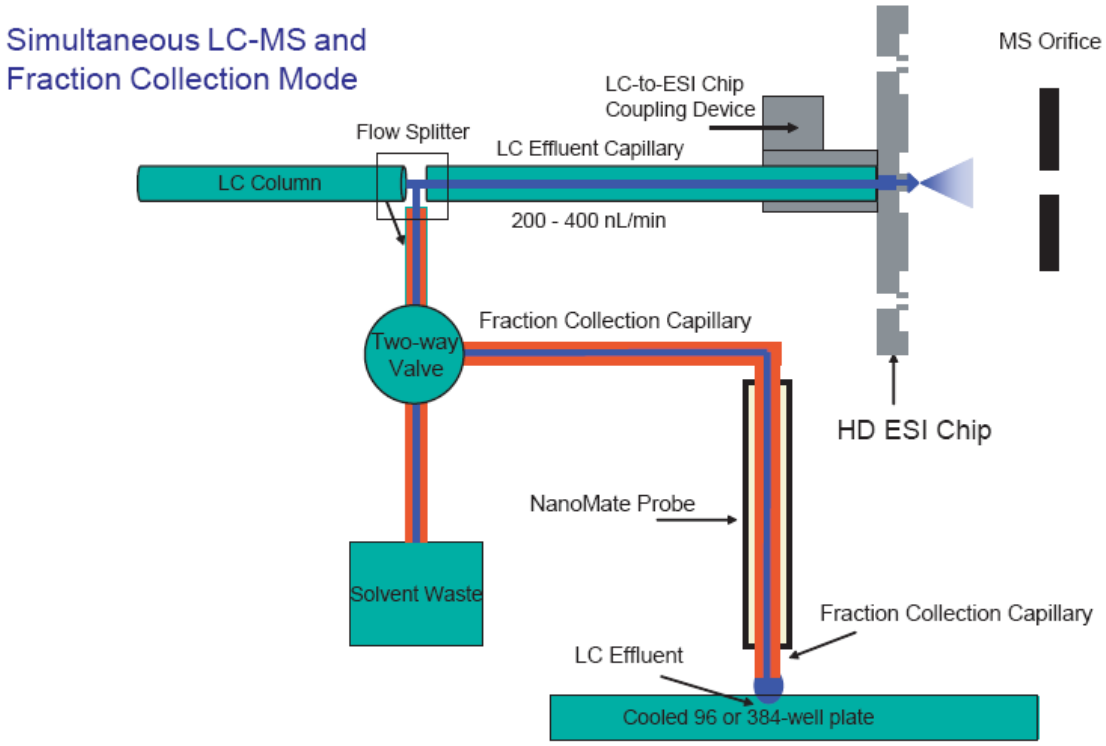

Figure 22. (A) ESI nanochip. (B) Schematic presentation of LC/MS coupled to NanoMate.

Structural characterization of F2-S1-Q6-D1B using NMR (described in NMR characterization) suggests that the inhibitory molecule is $InsP_6$. Therefore, exact mass measurements and subsequent tandem MS analyses of both F2-S1-Q6-D1B and the commercial $InsP_6$ were carried out on the new system under negative polarity to investigate the identity of the inhibitory molecule. As shown in the Figure 26 *inset*, F2-S1-Q6-D1B exhibited an exact mass $(M-H)^-$ of 658.8506 with an error of negative 5.3 ppm with respect to the calculated molecular mass of 658.8541, and the commercial $InsP_6$ showed an exact mass $(M-H)^-$ of 658. 8563 with an accuracy of 3.3 ppm, as shown in Figure 27 *inset*.

MS/MS

LC-MS/MS positive polarity

The LC/MS/MS spectra of the precursor ion at *m/z* 661 (obtained from F2-S1-Q6 ultrafiltered against a YM3 membrane) under positive polarity were acquired subsequent to LC/MS on QTRAP. Enhanced product ion (EPI) scans were performed subsequent to the EMS scan. In the EPI scan, the selection of the precursor ion is achieved in Q1 utilizing RF/DC isolation. The selected precursor ion is accelerated into a pressurized transmission collision cell to induce fragmentation. The ions emerging from Q2 are trapped in the Q3 LIT and subsequently mass selectively scanned out of the trap toward the ion detector (Hager and Yves Le Blanc, 2003; Hopfgartner et al., 2004).

The precursor ion $(M+H)^+$ at *m/z* 661 was subjected to collision energies of 40 and 80 eV, respectively. Figure 23 *inset* shows the MS/MS spectrum of the $(M+H)^+$ at *m/z* 661 obtained at 40 eV. The protonated ion at *m/z* 661 yielded a series of prominent

ions at *m/z* 643, 625, 607, 581, 563, 545, 527, 483, 465, 447, 429, 385, 367, 349, 287, 269, 259, 189, 179, 161, 99. After the inhibitory molecule was identified as $InsP_6$ by NMR, exact MS and MS/MS analyses under negative polarity, the cause of the generation of fragment ions under positive polarity could be explained by successive losses of H_2O (18 amu), HPO_3 (80 amu), or H_3PO_4 (98 amu). However, some fragment ions arose from multiple pathways, as shown in Figure 25. For example, the ion at *m/z* 367 can be formed not only from the ion at *m/z* 465 via loss of H_3PO_4, but from the ion at *m/z* 447 via loss of HPO_3 as well. Additionally, elimination of H_2O from the ion at *m/z* 385 can also generate the *m/z* 367 ion. Ions at *m/z* 259, 241, 179, 81 were due to further loss of CO from ions at *m/z* 287, 269, 207, and 109, respectively.

Figure 24 *inset* shows the MS/MS spectrum of the $(M+H)^+$ at *m/z* 661 obtained at 80 eV. Further dissociation intensified the low *m/z* fragment ions, whereas the abundances of the high *m/z* fragment ions decreased tremendously. Ions higher than *m/z* 447 were not observed. XIC of major fragment ions under both collision energies exhibited identical trace pattern as that of TIC of the precursor ion, suggesting that only one isomeric form was present in the precursor ion $(M+H)^+$ at *m/z* 661.

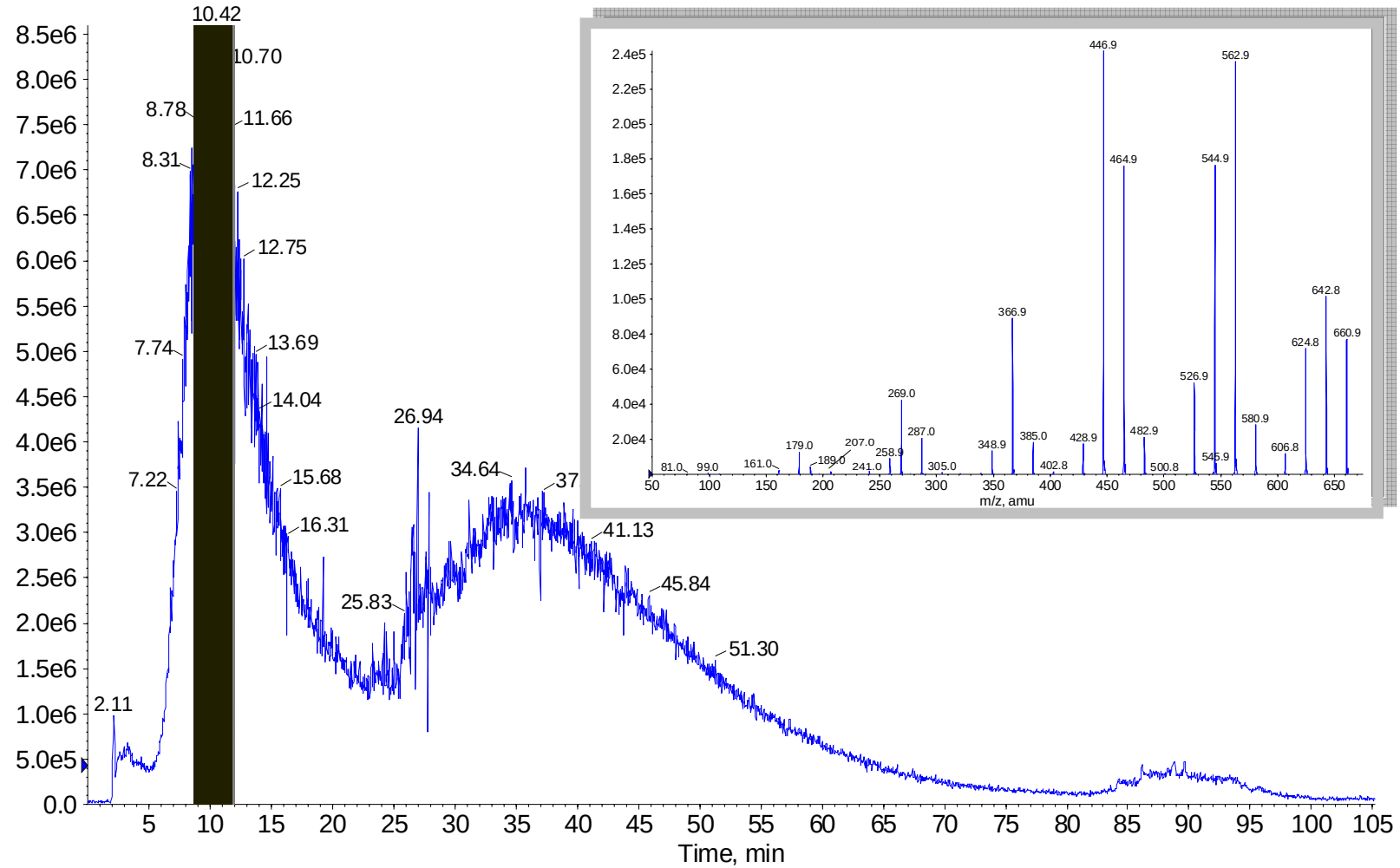

Figure 23. TIC and LC/MS/MS spectrum on precursor ion 661 from F2-S1-Q6 (the active fraction from Mini Q, desalted by 3000 Da cutoff membrane) at CE 40 eV.

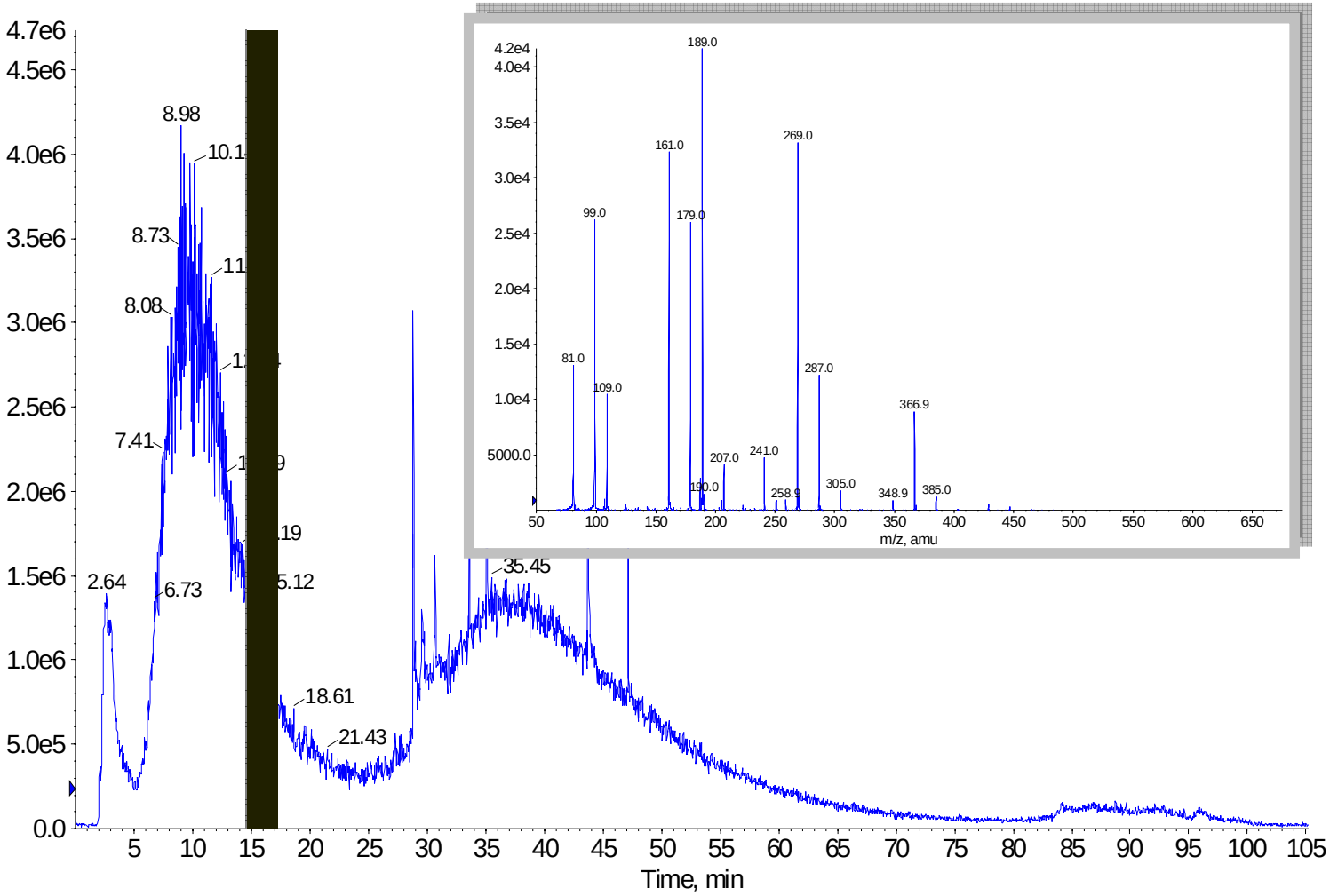

Figure 24. TIC and LC/MS/MS spectrum on precursor ion 661 from F2-S1-Q6 (the active fraction from Mini Q, desalted by 3000 Da cutoff membrane) at CE 80 eV.

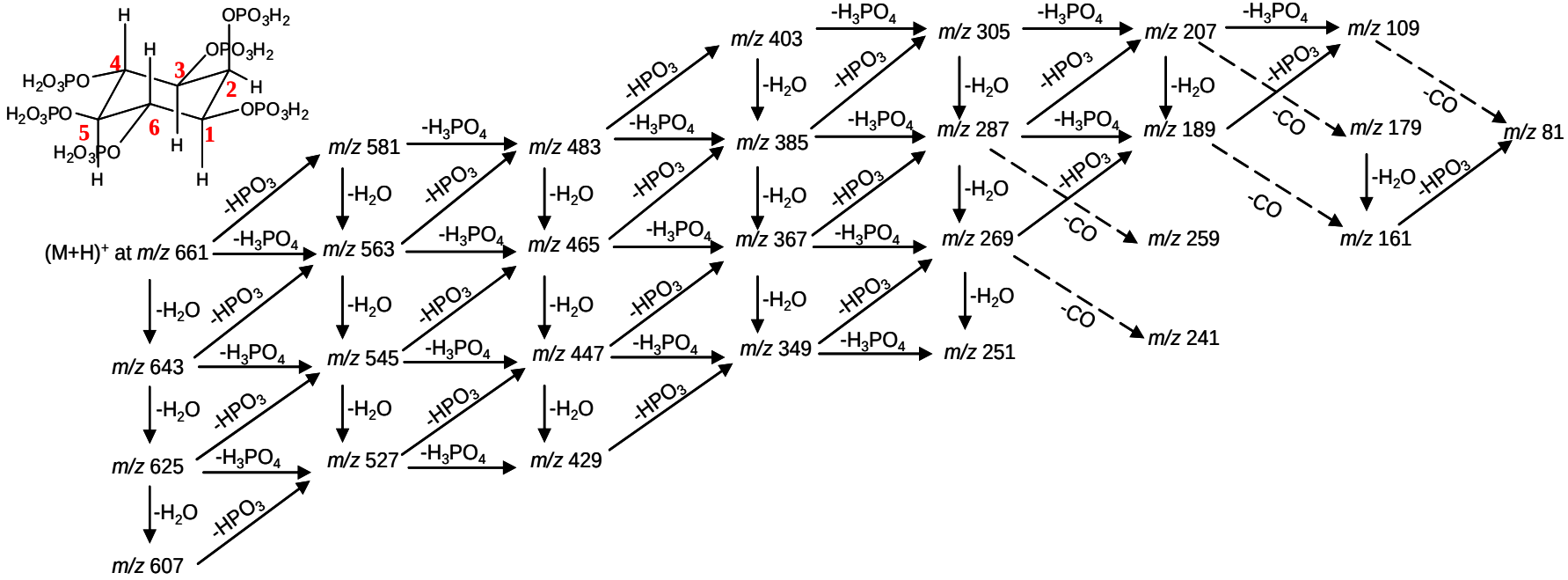

Figure 25. A schematic presentation of fragmentation pathways in LC/MS/MS under positive polarity, modified from (Hsu et al., 2003)

MS/MS negative polarity

Tandem mass spectra of the precursor ion at *m/z* 659 obtained from F2-S1-Q6-D1B and the commercial $InsP_6$ under negative polarity were acquired subsequent to the exact mass measurement on the QSTAR interfaced with NanoMate. Two collision energies of 40 and 80 eV were applied to the precursor ion $(M-H)^-$ at *m/z* 659, respectively. Spectra of F2-S1-Q6-D1B (Figures 26 and 28A) and the commercial $InsP_6$ (Figures 27 and 28B) under both collision energies were identical. Furthermore, MS/MS spectra acquired under negative polarity were consistent with those from positive mode, with each fragment ion lower by 2 amu. These results suggest that the pure inhibitory molecule is $InsP_6$ or one of its isomers.

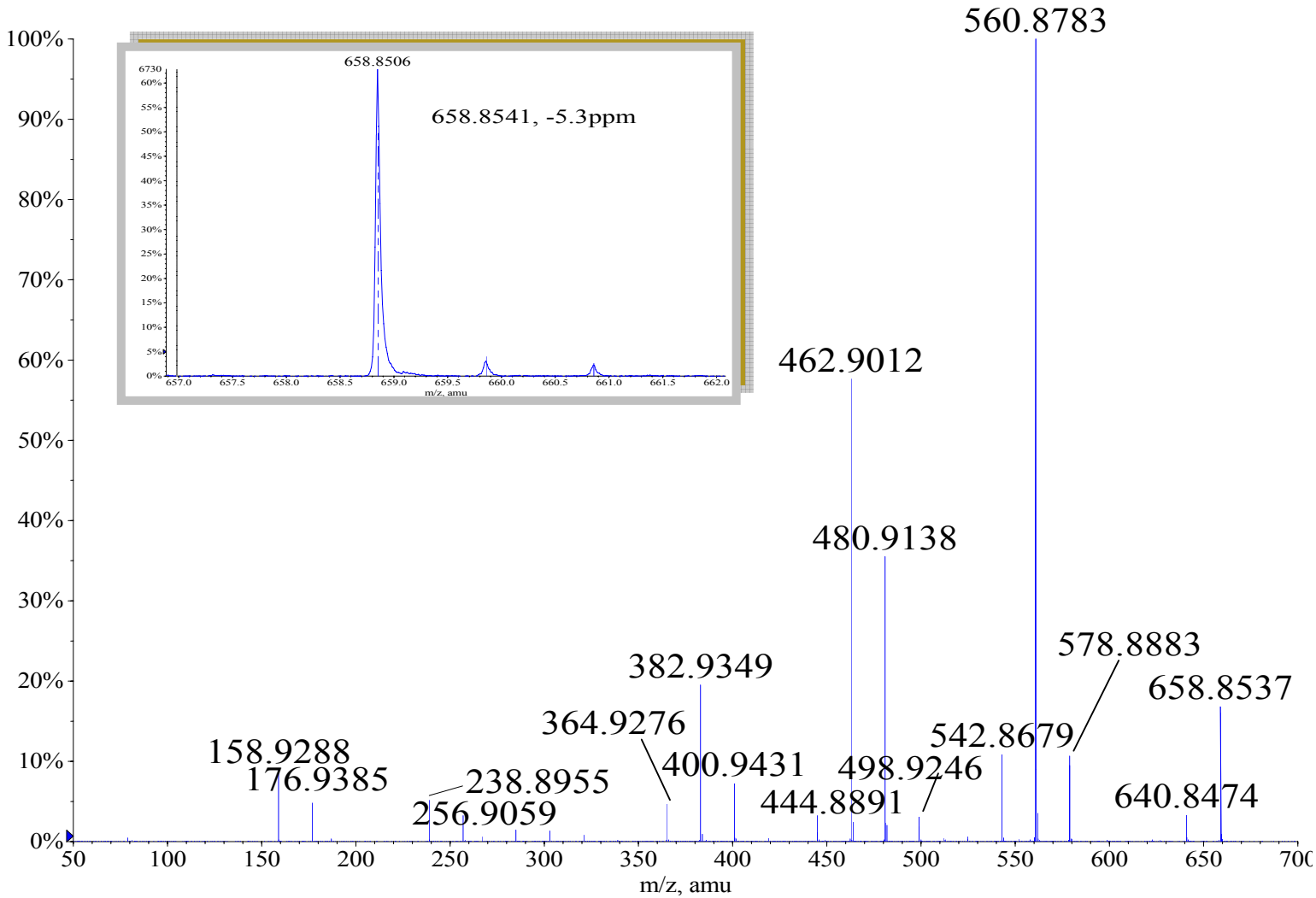

Figure 26. MS/MS on molecular ion 659 from full-term dry seed and exact MS of F2-S1-Q6-D1B (the active fraction from Superdex Peptide column) at CE 40 eV in negative polarity.

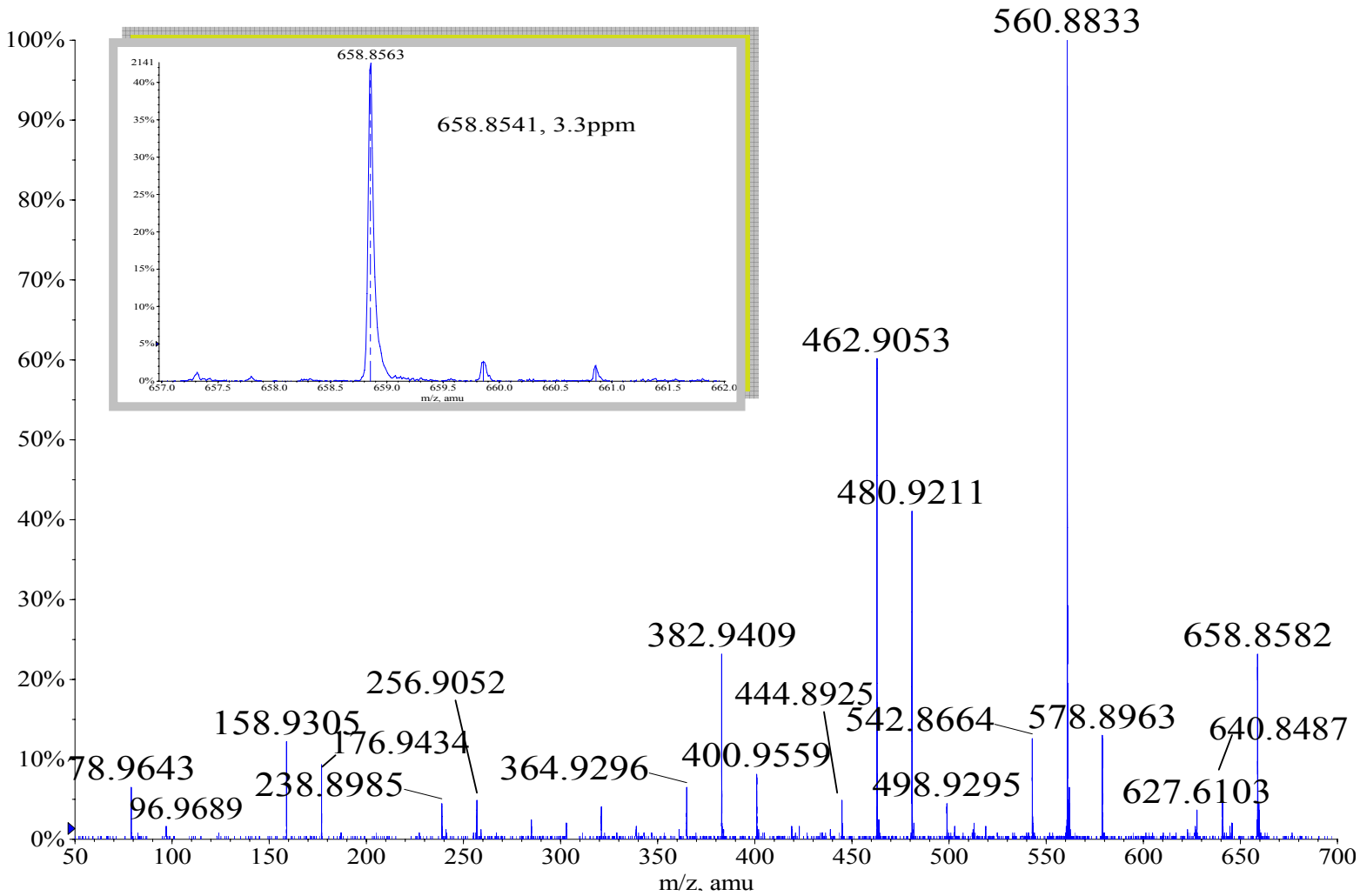

Figure 27. MS/MS on molecular ion 659 and exact MS of $InsP_6$ standard from Chromadex at CE 40 eV in negative polarity.

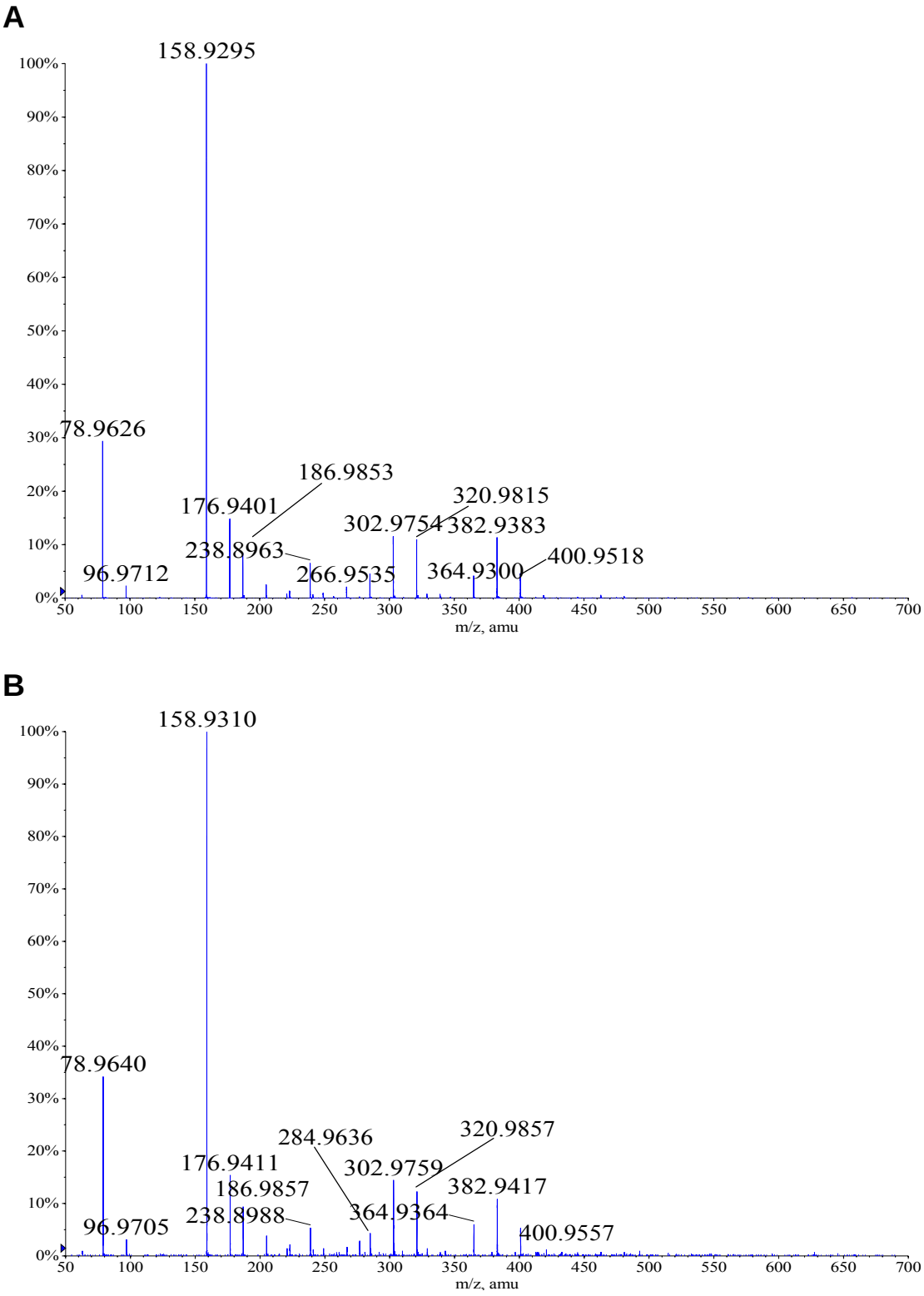

Figure 28. (A) MS/MS on molecular ion 659 of F2-S1-Q6-D1B (the active fraction from the Superdex Peptide column); (B) MS/MS on molecular ion 659 of $InsP_6$ standard from Chromadex, both at CE 80 eV in negative polarity.

NMR Characterization

One-dimensional NMR

The ^{13}C NMR spectra of F2-S1-Q6-D1B (Figure 32 bottom panel) revealed four distinct peaks at 77.40, 75.89, 74.51 and 73.39 ppm with an intensity ratio of 1:2:1:2, suggesting six carbons with two independent pairs of equivalent carbons and two non-equivalent individual carbons. Similar patterns were observed in both ^{1}H NMR (four distinct peaks at 4.59, 4.09, 3.82 and 3.76 ppm with an intensity ratio of 1:2:1:2, Figure 30 top panel) and ^{31}P NMR (four distinct peaks at 2.54, 2.29, 2.06 and 1.63 ppm with an intensity ratio of 1:2:1:2, Figure 31 top panel) spectra of F2-S1-Q6-D1B. A database search within SDBS based on ^{13}C NMR spectra found one match as *myo*-inositol. All these results suggest that the inhibitory molecule is an organophosphorus compound containing six phosphates, each directly linked to a (-CH) group of *myo*-inositol.

To confirm that the inhibitory molecule is indeed $InsP_6$, commercially available $InsP_6$ was used to obtain both 1-D and 2-D NMR spectra. The ^{1}H NMR, ^{31}P NMR and ^{13}C NMR spectra of both F2-S1-Q6-D1B and the commercial $InsP_6$ are presented in Figure 30, 31, 32, respectively. The pH of F2-S1-Q6-D1B was measured at 8.22 and all its spectra were recorded at this value. The commercial $InsP_6$ was prepared from its dodecasodium salt through cation exchange resin and the pH adjusted to the same value using NaOD, in order to circumvent the generation of extra NaCl. The ^{1}H chemical shift assignments were made according to Murthy *et al* (Bauman et al., 1999). The Chemical structure of $InsP_6$ is shown in Figure 29 with six carbons labeled. Assignments of ^{13}C and ^{31}P resonances were made from a 2D ^{1}H-^{13}C HSQC (Figure 35) and a 2D ^{1}H-^{31}P HSQC (Figure 37), respectively. Both chemical shifts and splitting patterns of F2-S1-

Q6-D1B are identical to those of the commercial $InsP_6$, suggesting that the inhibitory molecule in F2-S1-Q6-D1B is $InsP_6$. The chemical shift assignments and coupling constants are listed in Table 5-7.

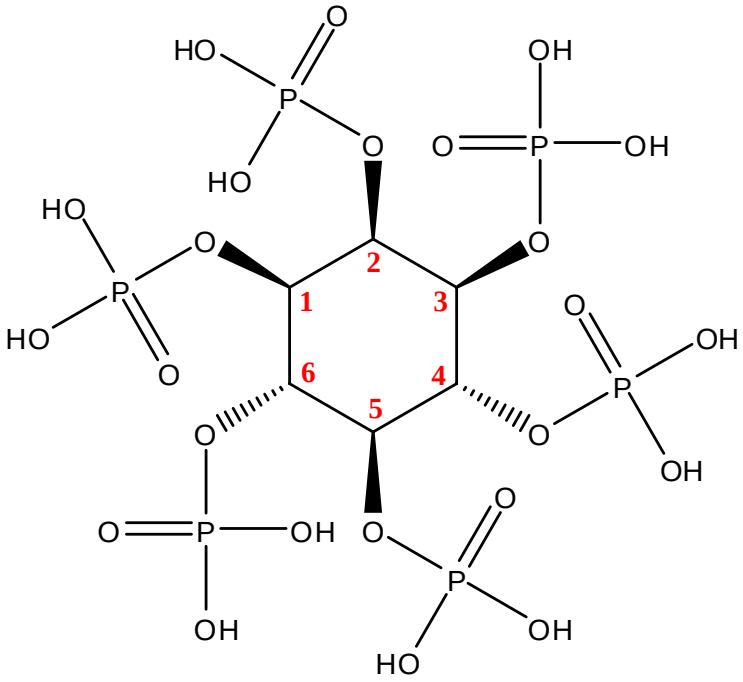

Figure 29. Chemical structure of $InsP_6$.

Table 5. ^{1}H chemical shift assignments and coupling constants of F2-S1-Q6-D1B and commercial $InsP_6$.

	^{1}H Chemical Shift	***Proton Position***	***Integration***	***Multiplicity***	***J (Hz)***
F2-S1-Q6-D1B	4.59	2	1	d	$J_{2\text{-}P1}$ (8.803)
	4.09	4/6	2	q	$J_{4/6\text{-}5}$ (9.048)
	3.82	5	1	m	$J_{4/6\text{-}5}$ (9.048)
	3.76	1/3	2	t	$J_{3\text{-}4}$ (8.314) $J_{1\text{-}6}$ (8.314)
Commercial $InsP_6$	4.56	2	1	d	$J_{2\text{-}P1}$ (9.048)
	4.08	4/6	2	q	$J_{4/6\text{-}5}$ (9.537)
	3.79	5	1	m	$J_{4/6\text{-}5}$ (9.537)
	3.74	1/3	2	t	$J_{3\text{-}4}$ (8.803) $J_{1\text{-}6}$ (8.803)

Table 6. ^{31}P chemical shift assignments of F2-S1-Q6-D1B and commercial $InsP_6$.

	^{31}P Chemical Shift	***Phosphate Position***	***Integration***	***Multiplicity***
F2-S1-Q6-D1B	2.54	5	1	s
	2.29	1/3	2	s
	2.06	2	1	s
	1.63	4/6	2	s
Commercial $InsP_6$	2.72	5	1	s
	2.54	1/3	2	s
	2.30	2	1	s
	1.75	4/6	2	s

Table 7. ^{13}C chemical shift assignments of F2-S1-Q6-D1B and commercial $InsP_6$.

	^{13}C Chemical Shift	***Carbon Position***	***Integration***	***Multiplicity***
F2-S1-Q6-D1B	77.40	5	1	s
	75.89	4/6	2	s
	74.51	2	1	s
	73.39	1/3	2	s
Commercial $InsP_6$	77.47	5	1	s
	75.77	4/6	2	s
	74.72	2	1	s
	73.38	1/3	2	s

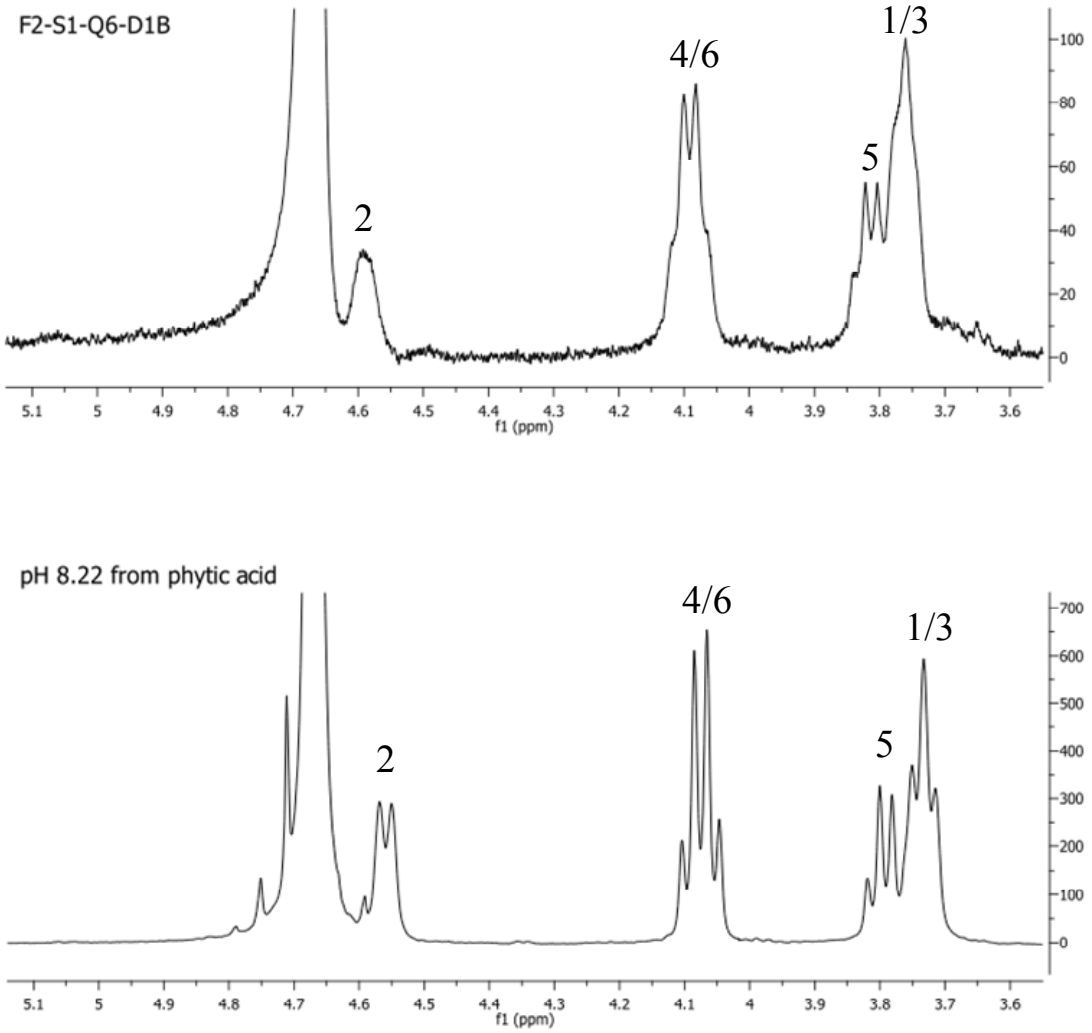

Figure 30. ^{1}H NMR spectra of F2-S1-Q6-D1B and $InsP_6$ standard at pH 8.22.

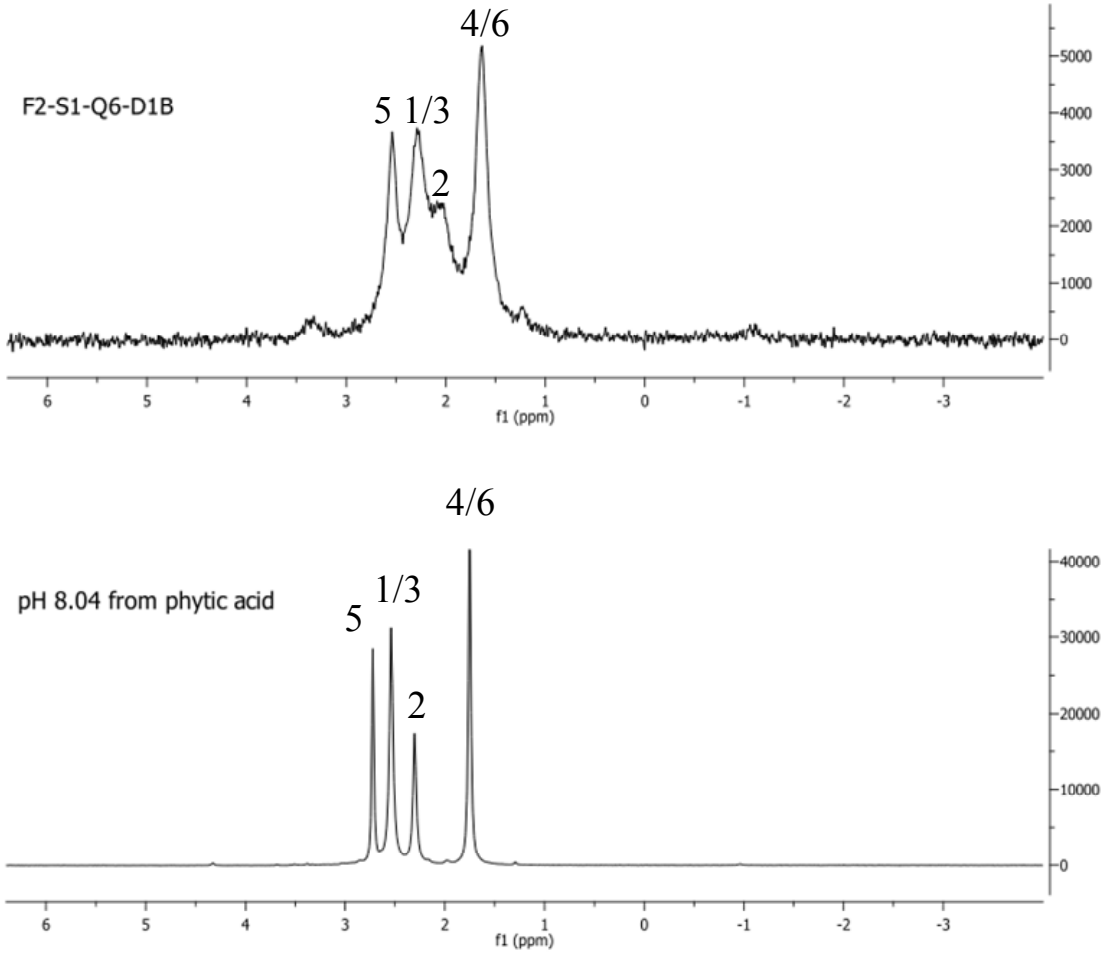

Figure 31. ^{31}P NMR spectra of F2-S1-Q6-D1B and $InsP_6$ standard at pH 8.04.

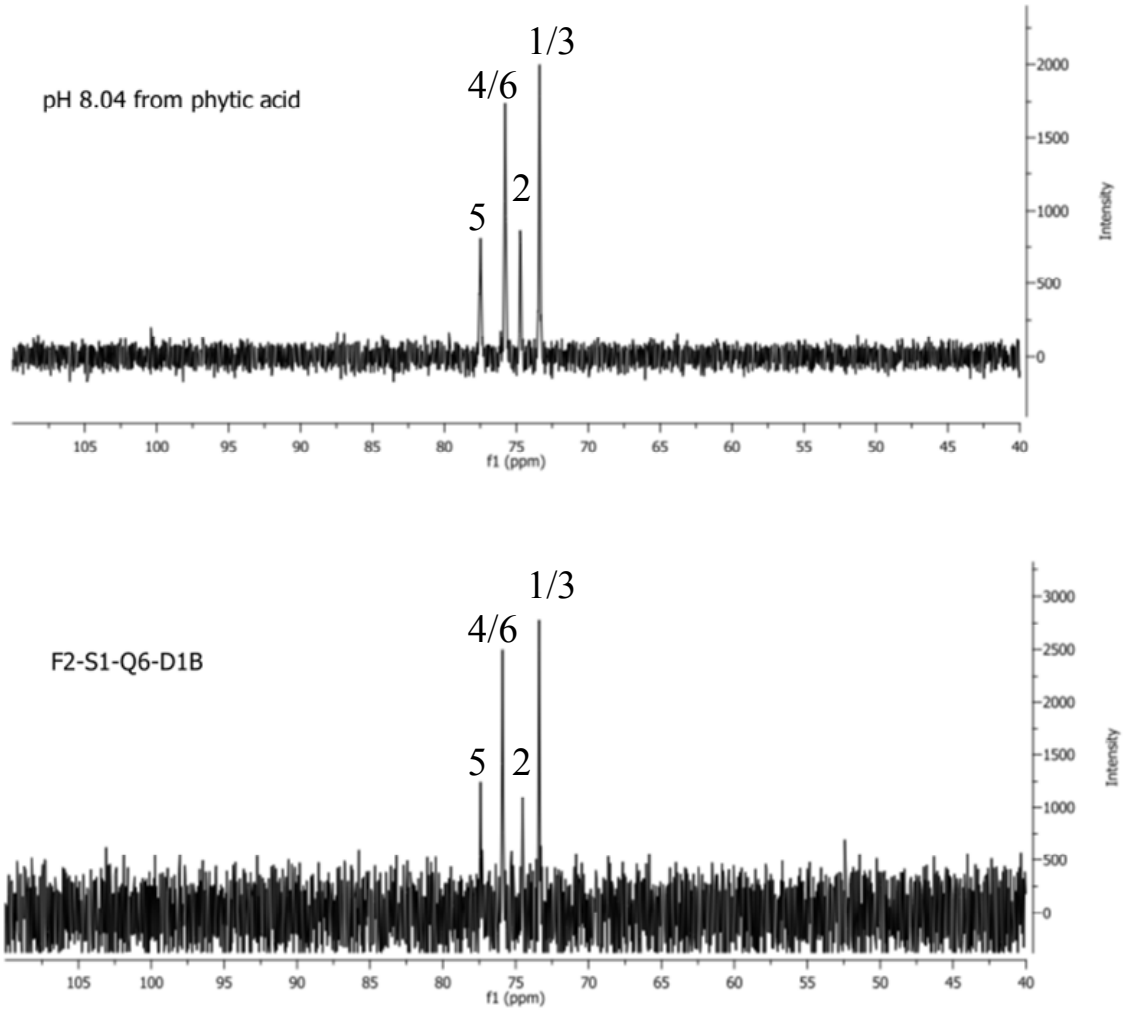

Figure 32. ^{13}C NMR spectra of F2-S1-Q6-D1B and $InsP_6$ standard at pH 8.04.

$InsP_6$ has six phosphomonoester groups attached to the inositol ring, and possesses six strong acid sites with pK_a ~1.8, two moderately weak acid sites with pK_a ~6.3, one weak acid site with pK_a ~8.6, and three least acidic protons with pK_a values of 9.2 to 9.6 (Barre et al., 1954; Isbrandt and Oertel, 1980). Initial NMR spectra of the commercial $InsP_6$ obtained from sodium phytate with its pH adjusted to 8.45 did not match very well with the spectra of F2-S1-Q6-D1B. Furthermore, ^{31}P NMR spectra are extremely sensitive to pH and various factors such as temperature, pH meter error and equilibration time can affect pH readings during measurement, although later commercial $InsP_6$ was adjusted to the same pH value as that of F2-S1-Q6-D1B. Therefore, a series of ^{1}H (Figure 33) and ^{31}P NMR (Figure 34) spectra were recorded over the pH range 8.0 – 8.5 of the commercial $InsP_6$. The ^{1}H NMR of the commercial $InsP_6$ revealed that spectra are identical at pH 8.04, 8.13 and 8.22, whereas ^{1}H resonances started shifting at pH 8.35. It is evident that the spectrum obtained from sodium phytate with its pH adjusted to 8.45 exhibited downfield chemical shifts of all corresponding ^{1}H resonances, most likely due to NaCl generated by dissociation of Na^+ from sodium phytate via the addition of HCl (Malinowski et al., 1966). ^{31}P NMR spectra changed drastically with different pH values, including both chemical shift and intensity ratios. For example, at pH 8.13, only three ^{31}P resonances were observed at 3:1:2, whereas after an increase of only 0.09 pH unit, another ^{31}P resonance appeared and the intensity ratio changed to 2:1:1:2. In addition, ^{31}P resonances have a trend to shift downfield as the pH increases.

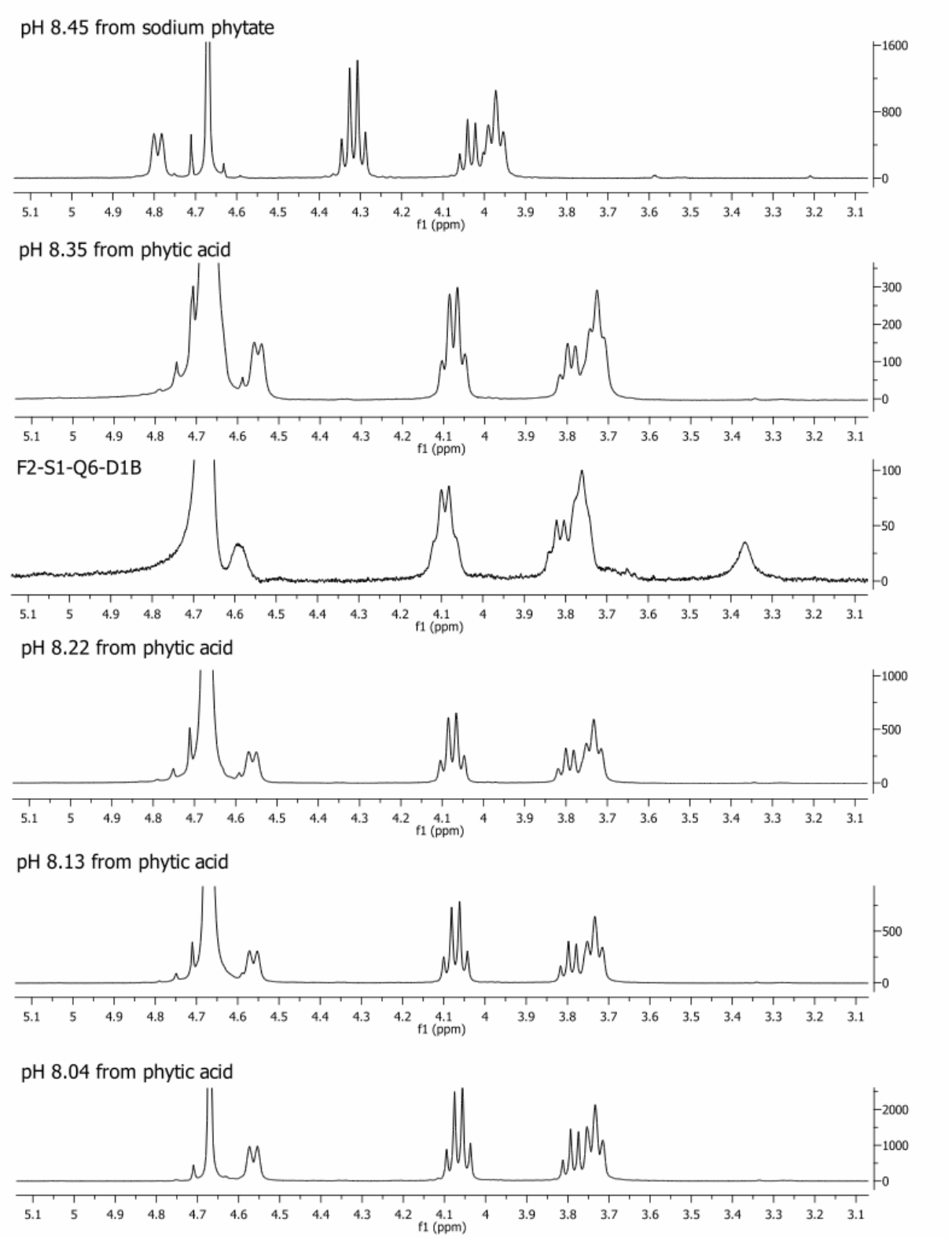

Figure 33. ^{1}H NMR spectra of F2-S1-Q6-D1B and $InsP_6$ standard at different pH over the range 8.0 -- 8.5.

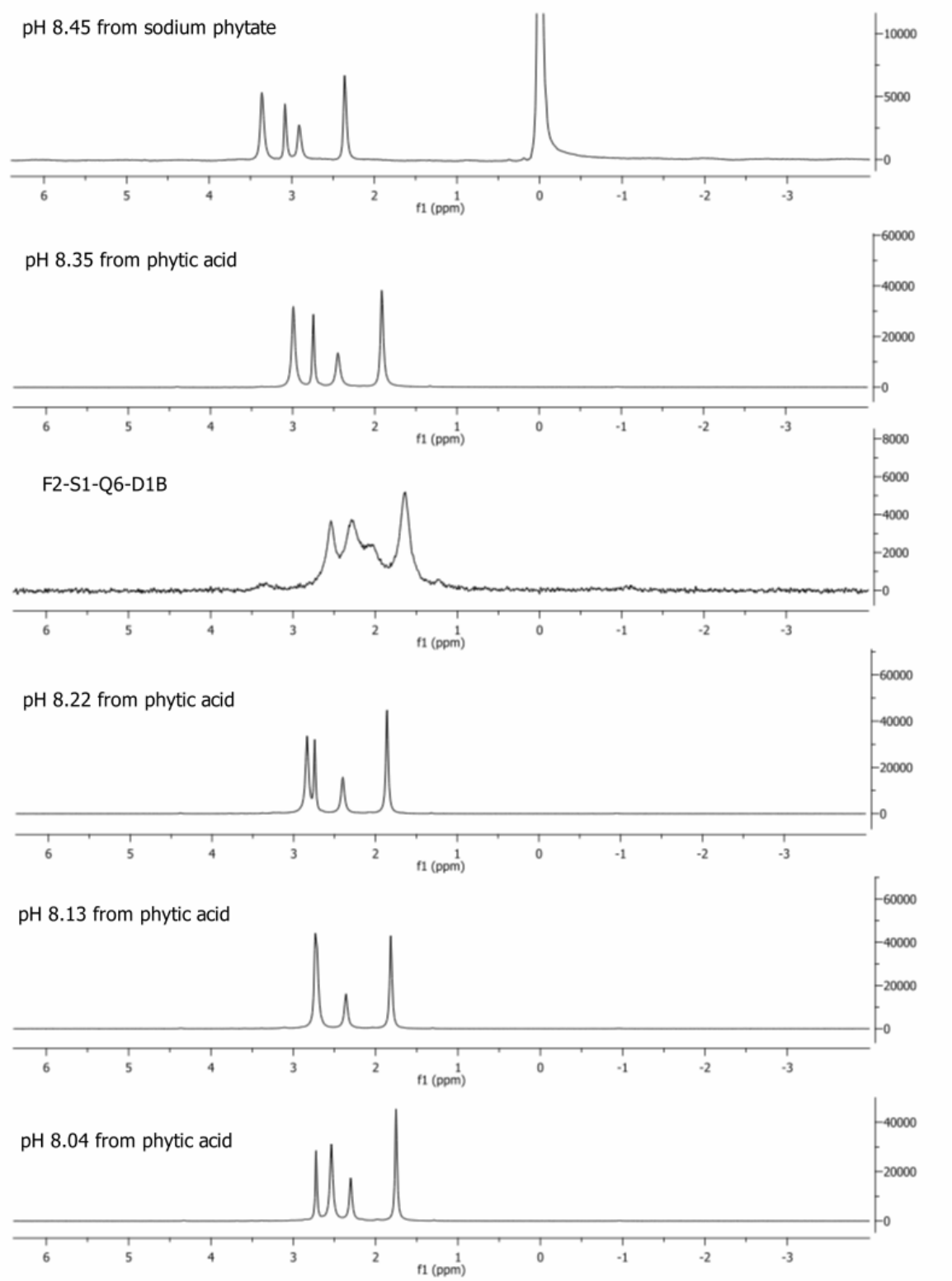

Figure 34. ^{31}P NMR spectra of F2-S1-Q6-D1B and $InsP_6$ standard at different pH over the range 8.0 -- 8.5.

Two-dimensional NMR

Two-dimensional ^{1}H-^{31}P HSQC, ^{1}H-^{13}C HSQC and ^{1}H-^{1}H COSY experiments were obtained for both F2-S1-Q6-D1B (Figures 35-37) and the commercial $InsP_6$ (Figures 38-40) to assign the chemical shifts as well as to compare the correlation patterns. All 2-D NMR of F2-S1-Q6-D1B showed identical correlation patterns to those obtained from the commercial $InsP_6$. Consistency in correlation patterns, chemical shifts and intensity ratios in all 1-D and 2-D NMR spectra strongly confirm that the pure molecule from the active fraction F2-S1-Q6-D1B is $InsP_6$.

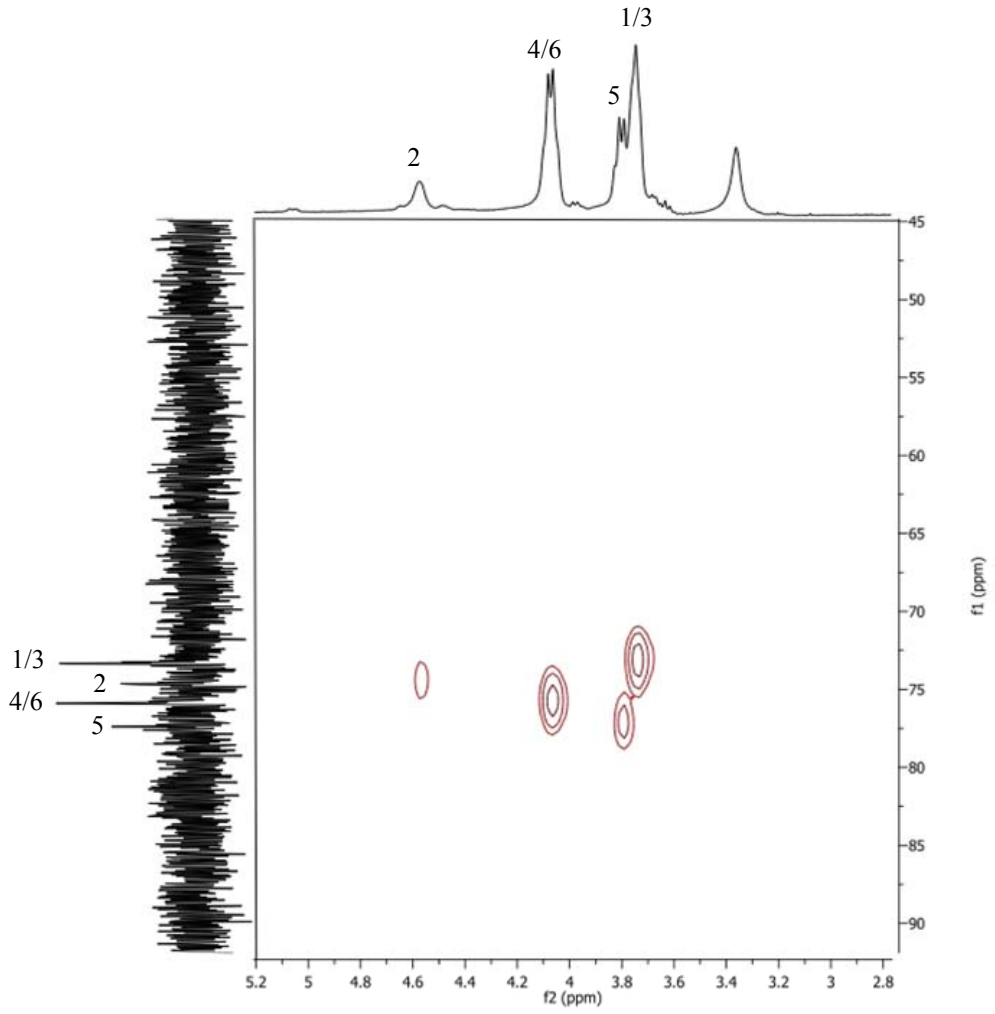

Figure 35. ^{1}H-^{13}C HSQC of F2-S1-Q6-D1B.

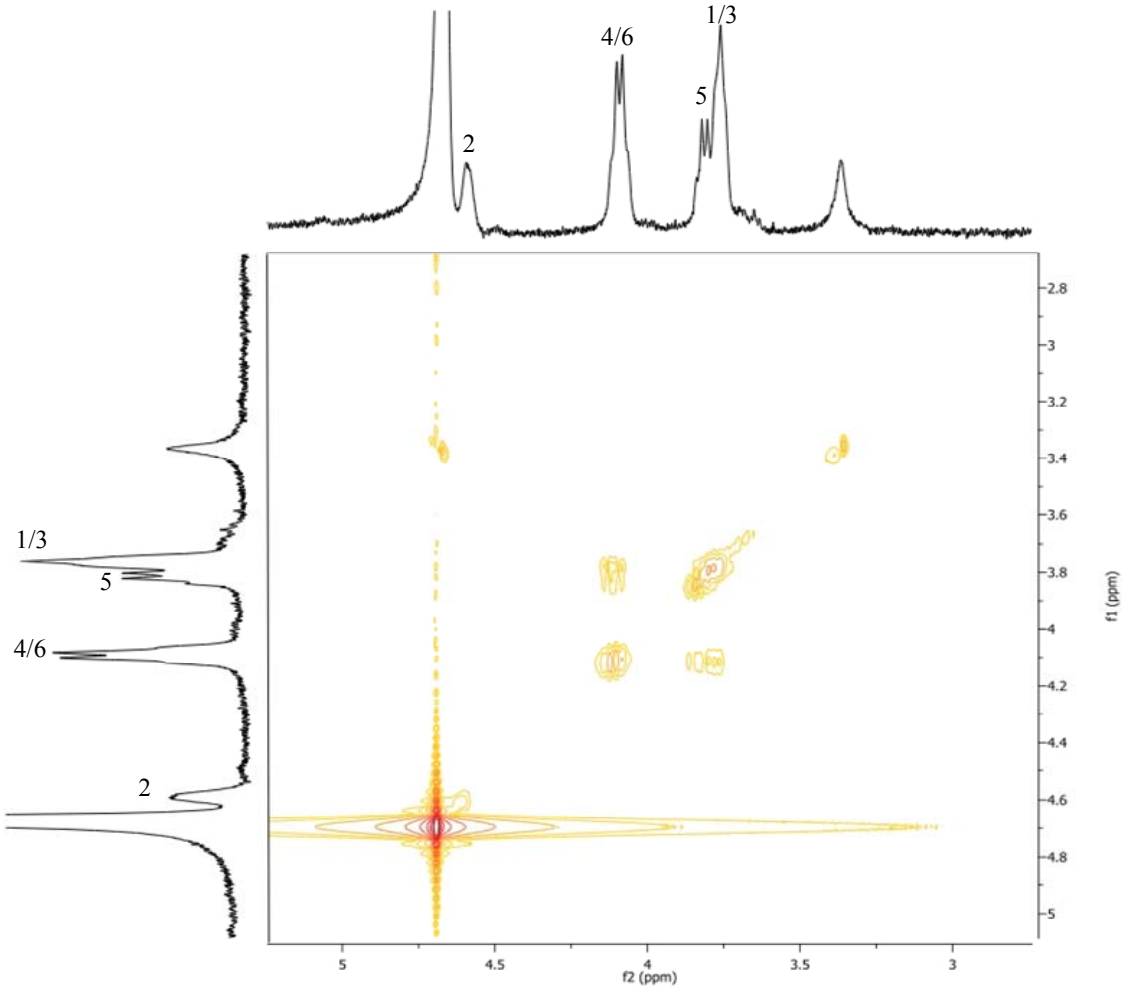

Figure 36. ^{1}H-^{1}H COSY of F2-S1-Q6-D1B.

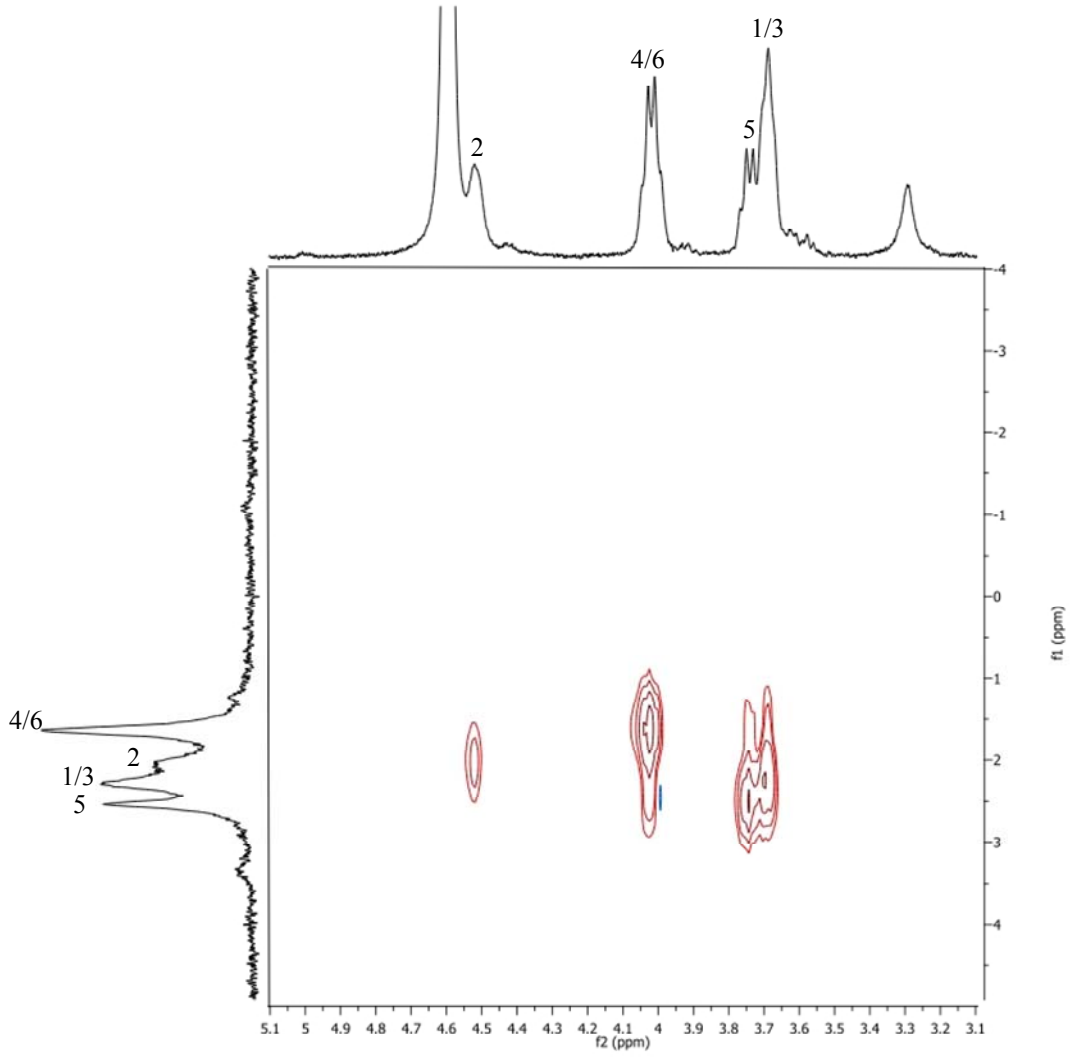

Figure 37. ^{1}H-^{31}P HSQC of F2-S1-Q6-D1B.

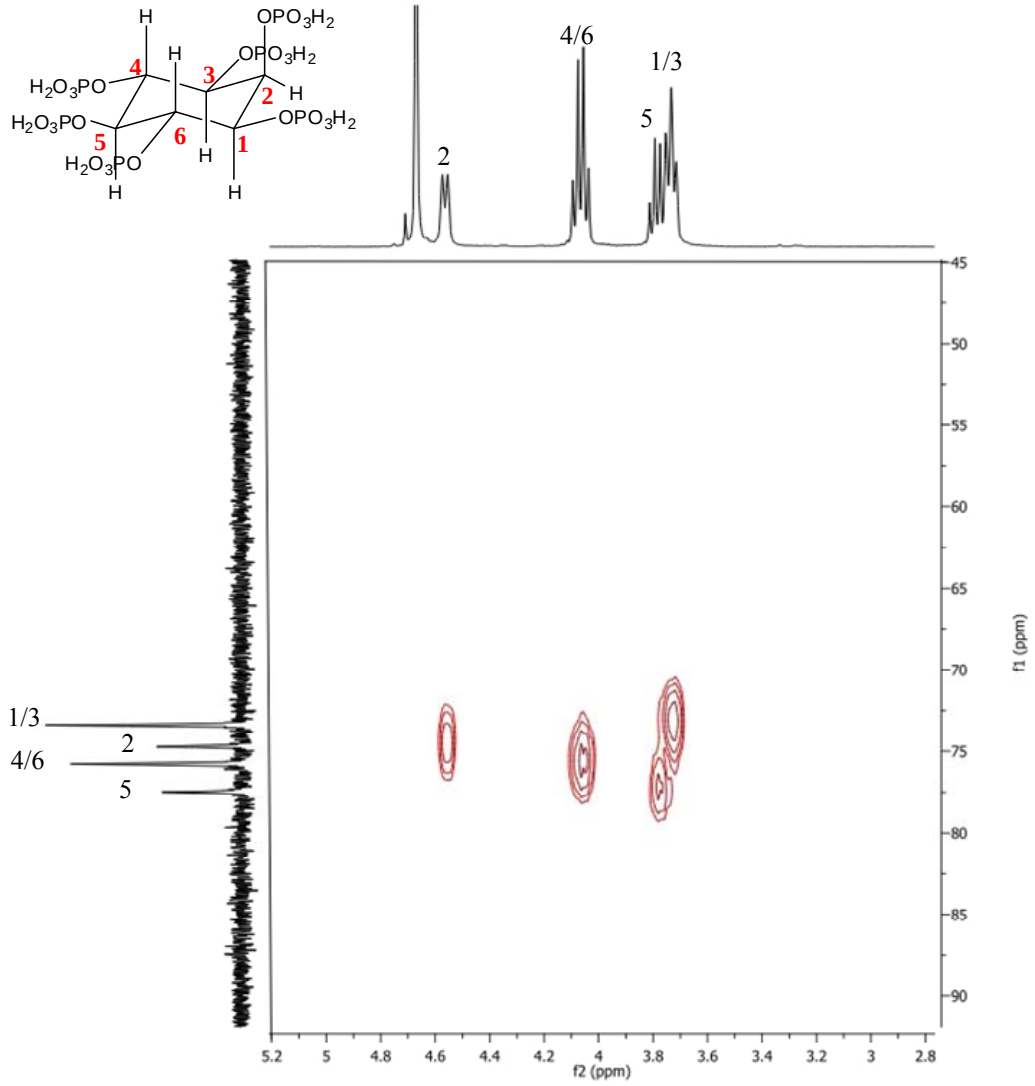

Figure 38. ^{1}H-^{13}C HSQC of $InsP_6$ standard.

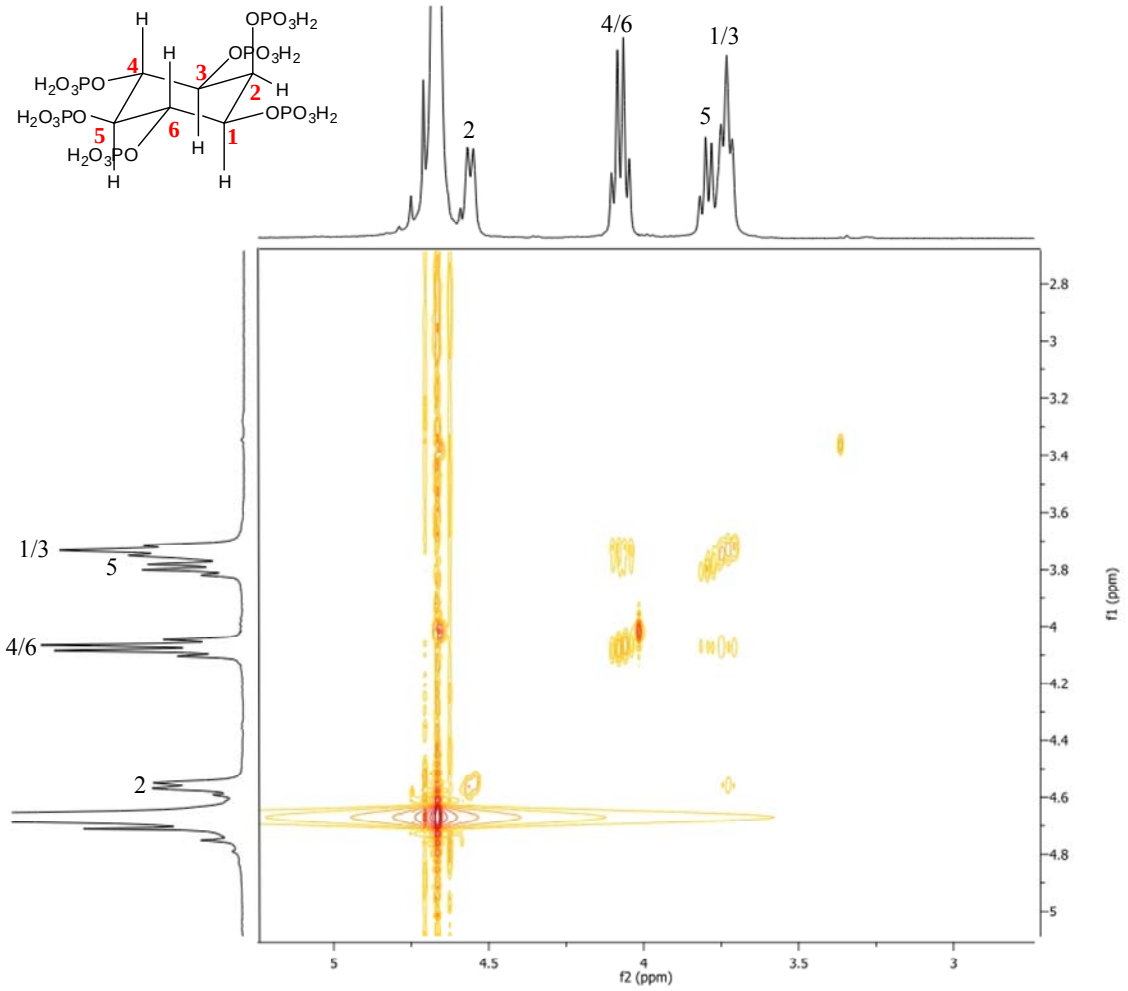

Figure 39. ^{1}H-^{1}H COSY of $InsP_6$ standard.

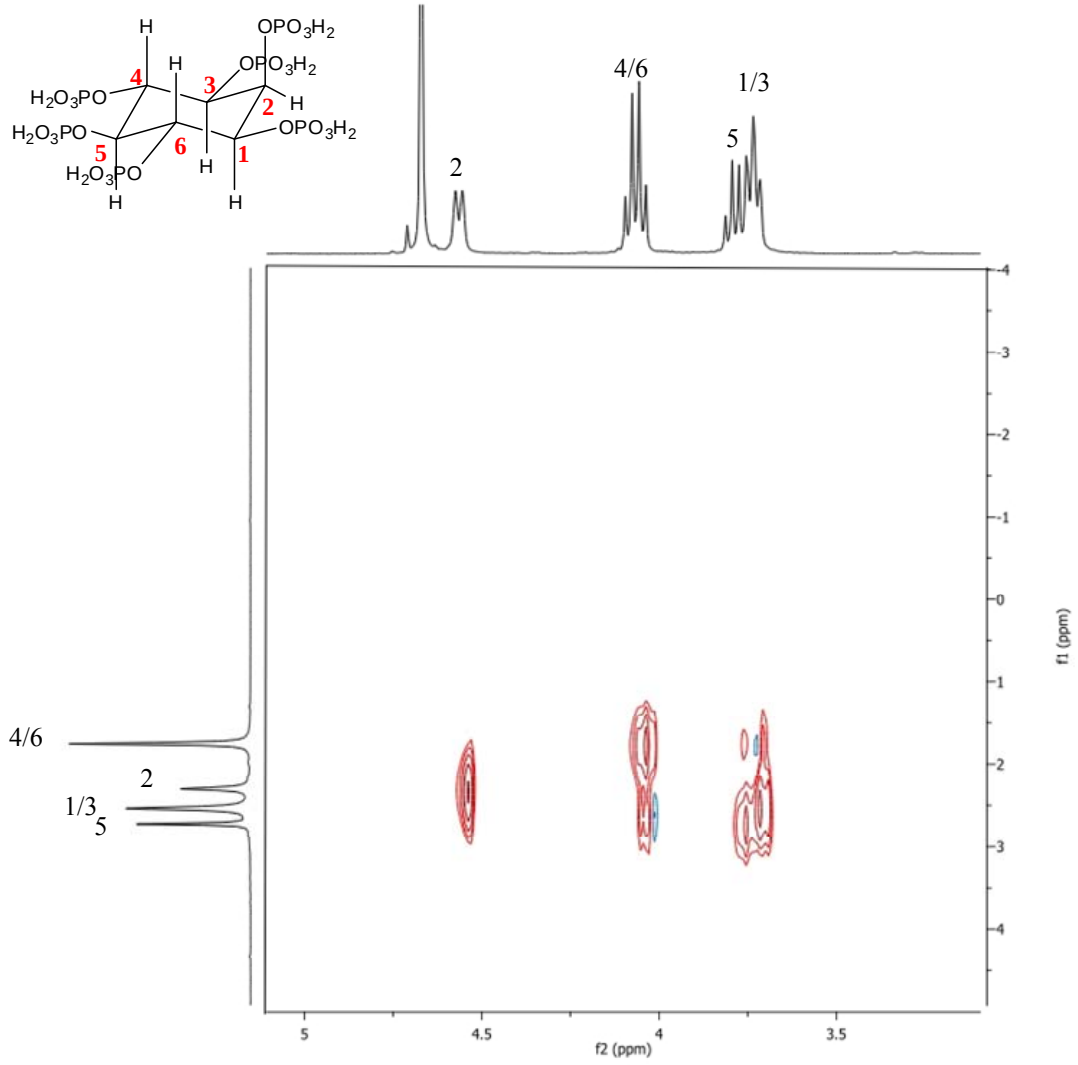

Figure 40. ^{1}H-^{31}P HSQC of $InsP_6$ standard.

Bioactivity of standard

A bioassay was carried out to investigate whether the commercial $InsP_6$ inhibits the early-stage somatic embryo growth, and whether there is a concentration response between this molecule and the bioactivity. The F2-S1-Q6-D1B fraction used for recording the NMR spectra had a pH of 8.22. $InsP_6$ possesses six strong acid sites with pK_a ~1.8, two moderately weak acid sites with pK_a ~6.3, one weak acid site with pK_a ~8.6, and three least acidic protons with pK_a values of 9.2 to 9.6 (Barre et al., 1954; Isbrandt and Oertel, 1980). Additionally, an array of sodium adduct ions were observed downstream of the $InsP_6$ peak in the LC/MS analyses. Therefore, the number of sodium cations associated with $InsP_6$ in F2-S1-Q6-D1B was assumed as eight. F2-S1-Q6-D1B corresponding to the extract from 100 FGs was previously weighed out at 0.11 mg (Table 4). Thus the mass of F2-S1-Q6-D1B was adjusted to 836 Da for the $InsP_6$-8Na salt during the calculation of the number of moles. F2-S1-Q6-D1B (20 FGs) was calculated to contain 26.3 nmoles of $InsP_6$, which corresponds to 658.9 pmoles in half a FG. Therefore, the commercial phytic acid dodecasodium salt hydrate (12 Na^+ attached) of 26.3 nmoles was used as a concentration factor of 1. A stock solution (0.53 mM) was made and concentration factors of 0.1, 0.2, 1 and 5 were generated by dilution (Table 8) and the bioassay was performed as described earlier.

All treatments of the commercial $InsP_6$ at four different concentrations inhibited the somatic embryo growth in a statistically significant manner (Figure 41). Furthermore, inhibition from the treatment with concentration factor 1 was the most significant. This result suggests a good correlation between the amount of $InsP_6$ purified from FG tissue

(1.3 nmoles per stage 9 or full-term FG) and the amount of $InsP_6$ inhibiting somatic embryo growth.

Table 8. $InsP_6$ standard preparation for bioassay.

Concentration factor to F2-S1-Q6-D1B	µg of dodecasodium phytate for each treatment	µl of stock solution added	pH (before adjustment)	pH (after adjustment)
5	121.6	250	7.52	5.71
1	24.3	50	6.84	5.68
0.2	4.9	10	6.51	5.71
0.1	2.4	5	6.30	5.70

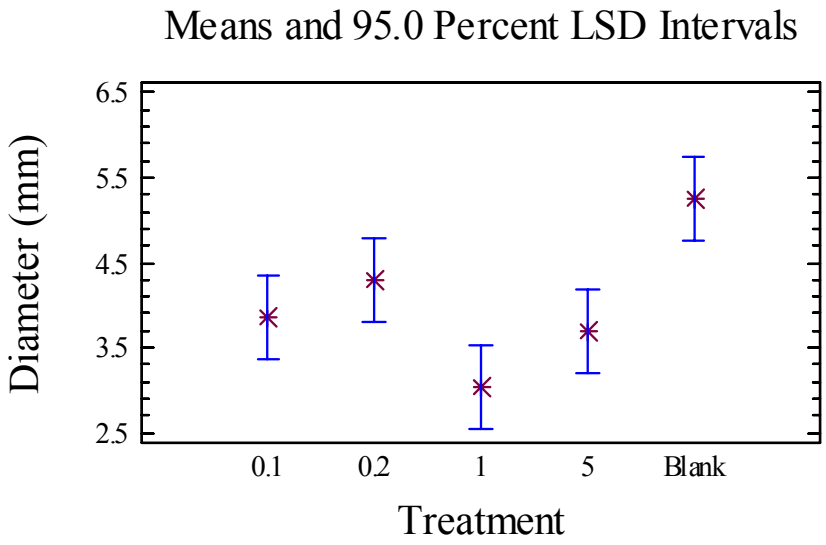

Figure 41. Bioassay result of treatment of $InsP_6$ standard with various concentrations.

Initial Characterizations as a Plant Peptide Hormone

MALDI analysis of trypsin digest

A small protein with a mass of 9607 Da was initially thought to be the inhibitory molecule present both in F2 and subfraction P3 from the Phenomenex Jupiter C5 column. Figure 42 shows the initial flow chart of separation and characterization of the inhibitory molecule. P3 was reduced by TBP (tributylphosphine), alkylated by iodoacetamide, and trypsin digested in the presence of NH_4HCO_3 and HCl according to the protocol provided with the Sigma kit. MALDI-TOF and TOF/TOF mass spectra of the resulting digest were acquired with the Applied Biosystems 4700 Proteomics Analyzer. Peptide mass fingerprint (PMF) search against NCBInr database was performed using a Mascot search engine with the submission of both MS and MS/MS spectra. The search was repeated with tryptic (both peptide ends tryptically cleaved) and semitryptic (one peptide end tryptically cleaved) cleavages. MS/MS spectra with a Mascot score higher than the significant score of 95% were assumed to be correct calls. Unfortunately, scores obtained from multiple peptide hits based on the P3 fraction were all below 80%, suggesting that no match was found in the database. *De novo* sequencing was performed through distinguishing different fragment ions directly from individual MS/MS spectra without resorting to database sequence information. However, too many peptide fragments made it impossible to assemble each complete polypeptide.

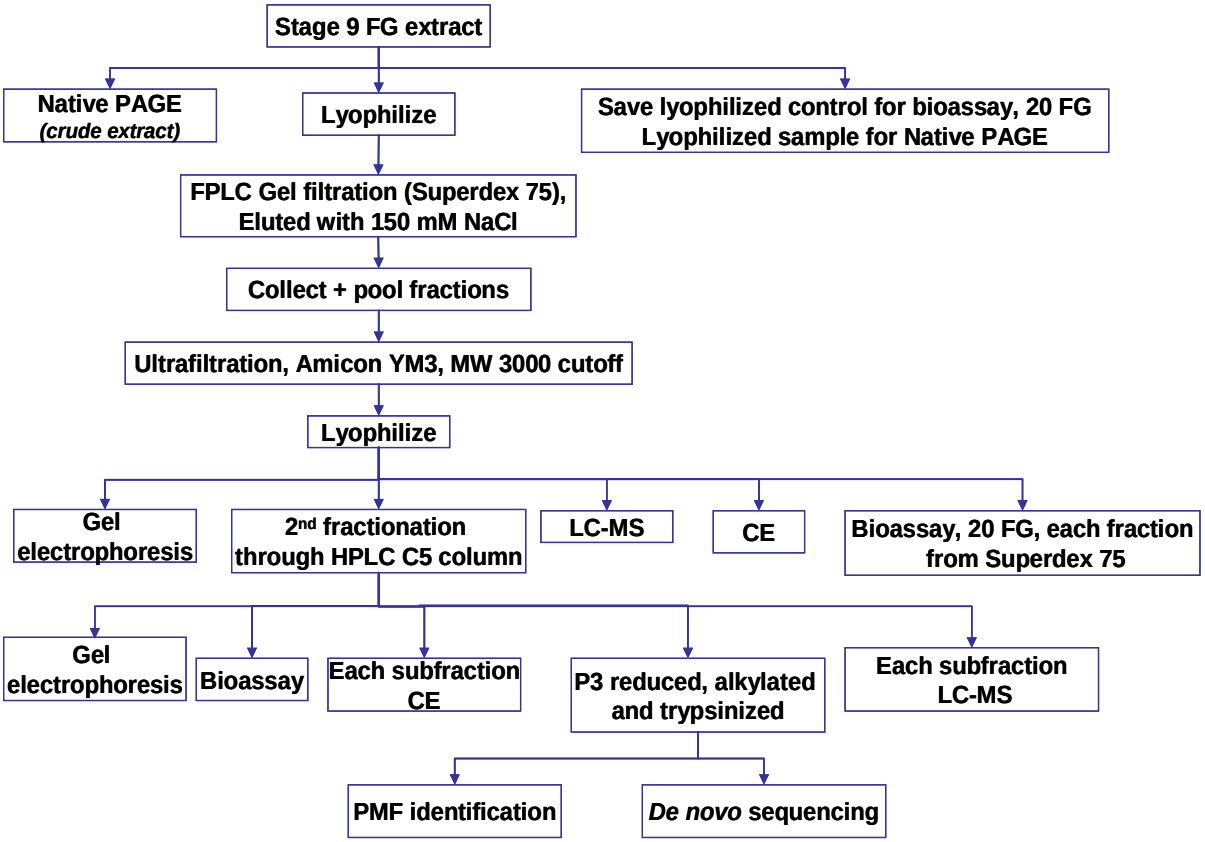

Figure 42. Initial flow chart of separation and characterization of the inhibitory molecule.

Gel and capillary electrophoresis

Gel electrophoresis (SDS-PAGE and Native-PAGE) was carried out to correlate with MS results. Fractions (F1 through F4) from the Superdex 75 column and subfractions (P1 through P3) from the Phenomenex Jupiter C5 column were separated by SDS-PAGE and stained by Coomassie Blue on a PhastSystem (GE Healthcare, Piscataway, NJ). Multiple protein bands were observed from the active fraction F2, and four distinct bands were labeled with arrows (Figure 43). However, none of the subfractions from the Jupiter C5 column showed any distinct bands, and neither did subfractions from the Mono S column (data not shown), although LC/MS detected one distinct protein of 9607 Da in the P3 subfraction from the C5 column and several small peptides ranging from 2000 to 3000 Da in the F2-S1 subfraction from the Mono S column. This lack of correlation between gel electrophoresis and MS indicated that the latter is significantly more sensitive than the former under such low concentrations of samples. Therefore, this gel electrophoresis methodology was abandoned for characterization of subsequent active fractions.

Capillary electrophoresis (CE) analyses including SDS-gel MW and IEF were performed on a Proteolab PA 800 (Beckman Coulter, Fullerton, CA), mainly for the investigation of new separation methodologies, but also for the correlation with MS results. Due to the lack of ability to collect separated fractions, CE could only be used for the structure characterization. Figure 44A shows the calibration electropherogram of the capillary (50 μmID × 57 cm length) using standards ranging from 10 to 225 kD. However, as shown in Figure 44B, most components in F2 and subfractions P1, P2, P3 were below 10 kD, suggesting that this SDS-gel MW CE protocol is not applicable to the

structure elucidation of the inhibitor. Therefore, this CE methodology was also abandoned for characterization of subsequent active fractions.

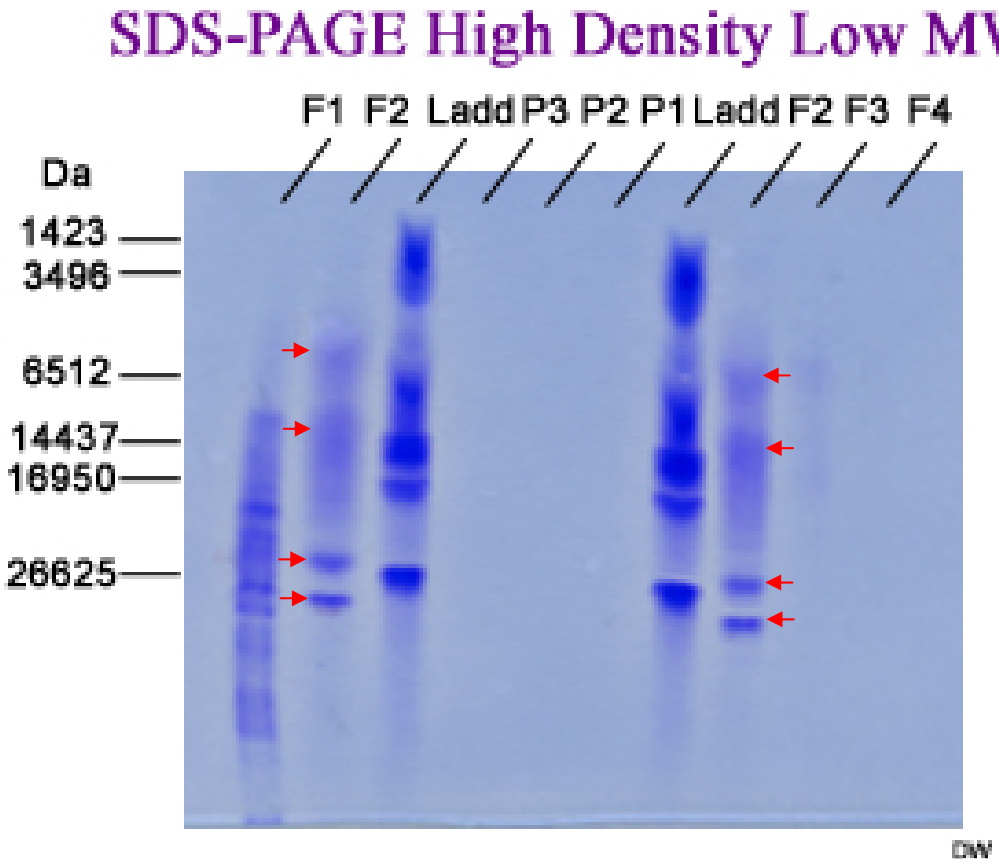

Figure 43. SDS-PAGE of fractions from the Superdex 75 and the Phenomenex Jupiter C5 columns.

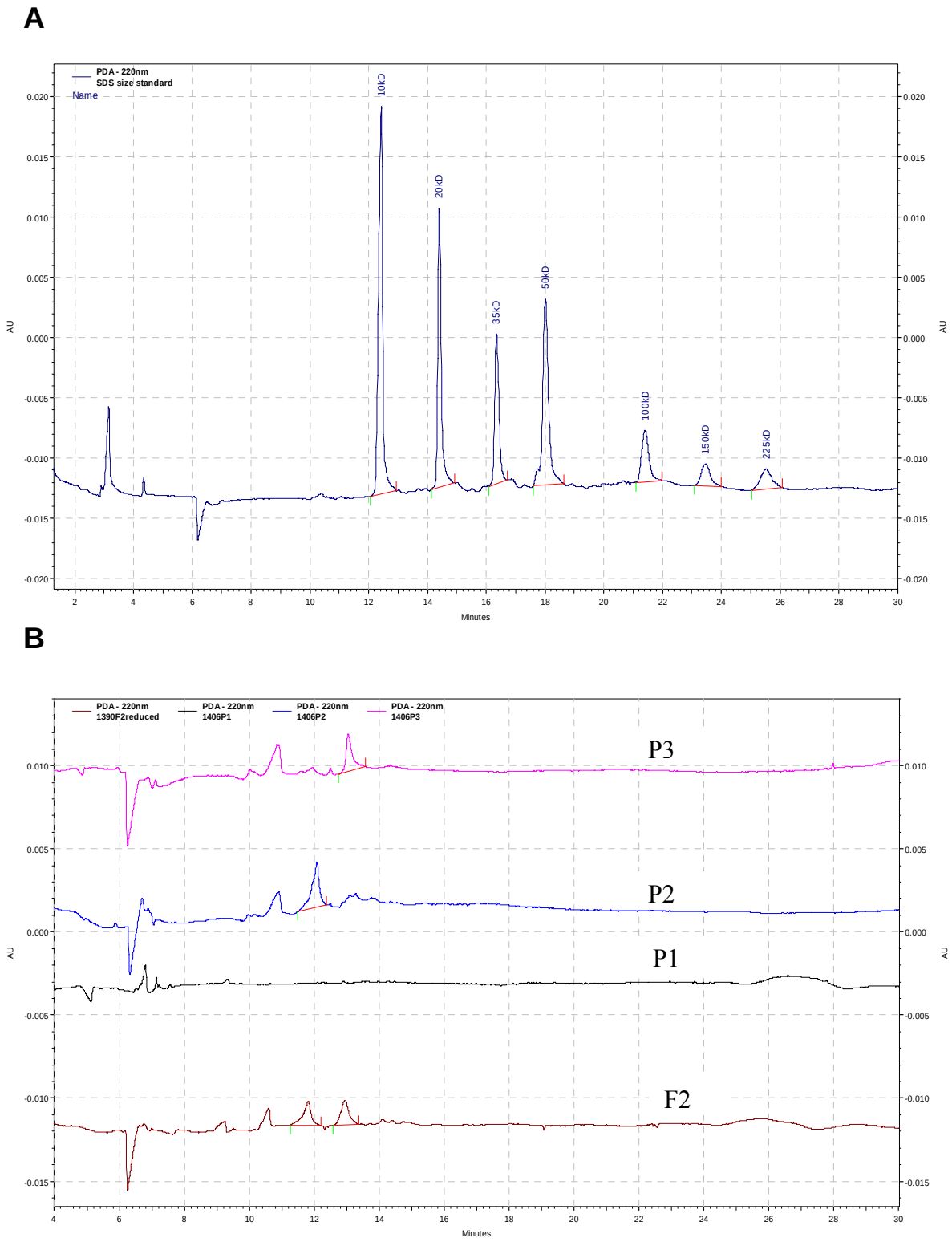

Figure 44. (A) Calibration electropherogram of the capillary (50 μmID × 57 cm length) using standards ranging from 10 to 225 kD; (B) electropherogram of CE separations of F2, P1, P2 and P3.

Separation and characterization of Stimulator

The preliminary results of the stimulator project were obtained by Dr. Charlie Oldham in our lab. Stage 2 or 3 FGs were water extracted and lyophilized to dryness. The lyophilized powder was subjected to 0.1% TFA precipitation. The resulting supernatant was loaded on a C18 solid-phase extraction cartridge and the flow-through was collected and lyophilized. The lyophilized product was separated by an Allsphere C8 HPLC column (4.6 × 250 mm, Alltech, Deerfield, IL) using acetonitrile as mobile phase A and potassium phosphate as mobile phase B. After the stimulator project was taken over by me, a further separation protocol of the bioactive fraction from C8 was established. An Allsphere semi-prep C18 HPLC column (10 × 250 mm, Alltech, Deerfield, IL) was used with methanol as mobile phase A and water as B, both containing 0.1% TFA, at a flow rate of 4.7 ml/min. A 30-min gradient was applied: 3% A for 12 min, 3% to 14% A over 13 min, 14% to 3% A for 5 min. The subfraction eluting from 3.7 to 4.5 min showed statistically significant inhibition to somatic embryo growth. Thus the bioactive subfraction was analyzed by LC/MS. Unlike the inhibitor which has multiple proteins present in the active fraction from the Superdex 75 column, the stimulator did not show any multiple charged state indicating peptides or proteins. This suggested that the stimulator is a small molecule, not a plant peptide hormone. Original flow chart of isolation and characterization of the stimulator is shown in Figure 45.

This project was then taken over by Dr. Veronica DeSilva from this point. She modified some of the isolation procedures by eliminating the C8 column and adding a Prevail C18 column (Waters, Milford, MA). The stimulator was later characterized as citric acid by means of proton NMR and fast atom bombardment MS. A good correlation

was found between the amount of citric acid isolated from the FG tissue (65 nmoles per stage 2-3 FG) and the amount of citric acid that stimulates colony growth (25 to 50 nmoles) when applied topically to early-stage somatic embryos (DeSilva et al., 2007).

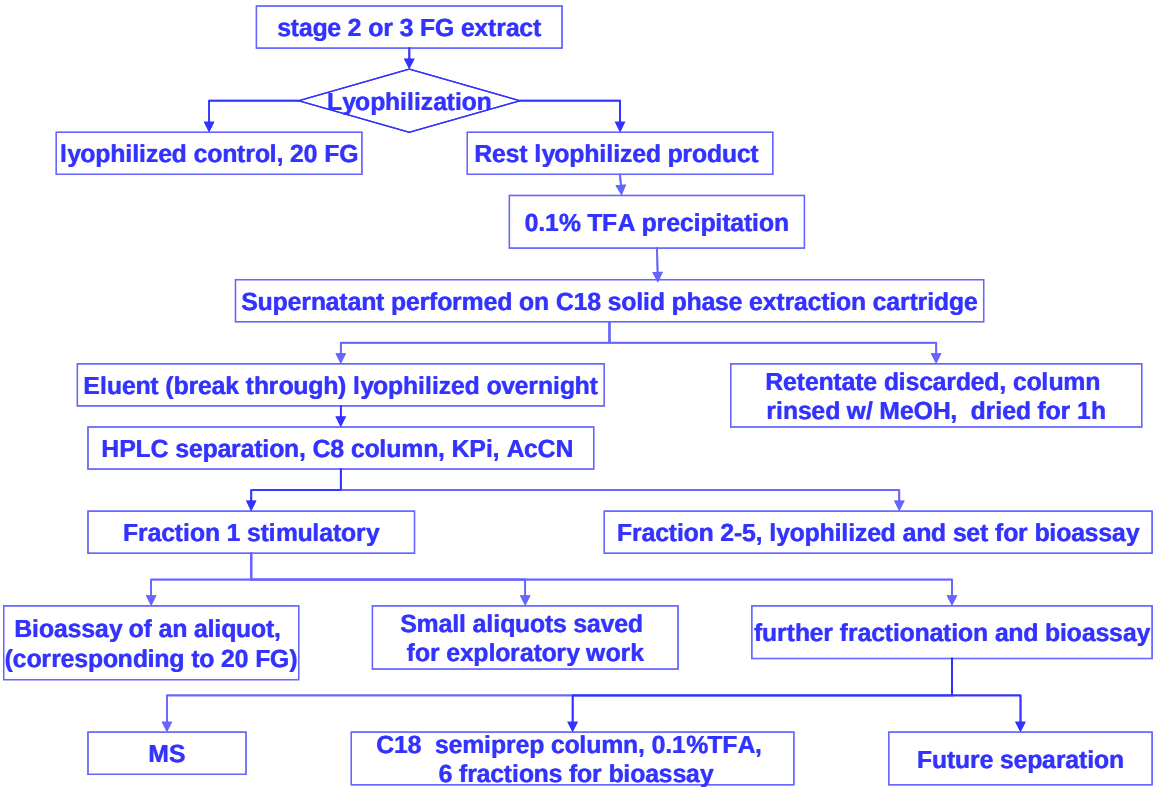

Figure 45. Original flow chart of isolation and characterization of the stimulator.

CHAPTER IV

DISCUSSION

Summary and importance of the discovery

We present here the first report of isolation of *myo*-inositol hexa*kis*phosphate ($InsP_6$) from FG tissue in LP seeds. The highly anionic $InsP_6$ was purified by water extraction, two gel filtrations and two ion exchange FPLC chromatographies. The results presented here also represent the first complete structural characterization of $InsP_6$ from a natural product. Identical exact mass and fragmentation patterns obtained from high resolution exact mass measurement and MS/MS analysis established that the purified compound from FG tissue is one of the isomers of inositol hexa*kis*phosphate. Direct structural identification of this FPLC purified inositol hexa*kis*phosphate was then performed using ^{1}H-, ^{31}P- and ^{13}C-NMR, ^{1}H-^{1}H COSY, ^{1}H-^{31}P HSQC and ^{1}H-^{13}C HSQC. The results unequivocally established that the molecule isolated from FG tissue is $InsP_6$.

We also report here the first evidence of inhibition of embryonic cell growth and development by $InsP_6$ in LP. SE in conifers is based on the natural occurrence of cleavage polyembryony *in vivo*. This technology has been serving as a model to study early regulatory and morphogenetic events in higher plants (Zimmerman, 1993; Quiroz-Figueroa et al., 2006; Imin et al., 2007). An early-stage somatic embryo multiplication assay was used as a search for inhibitory activities. This assay was also used recently to identify and isolate citric acid as a stimulator to growth of somatic embryos (DeSilva et al., 2007). We demonstrated that topical application of commercial $InsP_6$ to early-stage

somatic embryos indeed inhibits embryonic growth in a statistically significant manner. Furthermore, we found that there is a good correlation between the amount of $InsP_6$ purified from FG tissue (1.3 nmoles per full-term FG) and the amount of $InsP_6$ which inhibits somatic embryo growth.

$InsP_6$ is ubiquitous and the most abundant inositol phosphate derivative in eukaryotic cells. It is known for its anticancer activity by reducing the proliferation of malignant cells (Shamsuddin et al., 1992; Shamsuddin and Yang, 1995; Ferry et al., 2002). Additionally, $InsP_6$ increases differentiation of malignant cells leading to reversion to the normal phenotype with decreasing production of tumor markers (Shamsuddin and Vucenik, 2005). However, reduction of proliferation in plant cells has not been reported to date, and the real function of $InsP_6$ in plants is still an enigma. Our findings constitute the first observation of $InsP_6$ inhibiting cell proliferation in plants.

Purification and Identification of $InsP_6$

Due to its six anionic phosphate groups, $InsP_6$ has mainly been separated from other inositol phosphates using high-performance strong anion exchange chromatography (Skoglund et al., 1998; Talamond et al., 1998; Talamond et al., 2000; Carlsson et al., 2001) or ion-pair HPLC with refractive index detection (Hamada, 2002). The former technique can be performed using either of two chromatographic systems: one uses hydrochloric acid gradient elution with post-column reaction with a solution of iron nitrate and perchloric acid and UV detection at 295 nm (Chen and Li, 2003); the other uses a sodium hydroxide gradient with chemically suppressed conductivity detection (Talamond et al., 2000). $InsP_6$ purification from a parasitic cestode has also been

reported recently (Irigoin et al., 2002), in which $InsP_6$ was detected in the hydatid cyst wall of the larval stage of the cestode parasite *Echinococcus granulosus*. Purification was achieved by two sequential FPLC columns, a Source 15Q strong anion exchange column and a Superdex 75 gel filtration column (both from GE Healthcare). Dialysis was carried out using a 12 kD cut-off membrane after the Source 15Q column and the inhibitory activity of *in vitro* complement-activation assay remained afterwards. In addition, based on the calibration curve of Irigoin *et al.* using Superdex 75, $InsP_6$ eluted with a mass of approximately 3 kD. These results are in agreement with the results reported here, in that ultrafiltration against 3000 Da cut-off membrane after the Mini Q column for eight hours did not filter out $InsP_6$ and bioactivity still remained in the embryo multiplication assay.

Based on our calibration curve of the Superdex 75 column, the F2 fraction eluted in the mass range of 9kD to 16 kD. This is because $InsP_6$ can bind directly with charged groups of proteins or indirectly with the negatively charged groups of proteins mediated by a mineral cation such as K^+, Mg^{2+}, Ca^{2+}, Mn^{2+} and Zn^{2+}. For example, $InsP_6$ binds to nonvisual arrestins that desensitize G protein-coupled receptors, through interactions at the polar termini of Lys and Arg side chains. This $InsP_6$ binding regulates negatively interactions of arrestin with plasma membrane and nuclear signaling proteins by promoting arrestin cytosolic oligomerization (Milano et al., 2006). $InsP_6$ was also reported to form soybean protein-phytate-mineral complexes, which reduces bioavailability of minerals as well as protein digestibility and functionality (Honig and Wolf, 1991). In addition, negatively charged amino acid groups of alkaline phytase from *Bacillus* provides a favorable electrostatic environment for its substrate Ca^{2+}-$InsP_6$ (Ha et

al., 2000; Oh et al., 2006). An $InsP_6$-binding protein with a KD of 14 nM was isolated from detergent-solubilized rat brain membranes by means of an $InsP_4$ affinity column. SDS-PAGE analysis of this protein revealed that it comprises three subunits at 115, 105 and 50 kD. Photoaffinity experiments indicated that both 115- and 105-kD subunits possess recognition sites for $InsP_6$, whereas the 50-kD subunit lacks a specific recognition site (Theibert et al., 1992). Thus, multiple proteins or peptides in the mass range of 9kD to 16 kD co-eluted with $InsP_6$ via binding. This result was also supported by the detection of various proteins in LC/MS spectra of both F2 and F2-S1 fractions.

One step of strong cation exchange chromatography was included before the anion exchange in the final protocol. Since F2-S1 eluted before the salt gradient started, in retrospect, this step may not be necessary. However, it did remove significant amount of components including proteins from the F2 fraction and those components might not have been easily separated from two subsequent columns.

Inhibition to embryo growth was observed in both F2-S1-Q5 and F2-S1-Q6 fractions, but neither of them showed inhibition as significant as that of the F2-S1 control. There were two possibilities for the decrease in activity: the total amount of $InsP_6$ was divided between F2-S1-Q5 and F2-S1-Q6, since the ion at *m/z* 661 was observed in both fractions from LC/MS; a minor percentage of $InsP_6$ might have lost during ultrafiltration against water. The former contributed mainly to the activity decrease, in that $InsP_6$ behaves in dialysis at low ionic strength as if it had a higher molecular mass than predicted from its formula due to the high charge to mass ratio and the hydrogen bonding between phosphate groups of $InsP_6$ (Van der Kaay and Van Haastert, 1995; Hanakahi et al., 2000; Irigoin et al., 2002). This also explained why there was no significant

difference in yield of F2 and F2-S1 using either 1000 Da or 3000 Da cutoff ultrafiltration membranes.

The Superdex Peptide column was selected for the optimized desalting procedure to increase the yield as well as to remove plasticizer contaminants in F2-S1-Q6 detected from MS. The final active fraction, F2-S1-Q6-D1B, had no significant absorbance at three different wavelengths (215, 254, 280 nm), indicating a lack of aromatic amino acids, purine or pyrimidine moieties (Hanakahi et al., 2000). This result was not surprising in that $InsP_6$ has no appreciable UV absorbance at these wavelengths and could only be detected at 295 nm via post-column reaction (Chen and Li, 2003).

Mass Spectrometry Characterization

The fact that the $(M+H)^+$ ion at *m/z* 661 is consistently present through four successive active fractions indicate that the corresponding molecule is indeed from the FG tissue through the sequential fractionation and not produced from the purification process. The purity measured by means of LC/ESI-MS of the final active fraction F2-S1-Q6-D1B indicated that the active molecule is homogeneous and has an average mass of 660 Da. Exact mass measurement of F2-S1-Q6-D1B under negative polarity exhibited identical exact mass to the calculated molecular mass of $InsP_6$. Subsequent tandem MS analyses of both F2-S1-Q6-D1B and the commercial $InsP_6$ showed identical MS/MS spectra under both collision energies of 40 and 80 eV. All these results suggest that the pure inhibitory molecule is $InsP_6$ or one of its isomers.

When active fractions were approaching purity, they lost ability to bind to the C8 reversed phase capillary column in contrast to F2 and F2-S1 fractions, mainly because

there are no proteins available to react directly or indirectly with the phosphate groups on $InsP_6$. One alternative HPLC methodology for LC/MS, ion-pair chromatography, coupled to a double focusing inductively coupled plasma-sector field-mass spectrometry (ICP-SF-MS) was developed recently for the determination of $InsP_6$ and its degradation products ($InsP_1$ – $InsP_5$) (Helfrich and Bettmer, 2004). A C18 reversed phase column was used; eluent A was water and eluent B consisted of 10% (w/w) methanol, 20 mmol/L citrate and 0.04% (w/w) tetrabutylammonium hydroxide as the ion-pair reagent. The HPLC separation of the six phosphorus species was achieved in a 15-min gradient elution. However, no LC/ESI-MS of $InsP_6$ has been presented so far.

Although the error tolerance for the exact mass measurement under positive polarity was set at ±30 ppm, the empirical formula $C_6H_{18}O_{24}P_6$ corresponding to $InsP_6$ was not included in the candidate list. F2-S1-Q6 exhibited exact mass $(M+H)^+$ of 660.8479 with an error of negative 31.5 ppm with respect to the calculated molecular mass of $InsP_6$ at 660.8687. This huge error could only be caused by inaccurate calibration. However, with the lack of a candidate empirical formula, it was not possible to evaluate the calibration.

The LC/MS/MS spectrum under positive mode of F2-S1-Q6 at a collision energy of 40 eV was identical to those obtained at 30 and 35 eV as presented by Hsu *et al.* (Hsu et al., 2003). A series of prominent ions at *m/z* 643, 625, 607, 581, 563, 545, 527, 483, 465, 447, 429, 385, 367, 349, 287, 269, 259, 189, 179, 161, 99 were generated by successive losses of H_2O (18 amu), HPO_3 (80 amu), or H_3PO_4 (98 amu) from the precursor ion at *m/z* 661. Some fragment ions arose from multiple pathways, as described in early results. A further MS of the product ions was performed at *m/z* 563,

545 and 483 to elucidate the multiple pathways for the formation of ion at *m/z* 465. Additionally, they found that further loss of CO from ions at *m/z* 287, 269, 207, and 109 generated ions at *m/z* 259, 241, 179, 81, respectively, which resembled those observed for inositol at *m/z* 109 and 81. The latter result was supported by the product-ion spectrum of the *m/z* 109 ion. The presence of *m/z* 81 ion $(HPO3 + H)^+$ in the product-ion spectrum of *m/z* 99 $(H3PO4 + H)^+$ confirmed that ion at *m/z* 81 arose from a water loss from ion at *m/z* 99.

NMR Characterization

The $InsP_6$ standard solution used for MS analyses was in an initial attempt as the NMR standard. However, several unknown peaks showed in ^{1}H, ^{31}P and ^{13}C 1-D spectra, suggesting that the $InsP_6$ solution was not pure. Hamada (Hamada, 2002) reported that the commercial 40% or 50% phytic acid solution contains substantial amounts of its degradation products such as $InsP_3$, $InsP_4$ and $InsP_5$, which suggested that those unknown peaks were from the lower inositol phosphates. Thus a pure $InsP_6$ standard was needed for NMR spectra recording to compare with those from F2-S1-Q6-D1B. Phytic acid dodecasodium salt hydrate (98% pure, recrystallized) with twelve acidic protons replaced by sodium cations, has also been used as $InsP_6$ standard (Hamada, 2002; Chen and Li, 2003).

Since tandem MS results revealed that fragmentation pattern of F2-S1-Q6-D1B was identical to that of the commercial $InsP_6$, one can conclude that the purified compound is $InsP_6$, or one of its eight isomers. Figure 46 shows the nine stereoisomeric inositol hexa*kis*phosphate, including *myo*-, *neo*-, L-*chiro*, D-*chiro*, *allo*-, *scyllo*-, *epi*-, *cis*-

and *muco*-inositol hexa*kis*phosphate. However, no complete NMR studies have been published for the other eight stereoisomeric inositol hexa*kis*phosphate. Hypothesis of the identity of the stereoisomeric inositol hexa*kis*phosphate was based on ^{13}C NMR spectra of $InsP_6$ (Isbrandt and Oertel, 1980), *neo*-, L-*chiro*, D-*chiro*, *allo*-, *scyllo*-inositol hexa*kis*phosphate, *epi*-inositol (Podeschwa et al., 2003), and *cis*- and *muco*-inositol (Takahashi et al., 2001). $InsP_6$ showed four distinct ^{13}C peaks with an intensity ratio of 1:2:1:2 below pH 9.2. *neo*-inositol hexa*kis*phosphate possessed two ^{13}C peaks at 74.24 and 76.57 ppm with an intensity ratio of 2:1. Both L-*chiro*- and D-*chiro*-inositol hexa*kis*phosphate showed three ^{13}C peaks at 72.9, 73.3 and 76.5 ppm with an intensity ratio of 1:1:1. *allo*-inositol hexa*kis*phosphate had three distinct ^{13}C peaks at 71.13, 72.30 and 75.40 ppm. *scyllo*- inositol hexa*kis*phosphate, on the other hand, exhibited only one ^{13}C peak. Since no ^{13}C NMR spectra are available for *epi*-, *cis*- and *muco*- inositol hexa*kis*phosphate in literature and ^{13}C NMR spectra are not as pH dependent as ^{1}H and ^{31}P NMR spectra, ^{13}C NMR spectra of *epi*-, *cis*- and *muco*- inositol were used as the reference. Both *cis*- and *muco*-inositols have two ^{13}C peaks. *epi*-inositol also showed four distinct ^{13}C peaks as *myo*-inositol at 69.07, 72.29, 73.99 and 76.70 ppm, but the intensity ratio of *epi*-inositol (1:1:2:2) was different from that of *myo*-inositol.

Based on all these available information, only *myo*- and *epi*- inositol hexa*kis*phosphate were possible candidates, in that both $InsP_6$ and *epi*-inositol showed four ^{13}C peaks, the same number of ^{13}C peaks observed in F2-S1-Q6-D1B. The intensity ratio of 1:2:1:2 from F2-S1-Q6-D1B is in agreement with that from $InsP_6$. Moreover, no literature regarding *epi*-inositol hexa*kis*phosphate has been reported and *epi*-inositol is

nonexistent in nature (Vitelio et al., 2004). Taken together, $InsP_6$ is hypothesized to be the inhibitory molecule.

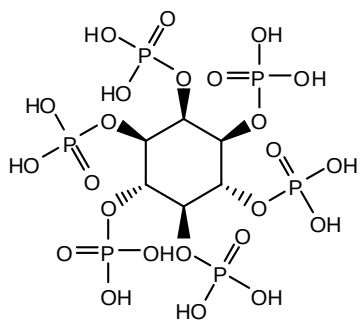

myo-inositol hexakisphosphate

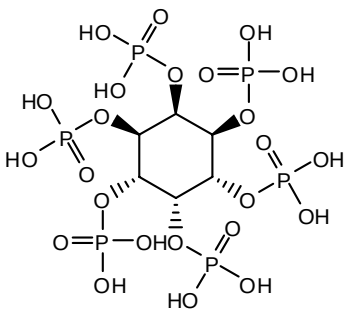

neo-inositol hexakisphosphate

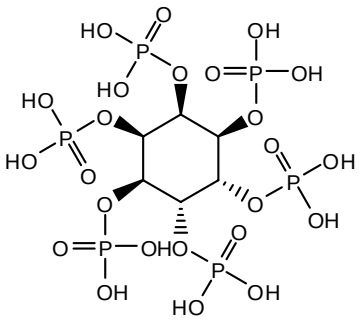

allo-inositol hexakisphosphate

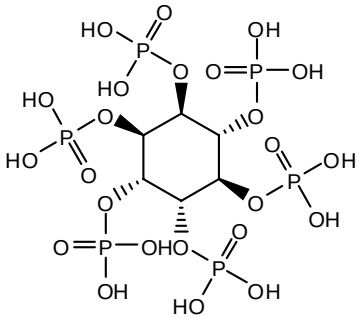

(-)-L-*chiro*-inositol hexakisphosphate

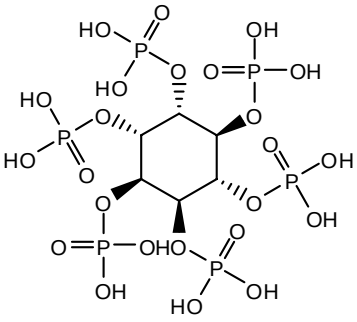

(+)-D-*chiro*-inositol hexakisphosphate

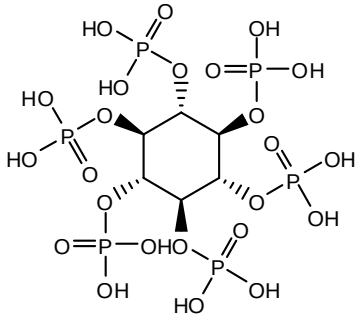

scyllo-inositol hexakisphosphate

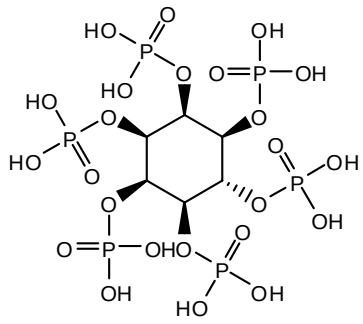

epi-inositol hexakisphosphate

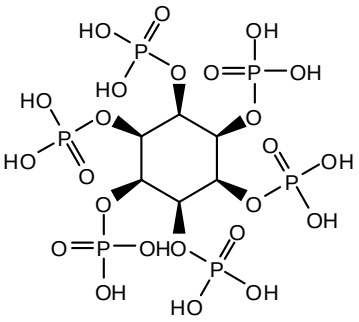

cis-inositol hexakisphosphate

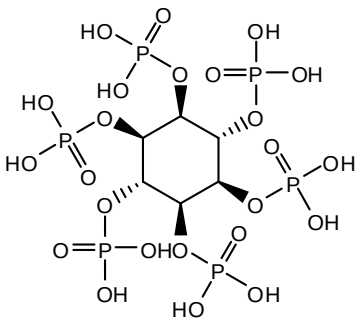

muco-inositol hexakisphosphate

Figure 46. Stereoisomeric inositol hexa*kis*phosphate.

Spectra were initially recorded at room temperature, but no peak splitting was detected. After the probe temperature was decreased to 7 ^{o}C, an evident splitting pattern was exhibited by $H_{1/3}$, H_5 and $H_{4/6}$. This result is in agreement with that of Bauman *et al* (Bauman et al., 1999), who reported previously that the coalescence temperature, T_c, for $H_{1/3}$, H_5 and $H_{4/6}$ was 15 ^{o}C at pH 9.3. Barrietos *et al.* reported that ^{1}H NMR spectra of $InsP_6$ are very pH dependent (Barrietos and Murthy, 1996), in that below pH 9.2, $InsP_6$ exists in the sterically-unhindered 1ax/5eq form (Figure 47), above pH 9.5 in the sterically-hindered 5ax/1eq form, whereas between pH 9.2 and 9.5, both forms are at equilibrium. Although all NMR spectra obtained from the commercial $InsP_6$ presented here were in the sterically stable 1ax/5eq form, initial NMR spectra at pH 1.6 and 2.6 (data not shown) showed dramatically different 1-D and 2-D spectra from those obtained over the pH range 8.0 – 8.5. Spectra at pH 1.6 and 2.6 are identical, showing three ^{1}H peaks at 1:2:3, four ^{31}P peaks at 1:2:2:1, four ^{13}C peaks at 1:2:1:2, all different chemical shifts in 1-D NMR spectra and different correlation patterns in 2-D NMR from those obtained over the pH range 8.0 – 8.5. ^{1}H, ^{31}P and ^{13}C spectra at various pH values are consistent with those of Barrietos and Isbrandt (Isbrandt and Oertel, 1980; Barrietos and Murthy, 1996).

The broader ^{31}P peaks from F2-S1-Q6-D1B relative to those from the commercial $InsP_6$ resulted mainly from approximately 20 fold higher concentration of the commercial $InsP_6$, and partially from paramagnetic ions such as Fe and Mn from the FG extract (Pullman et al., 2003b) involved in F2-S1-Q6-D1B causing sharp peaks to overlap (McDowell and Stewart, 2005).

Although the multiplicity of H_2 as doublet in F2-S1-Q6-D1B is not as evident as that in the commercial $InsP_6$, the peak width of both is identical. This unapparent doublet in F2-S1-Q6-D1B might be caused by substantial amounts of $InsP_6$-salt precipitates formed during several rounds of deuterium oxide dissolution and lyophilization, whereas the commercial $InsP_6$ did not undergo these processes. The $InsP_6$-salt precipitates are easy to form aggregates which cause peaks broader and unapparent split pattern.

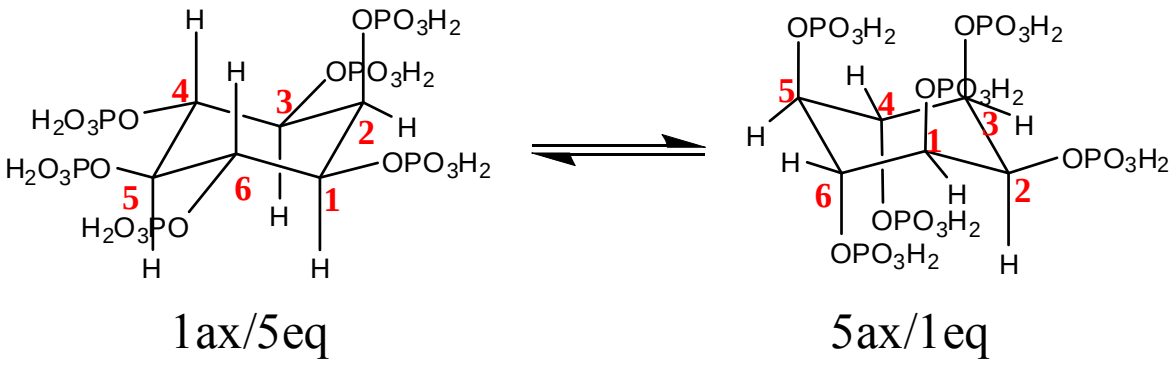

Figure 47. Two conformations of $InsP_6$.

Scale-up collection and concentration-dependent bioactivity

The inhibitory bioactivity of same amount of FG from full-term dry seeds was lower than that from stage 9.10-9.12 seeds, resulting from the degradation of $InsP_6$ from mechanical drying process (Pullman and Buchanan, 2003). The $InsP_6$ concentration-dependence of the inhibitory activity was investigated. A good correlation was observed between the amount of $InsP_6$ purified from FG tissue (1.3 nmoles per full-term FG) and the amount of $InsP_6$ inhibiting somatic embryo growth. However, this amount of $InsP_6$ purified from FG tissue is an underestimation of the actual content of $InsP_6$ in full-term FG, in that phosphorus in $InsP_6$ present in FG tissue of full-term white spruce seeds weighs 12.0 μg per FG, corresponding to 64.7 nmoles of $InsP_6$ per full-term FG (Reid et al., 1999). Although $InsP_6$ has never been characterized in LP, both LP and white spruce are conifers and $InsP_6$ levels in both full-term FG tissues should be similar.

Since $InsP_6$ can bind to hydrophobic proteins which are not water soluble, water extraction of FG would lose some $InsP_6$. Plus, only certain percentage of analyte would be recovered from each column chromatography and ultrafiltration, these steps would also contribute some loss of $InsP_6$. Additionally, the total amount of $InsP_6$ was divided between F2-S1-Q5 and F2-S1-Q6, and only F2-S1-Q6 was purified further for the final collection. The unique 11-step purification processes established here involved multiple sample transfers, which would inevitably lose $InsP_6$ in between. Hence, heat drying of seeds, water extraction of FG, successive FPLC purification and ultrafiltration, and inevitable sample transfer would explain the substantial loss of $InsP_6$ from its initial amount in FG tissue.

Proposed mechanism of inhibition

Can inhibition of somatic embryo growth by $InsP_6$ in plants share the same mechanism as some cancer cells in animals? $InsP_6$ has been known for its anticancer activity since the late 1980s. Reduction of the elevated rate of malignant cell proliferation to normal level has been observed both *in vivo* and *in vitro* in a dose- and time-dependent manner (Shamsuddin and Vucenik, 2005). Cells from different origins have different sensitivity to $InsP_6$, indicating that the mechanism of $InsP_6$ anticancer action varies in cell types. Although the cellular mechanisms behind the anticancer activity have been known for a while to involve cell proliferation and differentiation, there is still no clear agreement about the biochemical pathways (Shamsuddin and Vucenik, 2005).

$InsP_6$ has been found to impair epidermal growth factor- or phorbol ester (tumor promoter)-induced JB6 (a well-characterized cell culture model for studying tumor promotion) cell transformation and activator protein 1 activation. This impairment results from the block of epidermal growth factor-induced phosphatidylinositol-3 kinase (PtdIns 3-kinase) activity (Huang et al., 1997). Additionally, the structure of $InsP_6$ is similar to D-3-deoxy-3-fluoro-ptdIns, a potent PtdIns 3-kinase inhibitor (Powis et al., 1995). It is likely that $InsP_6$ can inhibit PtdIns 3-kinase in plants.

There are four families of PtdIns 3-kinases based on sequence homology and their preferred inositol lipid substrate(s). Only the PtdIns-specific Vps34p-related 3-kinase family has been found in all the eukaryotic cells. This kinase family phosphorylates only PtdIns at the D3-positon of the inositol ring, and is not able to phosphorylate PtdIns 4-monophosphate or PtdIns 4,5-bisphosphate. In mammals and yeast, PtdIns 3-kinases are

involved in mitogenesis, apoptosis, trafficking of membrane proteins, membrane ruffling, glucose uptake, chemotaxis, the oxidative burst response in neutrophils, and activation of intracellular signaling molecules such as *rac*, *ras*, *rab*, MAP kinase, protein kinase B/Akt, protein kinase C and JNK/p38 kinase (Munnik et al., 1998; Leevers et al., 1999; Meijer and Munnik, 2003).

Several PtdIns 3-kinase homologues have been cloned in plant species including soybean (Hong and Verma, 1994), *Arabidopsis thaliana* (Welters et al., 1994) and *Brassica napus* (Das et al., 2005). In *Arabidopsis thaliana*, the PtdIns 3-kinase *At*VPS34, has a significantly higher homology to yeast VPS34 than to the mammalian PtdIns 3-kinase (p110). Expression of antisense *At*VPS34 mRNA results in severe inhibition in growth and development of second-generation transformed plants. This lethal phenotype indicates that PtdIns 3-kinase also plays an important role in plant development and growth. The authors hypothesized that plant PtdIns 3-kinase is associated with vesicle transport of proteins to the vacuole. Recently, both PtdIns 3-kinase and PtdIns 4 -kinase activities have been observed during the induction of somatic embryogenesis in *coffea arabica* (Ek-Ramos et al., 2003). Products of both kinases, PtdIns 3- monophosphate and PtdIns 4-monophosphate, were detected in the somatic-embryo extracts of two early stages, cells without differentiated structures and the first differentiated stage. When wortmannin (an inhibitor to both PtdIns 3-kinase and PtdIns 4-kinase) was added to these two early-stage extracts, wortmannin suppressed the formation of both PtdIns 3-monophosphate and PtdIns 4-monophosphate in a dose-dependent manner. Furthermore, growth of somatic embryos was inhibited by wortmannin included in the induction medium during the first differentiated stage.

Although several molecular mechanisms can be suggested for the observed inhibition of early-stage somatic embryo multiplication by $InsP_6$, we hypothesize that $InsP_6$ exerts this role via the inhibition to PtdIns 3-kinase. Nevertheless, another possible cause, the block of access of minerals from medium for embryos to imbibe, can not be completely ruled out.

Proposed function *in vivo* of $InsP_6$

The function of $InsP_6$ in plants, except for the storage of phosphorus in seeds, is still at an early stage of investigation. $InsP_6$ accumulates in a linear fashion throughout seed development and degrades to lower-phosphate inositol phosphates during germination (Strother, 1980; Raboy and Dickinson, 1987). Abscisic acid (ABA), the plant drought-stress hormone, induces stomatal closure, conserving water and ensuring plant survival. Recently, Lemtiri-Chlieh *et al.* reported that ABA elevates $InsP_6$ levels, and $InsP_6$ inactivates the plasma membrane K^+-inward conductance which is a well characterized target of ABA response, in a cytosolic calcium-dependent manner in *Solanum tuberosum* stomatal guard cells (Lemtiri-Chlieh et al., 2000). $InsP_6$ also functions as an endomembrane-acting calcium release signal (Lemtiri-Chlieh et al., 2003). These findings suggest that $InsP_6$ is a downstream component of the ABA signaling pathway.

Seed dormancy is a temporary failure or block of a viable seed to germinate under physical conditions that are otherwise favorable for its germination. Germination initiates with the uptake of water by imbibition by the dry seed, followed by embryo expansion (Finch-Savage and Leubner-Metzger, 2006). When storage compounds accumulate during seed maturation, water content decreases, ABA accumulates, and desiccation tolerance and primary dormancy are established. Overexpression of genes involved in ABA anabolism increases seed ABA levels, enhances seed dormancy, and delays germination (Frey et al., 1999; Thompson et al., 2000; Lindgren et al., 2003; Nambara and Marion-Poll, 2003). In contrast, ABA deficiency is associated with the absence of primary dormancy and the precocious germination of mature seeds. ABA is

produced from the embryo and/or the maternal tissues during seed development. Reciprocal crosses and grafting experiments between wild-type and ABA-deficient mutants of *Arabidopsis* (Koornneef and Karssen, 1994; Nambara and Marion-Poll, 2003), tomato (Groot and Karssen, 1992; Hilhorst, 1995) and *Nicotiana plumbaginifolia* (Frey et al., 1999) revealed that only ABA produced by the embryo during seed development has the capacity to induce a lasting dormancy, whereas maternal ABA and exogenous ABA application during seed development fail to impose seed dormancy. ABA inhibits the transition from water uptake (phases 1 and 2) during germination to water uptake during post-germination growth (phase 3) (Kucera et al., 2005). Thus, ABA is a positive regulator of seed dormancy and downregulates seed germination.

Gibberellin (GA), on the other hand, releases dormancy, promotes germination, and counteracts ABA effects. Two other plant hormones, ethylene and brassinosteroid (BR), also counteract the inhibitory effects of ABA on seed germination. However, they act after dormancy has been released by gibberellin in most species (Kucera et al., 2005).

In seeds from temperate regions, dormancy is alleviated by a prolonged period of moist incubation at low temperatures (chilling or stratification). Recent findings (Andriotis et al., 2005) revealed that chilling alleviates hazel seed embryo dormancy with an early response of $InsP_6$ mobilization. $InsP_6$ levels in embryonic axes (the site where the block of germination is imposed) were reduced by 60% within the first three weeks at 5 ^{o}C, which was not detected in warm-imbibed tissue. Increased phytase activity was found during chilling. These results indicate that $InsP_6$ turnover to lower-phosphate inositol phosphates supports metabolic reactivation during dormancy alleviation and preparation for subsequent germination in hazel seeds.

Taken together, we hypothesize that the biological function of $InsP_6$ in plants is the regulation of seed germination and dormancy release via the crosstalk of ABA and GA, ethylene or BR. A complete description of this regulatory pathway is illustrated in Figure 48. When seeds approach maturation in fall, drought increases endogenous ABA levels, and ABA in turn elevates its downstream component $InsP_6$ and induces seed dormancy. In the end of winter, chilling directly activates the hydrolysis of $InsP_6$ to lower-phosphate inositol phosphates, or indirectly activates this hydrolysis via a signal hormone, such as GA, ethylene or BR. The $InsP_6$ turnover alleviates seed dormancy and induces germination.

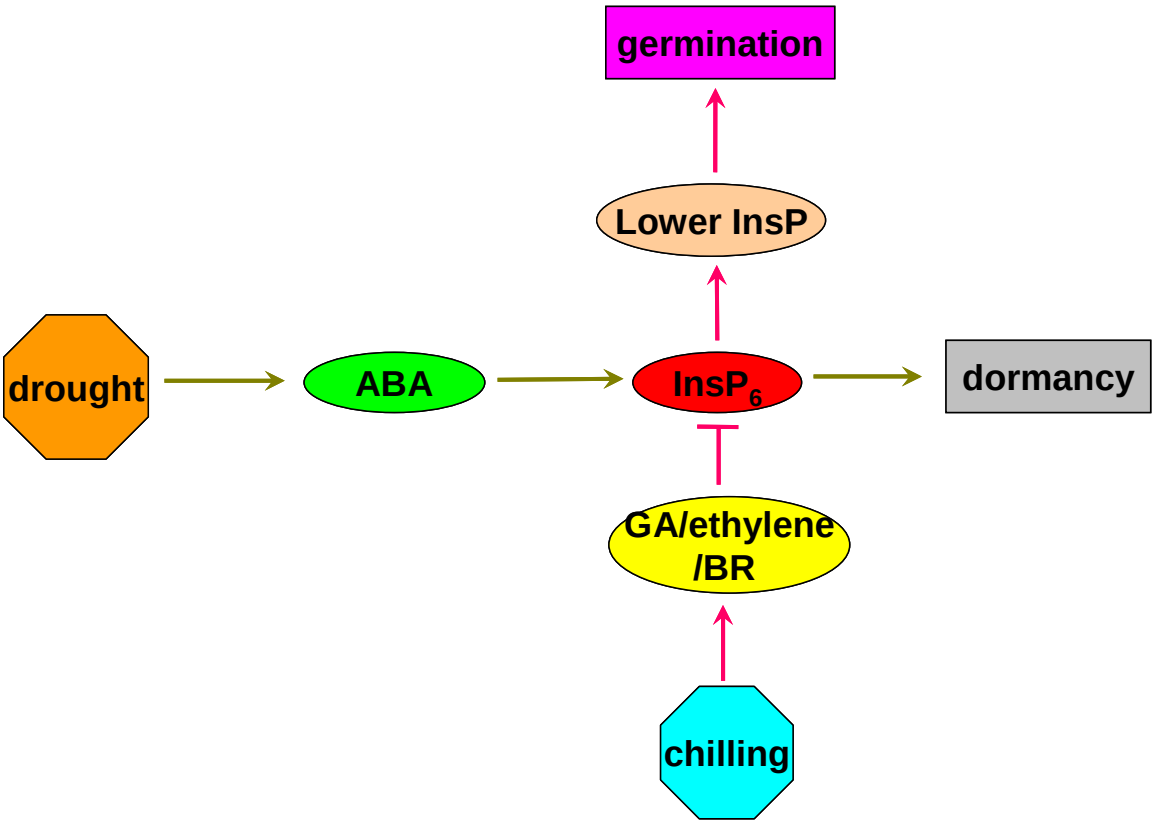

Figure 48. Hypothesized pathway of $InsP_6$ function *in vivo*. When seeds approach maturation in fall, drought increases endogenous ABA levels, and ABA in turn elevates its downstream component $InsP_6$ and induces seed dormancy (sap green route in horizontal orientation). At the end of winter, chilling directly activates the hydrolysis of $InsP_6$ to lower-phosphate inositol phosphates, or indirectly activates this hydrolysis via a signal hormone, such as GA, ethylene or BR. The $InsP_6$ turnover alleviates seed dormancy and induces germination (pink route in vertical orientation).

Impact of the discovery and future work

We herein present the first discovery of $InsP_6$ in FG of LP seeds and its inhibition to early-stage somatic embryo growth. The biochemical and physiological mechanisms in regulating this process, and perhaps other processes in plants, remain to be determined. We hypothesize that $InsP_6$ suppresses early-stage somatic embryo growth via the inhibition to PtdIns 3-kinase. More experiments need to be carried out to prove this hypothesis. First of all, the *in vitro* binding of $InsP_6$ on PtdIns 3-kinase and inhibition of $InsP_6$ to the PtdIns 3-kinase activity will be studied. Second, the PtdIns 3-kinase cDNA as well as the PtdIns 3-kinase activity need to be identified in the early-stage somatic embryos of LP. Third, the mechanism by which PtdIns 3-kinase regulates plant growth and development needs to be determined. Understanding the inhibition mechanism of $InsP_6$ would allow us to improve the SE technology by overcoming the current bottleneck, to elucidate enigmatic functions of $InsP_6$ in plants, and most importantly, to utilize this molecule properly.

The biological function of $InsP_6$ such as seed dormancy and germination remains to be answered. We hypothesize that $InsP_6$ participates in the crosstalk between the plant hormones ABA and GA/ethylene/BR to regulate seed dormancy and germination in response to environmental changes. If this hypothesis is true, monitoring lower-phosphate inositol phosphates is essential. Additionally, it would be intriguing to discover the signaling transduction pathway involving both $InsP_6$ and $Ins(1,4,5)P_3$ in the germination process.

REFERENCES

Advion. http://www.advion.com/biosystems_howitworks.php.

Andriotis, V.M., Smith, S.B., and Ross, J.D. (2005). Phytic acid mobilization is an early response to chilling of the embryonic axes from dormant oilseed of hazel (Corylus avellana). Journal of experimental botany **56,** 537-545.

Barre, R., Courtois, J.E., and Wormser, G. (1954). Bull. Soc. Chim. Biol. **36,** 455.

Barrietos, L., and Murthy, P. (1996). Conformational studies of *myo*-inositol phosphates. Carbohydrate research **296,** 39-54.

Barrietos, L., Scott, J.J., and Murthy, P. (1994). Specificity of hydrolysis of phytic acid by alkaline phytase from lily pollen. Plant physiology **106,** 1489-1495.

Bauman, A., Chateauneuf, G., Boyd, B., Brown, R., and Murthy, P. (1999). Conformational inversion processes in phytic acid: NMR spectroscopic and molecular modeling studies. Tetrahedron Lett. **40,** 4489-4492.

Blake, J. (1983). Tissue culture propagation of coconut, date, and oil palm. . In Tissue Culture of Trees, J.H. Dodds, ed (West Port, CT: Avi Publishing Co.), pp. 29-51.

Brand, U., Fletcher, J.C., Hobe, M., Meyerowitz, E.M., and Simon, R. (2000). Dependence of stem cell fate in Arabidopsis on a feedback loop regulated by CLV3 activity. Science **289,** 617-619.

Brearley, C.A., and Hanke, D.E. (1996). Metabolic evidence for the order of addition of individual phosphate esters in the myo-inositol moiety of inositol hexakisphosphate in the duckweed Spirodela polyrhiza L. The Biochemical journal **314 (Pt 1),** 227-233.

Butenko, M.A., Patterson, S.E., Grini, P.E., Stenvik, G.E., Amundsen, S.S., Mandal, A., and Aalen, R.B. (2003). Inflorescence deficient in abscission controls floral organ abscission in Arabidopsis and identifies a novel family of putative ligands in plants. Plant Cell **15,** 2296-2307.

Cairney, J., and Pullman, G.S. (2007). The cellualr and molecular biology of conifer embryogenesis. New Phytologist **176,** 511-536.

Cairney, J., Xu, N., MacKay, J., and Pullman, G.S. (2000). Transcript profiling: A tool to assess the development of conifer embryos. . In Vitro Cell. Dev. Biol. **36,** 155-162.

Carlsson, N.G., Bergman, E.L., Skoglund, E., Hasselblad, K., and Sandberg, A.S. (2001). Rapid analysis of inositol phosphates. Journal of agricultural and food chemistry **49,** 1695-1701.

Challa, A., Rao, D.R., and Reddy, B.S. (1997). Interactive suppression of aberrant crypt foci induced by azoxymethane in rat colon by phytic acid and green tea. Carcinogenesis **18,** 2023-2026.

Chen, Q.C., and Li, B.W. (2003). Separation of phytic acid and other related inositol phosphates by high-performance ion chromatography and its applications. Journal of chromatography **1018,** 41-52.

Chen, T.H.H., and K.K., K. (1987). cryopreservation of woody species. In Cell and tissue culture in forestry, J.M. Bonga and D.J. Durzan, eds (Martinus Nijhoff Publishers, Dordrecht), pp. 305-319.

Constabel, C.P., Yip, L., and Ryan, C.A. (1998). Prosystemin from potato, black nightshade, and bell pepper: primary structure and biological activity of predicted systemin polypeptides. Plant Mol. Biol. **36,** 55-62.

Cosgrove, D.J. (1980a). Inositol Phosphates: Their Chemistry, Biochemistry and Physiology (Amsterdam: Elsevier), pp. 191.

Cosgrove, D.J. (1980b). Inositolhexakisphosphates. In Inositol Phosphates. Their Chemistry, Biochemistry and Physiology, D.J. Cosgrove, ed (Netherlands: Elsevier Scientific Publishing Company), pp. 26-43.

Creighton, T.E., and Freeman, W.E. (1984). Proteins, structure and molecular properties. (New York).

Das, S., Hussain, A., Bock, C., Keller, W.A., and Georges, F. (2005). Cloning of Brassica napus phospholipase C2 (BnPLC2), phosphatidylinositol 3-kinase (BnVPS34) and phosphatidylinositol synthase1 (BnPtdIns S1)--comparative analysis of the effect of abiotic stresses on the expression of phosphatidylinositol signal transduction-related genes in B. napus. Planta **220,** 777-784.

Davies, P.J. (1995). Plant Hormones—Physiology, Biochemistry and Molecular Biology. (Dordrecht: The Netherlands: Kluwer Academic Publishers).

DeSilva, V., Bostwick, D., Burns, K., Oldham, C., Skryabina, A., Wu, D., Zhang, Y., May, S., and Pullman, G.S. (2007). Isolation and Characterization of a Molecule Stimulatory to Growth of Somatic Embryos from Early Stage Female Gametophyte Tissue of Loblolly Pine.

Dorsch, J.A., Cook, A., Young, K.A., Anderson, J.M., Bauman, A.T., Volkmann, C.J., Murthy, P.P., and Raboy, V. (2003). Seed phosphorus and inositol phosphate phenotype of barley low phytic acid genotypes. Phytochemistry **62,** 691-706.

Efanov, A.M., Zaitsev, S.V., and Berggren, P.O. (1997). Inositol hexakisphosphate stimulates non-Ca2+-mediated and primes Ca2+-mediated exocytosis of insulin by activation of protein kinase C. Proceedings of the National Academy of Sciences of the United States of America **94,** 4435-4439.

Eggleton, P., Penhallow, J., and Crawford, N. (1991). Priming action of inositol hexakisphosphate (InsP6) on the stimulated respiratory burst in human neutrophils. Biochimica et biophysica acta **1094,** 309-316.

Ek-Ramos, M.J., Palma, G.R., and Hernandez-Sotomayor, T. (2003). Changes in phosphatidylinositol and phosphatidylinositol monophosphate kinase activities during the induction of somatic embryogenesis in *Coffea arabica*. Physiol Plantarum **119,** 270-277.

Ferry, S., Matsuda, M., Yoshida, H., and Hirata, M. (2002). Inositol hexakisphosphate blocks tumor cell growth by activating apoptotic machinery as well as by inhibiting the Akt/NFkappaB-mediated cell survival pathway. Carcinogenesis **23,** 2031-2041.

Finch-Savage, W.E., and Leubner-Metzger, G. (2006). Seed dormancy and the control of germination. New Phytologist **171,** 501-523.

Flores, S., and Smart, C.C. (2000). Abscisic acid-induced changes in inositol metabolism in *Spirodela polyrrhiza*. Planta **211,** 823-832.

Frey, A., Audran, C., Marin, E., Sotta, B., and Marion-Poll, A. (1999). Engineering seed dormancy by the modification of zeaxanthin epoxidase gene expression. Plant molecular biology **39,** 1267-1274.

Gautheret, R.J. (1940). Nouvelles recherches sur le bourgeonnement du tissue cambial d'*Ulmus campestris cultive in vitro*. C.R. Acad. Sci. Paris **210,** 744-746.

Graf, E., Empson, K.L., and Eaton, J.W. (1987). Phytic acid. A natural antioxidant. The Journal of biological chemistry **262,** 11647-11650.

Grases, F., Garcia-Gonzalez, R., Torres, J.J., and Llobera, A. (1998). Effects of phytic acid on renal stone formation in rats. Scandinavian journal of urology and nephrology **32,** 261-265.

Groot, S.P.C., and Karssen, C.M. (1992). Dormancy and germination of abscisic acid-deficient tomato seeds. Plant physiology **99,** 952-958.

Gupta, K.P., Singh, J., and Bharathi, R. (2003). Suppression of DMBA-induced mouse skin tumor development by inositol hexaphosphate and its mode of action. Nutrition and cancer **46,** 66-72.

Ha, N.C., Oh, B.C., Shin, S., Kim, H.J., Oh, T.K., Kim, Y.O., Choi, K.Y., and Oh, B.H. (2000). Crystal structures of a novel, thermostable phytase in partially and fully calcium-loaded states. Nature structural biology **7,** 147-153.

Hager, J.W., and Yves Le Blanc, J.C. (2003). Product ion scanning using a Q-q-Q linear ion trap (Q TRAP) mass spectrometer. Rapid Commun Mass Spectrom **17,** 1056-1064.

Hamada, J.S. (2002). Scale-up potential of ion-pair high-performance liquid chromatography method to produce biologically active ionositol phosphates. Journal of chromatography **944,** 241-248.

Hanakahi, L.A., Bartlet-Jones, M., Chappell, C., Pappin, D., and West, S.C. (2000). Binding of inositol phosphate to DNA-PK and stimulation of double-strand break repair. Cell **102,** 721-729.

Harland, B.F., and Morris, E.R. (1995). Phytate: A good or bad food component? Nutrition Res. **15,** 733–754.

Hawkins, P.T., Poyner, D.R., Jackson, T.R., Letcher, A.J., Lander, D.A., and Irvine, R.F. (1993). Inhibition of iron-catalysed hydroxyl radical formation by inositol polyphosphates: a possible physiological function for myo-inositol hexakisphosphate. The Biochemical journal **294 (Pt 3),** 929-934.

Helfrich, A., and Bettmer, J. (2004). Determination of phytic acid and its degradation products by ion-pair chromatography (IPC) coupled to inductively coupled plasma-sector field-mass spectrometry (ICP-SF-MS). J Anal At Spectrom **19,** 1330-1334.

Hilhorst, H.W.M. (1995). A critical update on seed dormancy. I. Primary dormancy Seed Sci. Res. **5,** 61-73.

Hjertén, S. (1977). Fractionation of proteins by hydrophobic interaction chromatography, with reference to serum proteins. . In Proceedings Intl. Workshop on Technology for Protein Separation & Improvement of Blood Plasma Fractionation. (Reston, Virginia), pp. 410–421.

Hjertén, S., Yao, K., Eriksson, K.-O., and Johansson, B. (1986). Gradient and isocratic High Performance Hydrophobic Interaction Chromatography of proteins on agarose columns. . J. Chromatog. **359,** 99–109.

Hong, Z., and Verma, D.P. (1994). A phosphatidylinositol 3-kinase is induced during soybean nodule organogenesis and is associated with membrane proliferation. Proceedings of the National Academy of Sciences of the United States of America **91,** 9617-9621.

Honig, D.H., and Wolf, W.J. (1991). Phytate-mineral-protein composition of soybeans: gel filtration studies of soybean meal extracts. Journal of agricultural and food chemistry **39,** 1037-1042.

Hopfgartner, G., Varesio, E., Tschappat, V., Grivet, C., Bourgogne, E., and Leuthold, L.A. (2004). Triple quadrupole linear ion trap mass spectrometer for the analysis of small molecules and macromolecules. J Mass Spectrom **39,** 845-855.

Hsu, F.F., Turk, J., and Gross, M.L. (2003). Structural distinction among inositol phosphate isomers using high-energy and low-energy collisional-activated dissociation tandem mass spectrometry with electrospray ionization. J Mass Spectrom **38,** 447-457.

Huang, C., Ma, W.Y., Hecht, S.S., and Dong, Z. (1997). Inositol hexaphosphate inhibits cell transformation and activator protein 1 activation by targeting phosphatidylinositol-3' kinase. Cancer research **57,** 2873-2878.

Imin, N., Nizamidin, M., Wu, T., and Rolfe, B.G. (2007). Factors involved in root formation in Medicago truncatula. Journal of experimental botany **58,** 439-451.

Irigoin, F., Ferreira, F., Fernandez, C., Sim, R.B., and Diaz, A. (2002). myo-Inositol hexakisphosphate is a major component of an extracellular structure in the parasitic cestode Echinococcus granulosus. The Biochemical journal **362,** 297-304.

Isbrandt, L.R., and Oertel, R.P. (1980). Conformational states of myo-inositol hexakis(phosphate) in aqueous solution. A ^{13}C NMR, ^{31}P NMR, and Raman spectroscopic investigation. J. Am. Chem. Soc. **102,** 3144-3148.

Jain, S.M., Gupta, P.K., and Newton, R.J. (1995). Somatic Embryogenesis in Woody Plants, Vol 1 - History, Molecular and Biochemical Aspects, and Applications.

Jennissen, H.P., and Heilmeyer, I.M.G. (1975). General aspects of hydrophobic chromatography. Adsorption and elution characteristics of some skeletal muscle enzymes. Biochemistry **14,** 754–760.

Koornneef, M., and Karssen, C.M. (1994). Seed dormancy and germination. In Arabidopsis, E.M. Meyerowitz and C.R. Somerville, eds (New York: Cold Spring Harbor Laboratory Press), pp. 313-334.

Kucera, B., Cohn, M.A., and Leubner-Metzger, G. (2005). Plant hormone interactions during seed dormancy release and germination. Seed Science Research **15,** 281-307.

Kuhlmann, F.E., Apffel, A., Fischer, S.M., Goldberg, G., and Goodley, P.C. (1995). Signal enhancement for gradient reverse-phase high-performance liquid chromatography-electrospray ionization mass spectrometry analysis with trifluoroacetic and other strong acid modifiers by postcolumn addition of propionic acid and isopropanol. J Am Soc Mass Spectrom **825,** 186-192.

Kulaeva, O.N., and Prokoptseva, O.S. (2004). Recent Advances in the Study of Mechanisms of Action of Phytohormones. Biochemistry (Moscow) **69** 233-247.

L.F. Johnson, M.E.T. (1969). Structure of 'phytic acids'. Can. J. Chem. **47,** 63–73.

Larsson, O., Barker, C.J., Sjoholm, A., Carlqvist, H., Michell, R.H., Bertorello, A., Nilsson, T., Honkanen, R.E., Mayr, G.W., Zwiller, J., and Berggren, P.O. (1997). Inhibition of phosphatases and increased Ca2+ channel activity by inositol hexakisphosphate. Science (New York, N.Y **278,** 471-474.

Lasztity, R., and Lasztity, L. (1990). Phytic acid in cereal technology. Adv. Cereal Sci. Technol. **10,** 309–371.

Le Blanc, J.C., Hager, J.W., Ilisiu, A.M., Hunter, C., Zhong, F., and Chu, I. (2003). Unique scanning capabilities of a new hybrid linear ion trap mass spectrometer (Q TRAP) used for high sensitivity proteomics applications. Proteomics **3,** 859-869.

Leevers, S.J., Vanhaesebroeck, B., and Waterfield, M.D. (1999). Signalling through phosphoinositide 3-kinases: the lipids take centre stage. Current opinion in cell biology **11,** 219-225.

Lemtiri-Chlieh, F., MacRobbie, E.A.C., and Brearley, C.A. (2000). Inositol hexakisphosphate is a physiological signal regulating the K^+-inward rectifying conductance in guard cells. Proceedings of the National Academy of Sciences of the United States of America **97,** 8687–8692.

Lemtiri-Chlieh, F., MacRobbie, E.A., Webb, A.A., Manison, N.F., Brownlee, C., Skepper, J.N., Chen, J., Prestwich, G.D., and Brearley, C.A. (2003). Inositol hexakisphosphate mobilizes an endomembrane store of calcium in guard cells. Proceedings of the National Academy of Sciences of the United States of America **100,** 10091-10095.

Lindgren, L.O., Stalberg, K.G., and Hoglund, A.S. (2003). Seed-specific overexpression of an endogenous Arabidopsis phytoene synthase gene results in delayed germination and increased levels of carotenoids, chlorophyll, and abscisic acid. Plant physiology **132,** 779-785.

Loewus, F., and Murthy, P. (2000). myo-Inositol metabolism in plants. Plant Sci **150,** 1-19.

Lott, J.N.A., Ockenden, I., Raboy, V., and Batten, G.D. (2000). Phytic acid and phosphorus in crop seeds and fruits: a global estimate. Seed Sci. Res. **10,** 11-33.

Malinowski, E.R., Knapp, P.S., and Feuer, B.I. (1966). Nuclear magnetic resonance studies of aqueous electrolyte solutions. I. Hydration number of sodium chloride determined from temperature effects on proton shift J Chem Phys **45,** 4274-4279.

Matsubayashi, Y., and Sakagami, Y. (1996). Phytosulfokine, sulfated peptides that induce the proliferation of single mesophyll cells of Asparagus officinalis L. Proc. Natl. Acad. Sci. USA **93,** 7623–7627.

Mauseth, J. (1991). Botany: an introduction to plant biology. (Philadelphia Saunders College Publishers).

McDowell, R.W., and Stewart, I. (2005). An improved technique for the determination of organic phosphorus in sediments and soils by 31P nuclear magnetic resonance spectroscopy. Chemistry and Ecology **21,** 11-22.

McGurl, B., Pearce, G., Orozco-Cardenas, M., and Ryan, C.A. (1992). Structure, expression, and antisense inhibition of the systemin precursor gene Science **255,** 1570–1573.

Meijer, H.J., and Munnik, T. (2003). Phospholipid-based signaling in plants. Annual review of plant biology **54,** 265-306.

Milano, S.K., Kim, Y.M., Stefano, F.P., Benovic, J.L., and Brenner, C. (2006). Nonvisual arrestin oligomerization and cellular localization are regulated by inositol hexakisphosphate binding. The Journal of biological chemistry **281,** 9812-9823.

Mirov, N.T. (1967). The Genus Pinus. (The Ronald Press Company, New York).

Munnik, T., Irvine, R.F., and Musgrave, A. (1998). Phospholipid signalling in plants. Biochimica et biophysica acta **1389,** 222-272.

Nambara, E., and Marion-Poll, A. (2003). ABA action and interactions in seeds. Trends in plant science **8,** 213-217.

Narhi, L.O., Kita, Y., and Arakawa, T. (1989). Hydrophobic Interaction Chromatography in alkaline pH. Anal. Biochem. **182,** 266–270.

Narita, N.N., Moore, S., Horiguchi, G., Kubo, M., Demura, T., Fukuda, H., Goodrich, J., and Tsukaya, H. (2004). Overexpression of a novel small peptide ROTUNDIFOLIA4 decreases cell proliferation and alters leaf shape in Arabidopsis thaliana. Plant J **38,** 699-713.

Nelson, D.E., Rammesmayer, G., and Bohnert, H.J. (1998). Regulation of cell-specific inositol metabolism and transport in plant salinity tolerance. Plant Cell **10,** 753-764.

Oh, B.C., Kim, M.H., Yun, B.S., Choi, W.C., Park, S.C., Bae, S.C., and Oh, T.K. (2006). Ca(2+)-inositol phosphate chelation mediates the substrate specificity of beta-propeller phytase. Biochemistry **45,** 9531-9539.

Otegui, M.S., Capp, R., and Staehelin, L.A. (2002). Developing seeds of Arabidopsis store different minerals in two types of vacuoles and in the endoplasmic reticulum. Plant Cell **14,** 1311-1327.

Pearce, G., Strydom, D., Johnson, S., and Ryan, C.A. (1991). A polypeptide from tomato leaves activates the expression of proteinase inhibitor genes. Science **253,** 895–897.

Pearce, G., Moura, D.S., Stratmann, J., and Ryan, C.A. (2001a). Production of multiple plant hormones from a single polyprotein precursor. Nature **411,** 817–820.

Pearce, G., Moura, D.S., Stratmann, J., and Ryan, C.A., Jr. (2001b). RALF, a 5-kDa ubiquitous polypeptide in plants, arrests root growth and development. Proc Natl Acad Sci U S A **98,** 12843-12847.

Podeschwa, M., Plettenburg, O., Brocke, J., Block, O., Adelt, S., and Altenbach, H.J. (2003). Stereoselective synthesis of *myo*-, *neo*-, L-*chiro*, D-*chiro*, *allo*-, *scyllo*-, and *epi*-inositol systems via conduritols prepared from p-benzoquinone. Eur. J. Org. Chem**,** 1958-1972.

Porath, J. (1986). Salt-promoted adsorption: recent developments. J. Chromatog. **376,** 331–341.

Powis, G., Berggren, M., Gallegos, A., Frew, T., Hill, S., Kozikowski, A., Bonjouklian, R., Zalkow, L., Abraham, R., Ashendel, C., and et al. (1995). Advances with phospholipid signalling as a target for anticancer drug development. Acta biochimica Polonica **42,** 395-403.

Pullman, G.S., and Webb, D.T. (1994). An embryo staging system for comparison of zygotic and somatic embryo development. In TAPPI R&D Divison Biological Sciences Symposium (Minneapolis, Minnesota), pp. pp31-34.

Pullman, G.S., and Buchanan, M. (2003). Loblolly pine (Pinus taeda L.): stage-specific elemental analyses of zygotic embryo and female gametophyte tissue. . Plant Sci **164,** 943-954.

Pullman, G.S., Zhang, Y., and Phan, B.H. (2003a). Brassinolide improves embryogenic tissue initiation in conifers and rice. Plant cell reports **22,** 96-104.

Pullman, G.S., Chopra, R., and Chase, K.M. (2006). Loblolly pine (Pinus taeda L.) somatic embryogenesis: Improvements in embryogenic tissue initiation by supplementation of medium with organic acids, Vitamins B12 and E. Plant Sci **170,** 648-658.

Pullman, G.S., Montello, P., Cairney, J., Xu, N., and Feng, X. (2003b). Loblolly pine (*Pinus taeda* L.) somatic embryogenesis: maturation improvements by metal analyses of zygotic and somatic embryos. Plant Sci **164,** 955-969.

Pullman, G.S., Johnson, S., Peter, G., Cairney, J., and Xu, N. (2003c). Improving loblolly pine somatic embryo maturation: comparison of somatic and zygotic embryo morphology, germination, and gene expression. Plant cell reports **21,** 747-758.

Quiroz-Figueroa, F.R., Rojas-Herrera, R., Galaz-Avalos, R.M., and Loyola-Vargas, V.M. (2006). Embryo production through somatic embryogenesis can be used to study cell differentiation in plants PLANT CELL TISSUE AND ORGAN CULTURE **86,** 285-301

Raboy, V. (1997). Accumulation and storage of phosphate and minerals. In Cellular and molecular biology of plant seed development, B.A. Larkins and I.K. Vasil, eds (Kluwer Academic Publishers), pp. 441-477.

Raboy, V. (2003). myo-Inositol-1,2,3,4,5,6-hexakisphosphate. Phytochemistry **64,** 1033-1043.

Raboy, V., and Dickinson, D. (1987). The timing and rate of phytic acid accumulation in developing soybean seeds. Plant physiology **85,** 841-844.

Raboy, V., Gerbasi, P.F., Young, K.A., Stoneberg, S.D., Pickett, S.G., Bauman, A.T., Murthy, P.P., Sheridan, W.F., and Ertl, D.S. (2000). Origin and seed phenotype of maize low phytic acid 1-1 and low phytic acid 2-1. Plant physiology **124,** 355-368.

Raven, P.H. (1992). Biology of Plants. (New York, NY: Worth Publishers).

Reid, D.A., Lott, J.N.A., Attree, S.M., and Fowke, L.C. (1999). Mineral nutrition in white spruce (Picea glauca [Moench] Voss) seeds and somatic embryos. I. phosphorus, phytic acid, potassium, magnesium, calcium, iron and zinc. Plant Sci **141,** 11-18.

Roberts, D.R., Webster, F.B., Flinn, B.S., Lazaroff, W.R., and Cyr, D.R. (1993). Somatic embryogenesis of spruce. In Synseeds: Applications of synthetic seeds to crop improvement, K. Redenbaugh, ed (Boca Raton, FL: CRC Press, Inc.), pp. 427-449.

Sakamoto, K., Venkatraman, G., and Shamsuddin, A.M. (1993). Growth inhibition and differentiation of HT-29 cells in vitro by inositol hexaphosphate (phytic acid). Carcinogenesis **14,** 1815-1819.

Salisbury, F.B., and Ross, C.W. (1992). Plant Physiology. (Belmont, CA: Wadsworth Publishing Company).

Sasakawa, N., Sharif, M., and Hanley, M.R. (1995). Metabolism and biological activities of inositol pentakisphosphate and inositol hexakisphosphate. Biochem Pharmacology **50,** 137-146.

Sasakawa, N., Ferguson, J.E., Sharif, M., and Hanley, M.R. (1994). Attenuation of agonist-induced desensitization of the rat substance P receptor by microinjection of inositol pentakis-and hexakisphosphates in Xenopus laevis oocytes. Molecular pharmacology **46,** 380-385.

Schultz, R.P. (1999). Loblolly: the pine for the twenty-first century. New Forests **17,** 71-88.

Seeds, A.M., Sandquist, J.C., Spana, E.P., and York, J.D. (2004). A molecular basis for inositol polyphosphate synthesis in Drosophila melanogaster. The Journal of biological chemistry **279,** 47222-47232.

Shamsuddin, A.M., and Yang, G.Y. (1995). Inositol hexaphosphate inhibits growth and induces differentiation of PC-3 human prostate cancer cells. Carcinogenesis **16,** 1975-1979.

Shamsuddin, A.M., and Vucenik, I. (2005). IP6 & inositol in cancer prevention and therapy. Curr Cancer Therapy Rev **1,** 259-269.

Shamsuddin, A.M., Baten, A., and Lalwani, N.D. (1992). Effect of inositol hexaphosphate on growth and differentiation in K562 erythroleukemia cell line. Cancer Lett **64,** 195-202.

Shan, X.Y., Wang, Z.L., and Xie, D. (2007). Jasmonate signal pathway in Arabidopsis. J Int Plant Biol **49,** 81-86.

Sharp, W.R., Evans, D.A., and Sondahl, M.R. (1982). Application of somatic embryogenesis to crop improvement. In Plant Tissue Culture, Proc. 5th Intern. Cong. Plant Tissue and Cell Culture, A. Fujiwara, ed (Japanese Assoc. for Plant Tissue Culture), pp. 759-762.

Shears, S.B. (2001). Assessing the omnipotence of inositol hexakisphosphate Cellular Signalling **13,** 151-158.

Singh, R.P., Agarwal, C., and Agarwal, R. (2003). Inositol hexaphosphate inhibits growth, and induces G1 arrest and apoptotic death of prostate carcinoma DU145 cells: modulation of CDKI-CDK-cyclin and pRb-related protein-E2F complexes. Carcinogenesis **24,** 555-563.

Skoglund, E., Carlsson, N.G., and Sandberg, A.S. (1998). High-performance chromatographic separation of inositol phosphate isomers on strong anion exchange columns. Journal of agricultural and food chemistry **46,** 1877-1882.

Sommer, H.E., and Wetzstein, H.Y. (1984). Hardwoods In Handbook of Plant Cell Culture, P.V. Ammirato, D.A. Evans, W.R. Sharp, and Y. Yamada, eds (MacMillan Publishing Co., New York), pp. 511-540.

Srinivasan, R., and Ruckenstein, E. (1980). Role of physical forces in hydrophobic interaction chromatography. . Separation & Purification Methods **9,** 267–370.

Stenvik, G.E., Butenko, M.A., Urbanowicz, B.R., Rose, J.K., and Aalen, R.B. (2006). Overexpression of INFLORESCENCE DEFICIENT IN ABSCISSION activates cell separation in vestigial abscission zones in Arabidopsis. Plant Cell **18,** 1467-1476.

Stephens, L.R., and Irvine, R.F. (1990). Stepwise phosphorylation of *myo*-inositol leading to *myo*-inositol hexakisphosphate in Dictyostelium. Nature **346,** 580-583.

Stevenson-Paulik, J., Odom, A.R., and York, J.D. (2002). Molecular and biochemical characterization of two plant inositol polyphosphate 6-/3-/5-kinases. The Journal of biological chemistry **277,** 42711-42718.

Strother, S. (1980). Homeostasis in germinating seeds. Ann. Bot. **45,** 217-218.

Takahashi, H., Kittaka, H., and Ikegami, S. (2001). Novel synthesis of enantiomerically pure natural inositols and their diastereoisomers. J. Org. Chem. **66,** 2705-2716.

Takayama, S., and Isogai, A. (2005). Self-incompatibility in plants. Annu Rev Plant Biol **56,** 467-489.

Talamond, P., Gallon, G., and Treche, S. (1998). Rapid and sensitive liquid chromatographic method using a conductivity detector for the determination of phytic acid in food. Journal of chromatography **805,** 143-147.

Talamond, P., Doulbeau, S., Rochette, I., and Guyot, J.P. (2000). Anion-exchange high-performance liquid chromatography with conductivity detection for the analysis of phytic acid in food. Journal of chromatography **871,** 7-12.

Tanfor, C., and sons, J.W. (1973). The hydrophobic effect: formation of micelles and biological membranes. (New York).

Theibert, A.B., Estevez, V.A., Mourey, R.J., Marecek, J.F., Barrow, R.K., Prestwich, G.D., and Snyder, S.H. (1992). Photoaffinity labeling and characterization of isolated inositol 1,3,4,5-tetrakisphosphate- and inositol hexakisphosphate-binding proteins. The Journal of biological chemistry **267,** 9071-9079.

Thompson, A.J., Jackson, A.C., Symonds, R.C., Mulholland, B.J., Dadswell, A.R., Blake, P.S., Burbidge, A., and Taylor, I.B. (2000). Ectopic expression of a tomato 9-cis-epoxycarotenoid dioxygenase gene causes over-production of abscisic acid. Plant J **23,** 363-374.

Timmis, R. (1998). Bioprocessing for tree production in the forest industry: conifer somatic embryogenesis. Biotechnol. Prog. **14,** 156-166.

Trotochaud, A.E., Jeong, S., and Clark, S.E. (2000). CLAVATA3, a multimeric ligand for the CLAVATA1 receptor-kinase. Science **289,** 613-617.

Vallejo, M., Jackson, T., Lightman, S., and Hanley, M.R. (1987). Occurrence and extracellular actions of inositol pentakis- and hexakisphosphate in mammalian brain. Nature **330,** 656-658.

van de Sande, K., Pawlowski, K., Czaja, I., Wieneke, U., Schell, J., Schmidt, J., Walden, R., Matvienko, M., Wellink, J., van Kammen, A., Frannsen, H., and Bisseling, T. (1996). Modification of phytohormone response by a peptide encoded by ENOD40 of legumes and a nonlegume. Science **273,** 370–373.

Van der Kaay, J., and Van Haastert, P.J. (1995). Desalting inositolpolyphosphates by dialysis. Anal. Biochem. **225,** 183-185.

Verbsky, J.W., Chang, S.C., Wilson, M.P., Mochizuki, Y., and Majerus, P.W. (2005). The pathway for the production of inositol hexakisphosphate in human cells. The Journal of biological chemistry **280,** 1911-1920.

Visser, J., and Strating, M. (1975). Separation of lipoamide dehydrogenase isoenzymes by affinity chromatography. Biochim. Biophys. Acta **384,** 69–80.

Vitelio, C., Bellomo, A., Brovetto, M., Seoane, G., and Gonzalez, D. (2004). Concise chemoenzymatic synthesis of epi-inositol. Carbohydrate research **339,** 1773-1778.

von Arnold, S., and Hakman, I. (1988). Regulation of somatic embryo development in Picea abies by abscisic acid (ABA). J. Plant Physiol. **132,** 164-169.

Vucenik, I., and Shamsuddin, A.M. (1994). [3H]inositol hexaphosphate (phytic acid) is rapidly absorbed and metabolized by murine and human malignant cells in vitro. J Nutr **124,** 861–868.

Wang, Z.Y., and He, J.X. (2004). Brassinosteroid signal transduction--choices of signals and receptors. Trends Plant Sci **9,** 91-96.

Wattenberg, L.W., and Chalcones. (1995). *myo*-Inositol and other novel inhibitors of pulmonary carcinogenesis. J Cell Biochem (Suppl) **22,** 162-168.

Welters, P., Takegawa, K., Emr, S.D., and Chrispeels, M.J. (1994). AtVPS34, a phosphatidylinositol 3-kinase of Arabidopsis thaliana, is an essential protein with homology to a calcium-dependent lipid binding domain. Proceedings of the National Academy of Sciences of the United States of America **91,** 11398-11402.

Wen, J., Lease, K.A., and Walker, J.C. (2004). DVL, a novel class of small polypeptides: overexpression alters Arabidopsis development. Plant J **37,** 668-677.

Winton, L.L. (1970). Shoot and tree production from aspen tissue cultures. Am. J. Bot. **57,** 904-909.

York, J.D., Odom, A.R., Murphy, R., Ives, E.B., and Wente, S.R. (1999). A phospholipase C-dependent inositol polyphosphate kinase pathway required for efficient messenger RNA export. Science (New York, N.Y **285,** 96-100.

Yoshida, K.T., Wada, T., Koyama, H., Mizobuchi-Fukuoka, R., and Naito, S. (1999). Temporal and spatial patterns of accumulation of the transcript of Myo-inositol-1-phosphate synthase and phytin-containing particles during seed development in rice. Plant physiology **119,** 65-72.

Zimmerman, J.L. (1993). Somatic embryogenesis: A model for early development in higher plants. Plant Cell **5,** 1411-1423.

VITA

DI WU

Di Wu was born on October 26, 1980, in Shanghai, China. She graduated from Shanghai High School, Shanghai, China, in 1998. She obtained her B. E. degree in Polymer Engineering and Science from Shanghai Jiao Tong University, Shanghai, China, in 2002. She had two internships at GE and Schering-Plough (China) Ltd., Shanghai, China, in 2001 and 2002. She entered the School of Chemistry and Biochemistry at Georgia Institute of Technology in August 2002 to pursue a Ph. D. degree under the guidance of Dr. Sheldon W. May.